A STUDY OF VIBRATION ISOLATION OF ENGINE MOUNT SYSTEM

Ruiping Wang

A Thesis

in

The Department

of

Mechanical and Industrial Engineering

Presented in Partial Fulfillment of the Requirements
for the Degree of Master of Applied Science (Mechanical Engineering) at
Concordia University
Montreal, Quebec, Canada

March 27, 2005

Your file Votre référence
ISBN: 0-494-04434-9
Our file Notre référence
ISBN: 0-494-04434-9

ABSTRACT

A STUDY OF VIBRATION ISOLATION OF ENGINE MOUNT SYSTEM

Ruiping Wang

The engine excitation forces, arising from gas pressure and unbalance force, are widely considered among the main vibration sources for the road vehicles. Even though the current engine mount designs are acceptable for vibration isolation of the transmitted forces from engine to chassis, the performance improvement of the engine mounting system is still required for the tendency of light weight and higher power of the vehicle. In this thesis, a coupled three degree-of-freedom engine mount system with both elastomeric and hydraulic mounts, are developed. The system performance is evaluated through simulation with the purpose of isolating the vibrations in entire frequency range and under engine excitation force.

The engine dynamic model is established based on the analysis of the kinematics and dynamics of its components and gas variation. The unbalanced inertia force caused by engine reciprocating and rotating parts is derived as the vertical excitation force. The net torque, generated by the inertia forces and gas pressure, is formulated using geometrical relationship of the engine components. Two types of individual mounts, including a nonlinear elastomeric mount and a flexible chamber hydraulic mount, are selected from the reported work. The validation of their characteristics is implemented in a single degree-of-freedom (SDOF) system with the response carried out in the time and frequency domain. The internal specific parameters of the hydraulic mount, such as chamber pressure, chamber volume change and the flow, are used to assess the hydraulic

mount properties in static and dynamic situations. The influences of excitation frequency and amplitude are performed to analyze the mounts characteristics. The results reveal reasonably good agreement between the selected model and the computed response characteristics under excitations.

The optimization method of Sequential Quadratic Programming (SQP) is applied to optimize the system design parameters successfully minimizing the objective function integrated by the transmitted forces in the entire frequency range. The optimization work is based on the three degree-of-freedom (three-DOF) model with elastomeric mounts. The vibration transmissibility characteristics of the system are employed to analyze the model. The engine mount system model with hydraulic mounts is evaluated by using the optimal locations of the elastomeric mount, which is proved to not always fit well for other mounts.

ACKNOWLEDGEMENTS

I would like to express sincere gratitude to my supervisors, Dr. Subhash Rakheja and Dr. Henry Hong, for their constant guidance and dedication throughout the realization of this work. I will be indebted for their valuable advice and contributions, as well as their patience. I also wish to thank various researchers whose data and conclusions have been employed in this study.

Finally, I would like to express my appreciation to my father, Gongzeng and my daughter, Nancy, who provided general encouragement and understanding during the completion of my thesis work, especially in the final stage.

TABLE OF CONTENTS

LIST OF FIGURES

LIST OF TABLES

CHAPTER 1

INTRODUCTION AND REVIEW OF LITERATURE

1.1 General

In the past few decades there have been many research achievements in the field of engine mounting system design. The vehicle engine mounting system usually comprises either three or four elastic or visco-elastic mounts that are installed between the engine and the vehicle structure. Although the current designs of mounts used in the modern engine mounting systems are known to be effective in isolating the driver and passenger from both the noise and vibration generated by the engine, further improvements in the performance of engine mounting systems are still desirable for enhancement of occupant comfort and to adapt for changing requirements for vehicle weight reduction and increase in power. To achieve this purpose, different types of engine mounts have been developed, such as elastomeric, hydraulic, and active mounts. Various optimization approaches have also been employed to identify optimal mount stiffness, damping and location to minimize the transmitted vibration. A majority of the studies on engine mounts consider idealized excitations due to engine, and uniform load distribution of different mounts. The optimal mount properties, thus obtained, may not be applicable for implementation in actual engines, which cause distinct excitation forces and uneven loads on different mounts.

In this dissertation research, the nature of engine excitation force is characterized through consideration of the physical operation. The force and moment excitations arising from the engine are also derived using reported experimental data corresponding to specific crank angles and gas pressures. The analytical description of the excitation

force is applied as input signal for studying of typical nonlinear rubber mounts and the comparable nonlinear hydraulic mounts. The effect of load distribution of different mounts is further studied through development and analysis of a three-degrees-of freedom model of the engine mounting system, in which the engine and gear box are considered as a rigid body. An optimization algorithm based on the Sequential Quadratic Programming (SQP) is applied to solve for the constrained nonlinear multivariable objective function to achieve improved vibration isolation. The influences of different rubber and hydraulic mounts properties on the performance of the entire engine mounting system are evaluated on the basis of the simulation results in both the time and frequency domains based on the optimized engine mount location.

1.2 Literature Review

The research works in the field of engine mounting systems include the analysis of an engine's dynamic force, different types of engine mounts (elastometric, hydraulic, active, etc.), and optimization techniques for identifying optimal mounts properties to reduce the transmitted vibration and force imposed on the vehicle chassis. The relevant literatures reported in these areas are reviewed to build the knowledge and scope of the dissertation work. The reported studies are grouped and discussed under four relevant areas which are listed below:

(i) Characteristics of engine excitation

(ii) Elastomeric engine mounts

(iii) Hydraulic engine mounts

(iv) Optimization methods to determine optimal engine mounting system

1.2.1 Characteristics of Engine Excitation

A vast number of reported studies have established that the engine is one of the main sources of vibration transmitted to the vehicle chassis, which is attributed to its unbalance and disturbance forces transmitted to the vehicle [19, 75]. Without isolation, these forces could cause rapid fatigue of vehicle components and discomfort for the occupant [28]. Considering that the design of effective mounts strongly relies upon the nature of engine vibration, the need to characterize the engine excitation forces under applicable operating conditions has been emphasized for studies on the engine mounting system [29]. The vibration and force excitations due to the engine is a complex function of the gas pressure, firing, unbalance and operating conditions, such as load torque and speed. The disturbance forces, arising from the engine, can be characterized through systematic considerations of the engine components and gas pressures.

Excitation force

The motion of the engine block is strongly dependent upon the excitation forces generated by the engine, the design and analysis of the engine mounting system thus necessitates characterization of the engine's excitation forces. For an internal combustion engine, the dynamic disturbances are primarily caused by two phenomena [3, 4, 9]. The first component is due to gas pressure forces associated with combustion and expansion of the fuel-air mixture. The second component is attributed to the variable inertia associated with the slider-crank mechanism of the engine, and dynamic motions of the components. The inertia force caused by the rotating and reciprocating components, including the piston, connecting rod and crank, contribute to vertical excitation force and excitation torque [4]. Furthermore, the variations in the gas pressure yield the principal

force of disturbance at low engine speeds, while the inertia forces may be considerably larger at higher speeds. Both the gas pressure and inertia forces are considered to yield the resultant force on the piston that is reduced by the shearing force generated between the piston assembly and the cylinder wall [3]. The net result is a force along the connecting rod axis that resolves itself into a force and a torque on the crankshaft. Consequently, the gas pressure and inertia forces may be combined to determine the net force acting along the center-line of the cylinder [9].

In a multi-cylinder engine, the motion produced by the group of cylinders is the resultant of motions produced by the individual cylinders. The nature of the unbalance disturbance force depends on the number of cylinders and their arrangement within the engine. For example, for a four-cylinder, four-stroke engine with cylinders uniformly spaced in line, the first order forces as identified from the Fourier series representation, are balanced [2-4]; the second order forces point in the same direction. These components thus result in an unbalanced force. Six and eight cylinder engines do not exhibit such inertia force but are known to cause oscillatory torque [2].

The presence of unbalance forces and variations in the gas pressure cause various vibration modes of the engine leading to motions along the translational and rotational axes (Figure 1.1) [61]. Apart from the magnitude of the unbalance force, the frequency of this force strongly depends upon the engine speed and the stroke number [8]. For a four cylinder, four-stroke engine, the frequency of fundamental disturbances is of the second order of the engine speed. The predominant frequency of unbalance force lies in the 20-200Hz range for engine operating speed in the range of 600-6000rpm. For an eight-cylinder engine, the frequency of the disturbance torque is of the fourth order of engine

speed [3]. The frequency of unbalance excitation would lie in the range of 40-400Hz for the same operating speed. In general, at low engine speeds (near idle) the engine disturbance will result in an annoying shaking of the vehicle. At higher speeds, a booming sound could be created inside the vehicle compartment, when the engine's disturbance force coincides with the acoustic resonance of the passenger compartment.

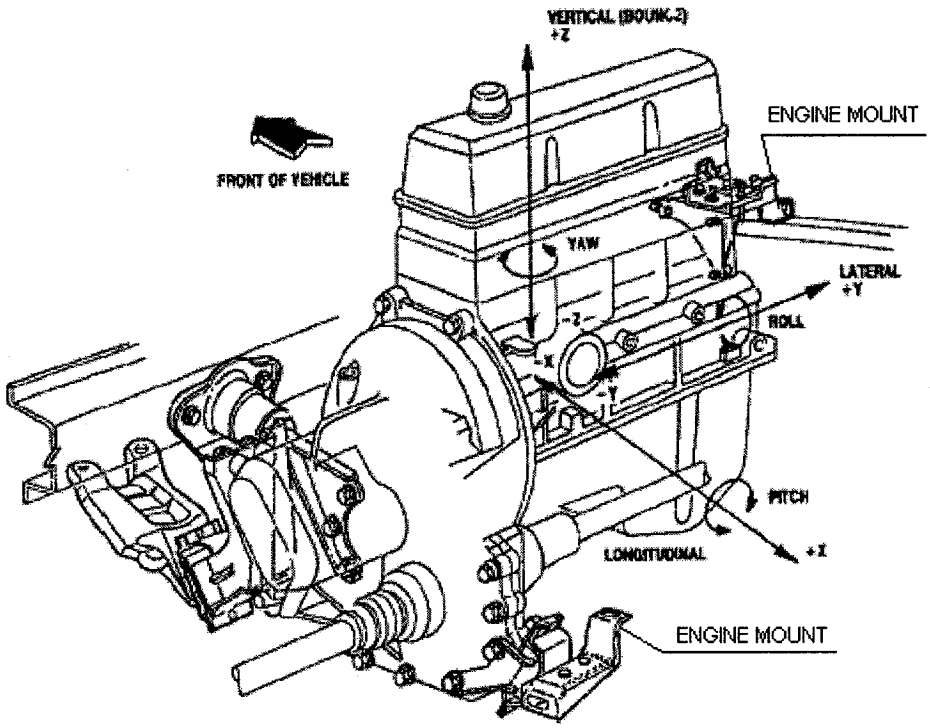

Figure 1.1: A schematic of the engine illustrating 6-DOF motion [61].

Engine model

A vast number of analytical engine models have been developed and analyzed to study the variations in the engine inertia force and excitation torque [6, 9, 10, 12]. The engine system is considered as a torsional dynamic system in many of these studies, which focus on the analysis of the excitation torque [7]. Doughty [9] introduced a fundamental model of the torsional vibration of the internal combustion (IC) engine, as

shown in Figure 1.2, where J_1 and J_2 are the mass moments of inertia due to crankshaft and the load. I_0 and I_2 are the mass moments of inertia of the slide-crank components and k_0 is the torsional stiffness of the shaft. The simplified model of a two-stroke single cylinder engine with load was developed and analyzed to derive the essential features of the IC engine torsional dynamic system, such as the natural frequencies and the forced vibration response [9]. The study established a relation between the motions of the engine slider-crank mechanism subject to combustion gas pressure and using the constant inertia model subject to torque expressed by a Fourier series. Furthermore, the simplified model did not include the damping, while the equations of motion were linearized.

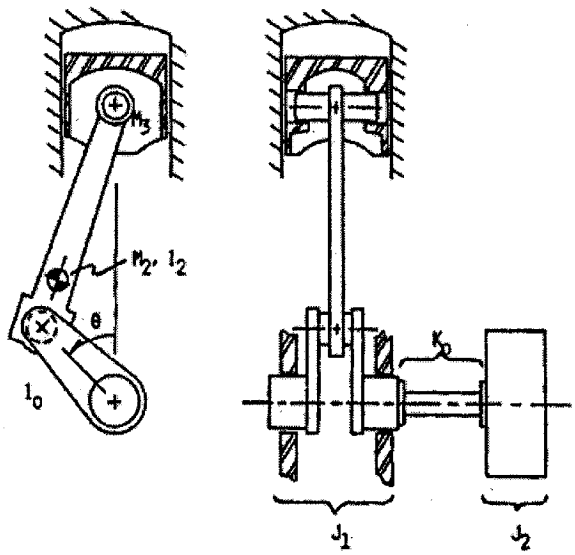

Figure 1.2: Single Cylinder IC Engine with Load [9].

Shiao et al. [75] derived the nonlinear governing equations for the internal combustion engine kinematics and dynamic forces by applying Newtonian and Lagrangian methods. The study also discussed the discrepancy between nonlinear time-varying inertia model and the earlier constant inertia models in terms of variations in the

shaft velocity and acceleration. While the constant mass moments of inertia models showed satisfactory results at low-speed operation, the results revealed considerable deviations at high speeds. When compared to those derived form the variable inertia model, the study concluded that the constant inertia assumption yields inaccurate estimates of the inertial forces at high speeds, and cannot predict the dynamic responses and failure of many engine components. Rizzoni [6] filled some of the existing gaps to the unresolved problems in the complex task of modeling the performance of the internal combustion engine. A robust model for the steady-state dynamic analysis of the spark ignition (SI) engine was proposed based upon rational parameter models of the rotating and reciprocating assemblies subject to stochastic excitations. The study developed a relationship between the cylinder pressure, net engine torque, and acceleration of the crankshaft. This relationship is explained in terms of a lumped, constant parameter electrical circuit model, considered valid under all engine-operating conditions. The net engine torque is thus expressed as a sum of torques due to gas pressure force, friction and pumping losses, and reciprocating inertia forces.

Experimental verification of the proposed equivalent circuit model demonstrated that the measured crankshaft acceleration can yield significant information regarding engine torque and cylinder pressure, the two fundamental engine performance variables. The proposed measurement of crankshaft acceleration is relatively inexpensive and feasible for production vehicle engines. Rizzoni [10] further developed a global model for the IC engine, which incorporated a robust submodel for the dynamics of the IC engine. The engine submodel is viewed as a system with input from the cylinder pressure, and outputs as the crankshaft angular acceleration and crankshaft torque. In the model, the cylinder

pressure is deterministically related to net engine torque through the geometry and dynamics of the reciprocating assembly. The relationship between net engine torque and crankshaft angular acceleration is described through a passive second-order electrical circuit with constant parameters. Experimental results confirmed the validity of the model over a wide range of engine operating conditions, including transient conditions. The robustness of the model was demonstrated over a range of engine operating conditions. Furthermore, the validity of the crankshaft acceleration transient response was demonstrated. The model was thus considered to provide an effective and compact solution to the problem of modeling the dynamics of the SI engine. Time-varying friction and pumping losses, however, were considered negligible in this model. The proposed equivalent circuit model of engine is presented in Figure 1.3, where $T_e(N), N = 1,2,...,N$ is the torque developed by each cylinder, and C_N is the corresponding capacitance representing the stiffness of the crankshaft between individual cylinders.

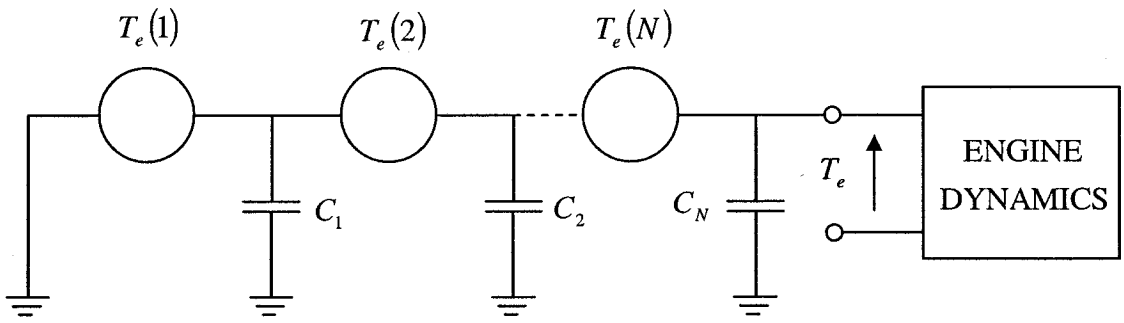

Figure 1.3: Equivalent circuit model of an SI engine [10].

Cho et al. [12] proposed a mean torque predictive model subject to mean pressure. Experiments were carried out to validate the simulation model for step changes of the throttle at a constant engine speed. The indicated mean effective pressure was predicted

cycle by cycle, while the engine model was simulated in real time along with an engine operation in a test cell.

The majority of the reported models consider relatively small magnitudes of torsional vibration. The engine excitation torque, however, has been identified as the major source of excitation to the driveline under higher magnitudes of torsional vibration [7, 9-13]. In many reported models, the automotive driveline systems are assumed as a set of inertia discs representing rotating masses linked by linear springs, representing the torsional stiffness of the rotating shafts. The dynamic torques developed by individual cylinders are properly phased and applied to each cylinder inertia, and coupled to the dynamic models for the driveline. The model parameters have been evaluated experimentally in many studies [7, 10-12]. The reported models have been analyzed under excitations at frequencies up to 500 Hz. The results suggested the presence of many resonant frequencies of the driveline system at frequencies below 50Hz.

One of the typical torsional dynamic models was studied by Rabeih [7], which confirmed that the torsional vibration response of the coupled driveline system are closely related to the torsional vibration of the individual system components, such as fluctuating engine torque. The total fluctuating torque applied to the crankshaft is the sum of the gas pressure torque and the reciprocating masses inertia torque. The gas pressure torque T_g can be adequately represented by a Fourier series comprising a steady part T_0, and a fluctuating component [10]. While the steady component of the torque determines the mean output power from the engine, it does not excite torsional vibration modes of the system. This component is thus neglected in the dynamic analysis of the engine and the driveline. Figure 1.4 illustrates the schematic of a coupled system model proposed by

Rabeih [7]. Owing to the periodic nature of the gas pressure, the torque due to gas pressure is usually expressed in the form of the Fourier series, given by [7]:

$$T_g = T_0 + \sum_{k}^{h_0} a_k \cos(k\omega t) + \sum_{k}^{h_0} b_k \sin(k\omega t) \tag{1.1}$$

where $k = 0.5,1,1.5,...,$ for a four-stroke engine, and h_0 is the maximum number of required harmonic orders, often chosen in the 8-12 range [7]. a_k and b_k are the Fourier coefficients, and ω is the fundamental frequency of the gas pressure in rad/s.

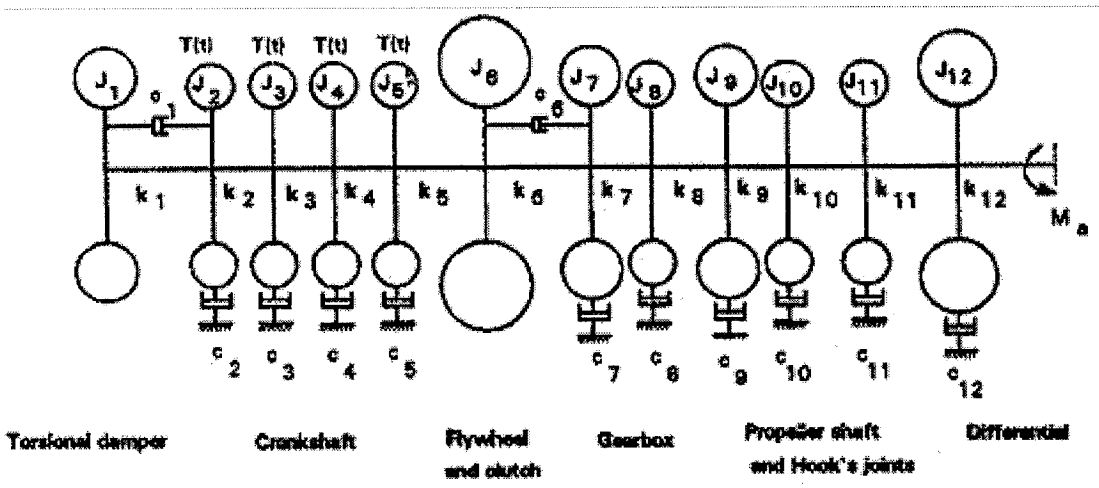

Figure 1.4: Driveline torsional vibration model [7].

Zweiri [16-18] developed three models to study the non-linear transient dynamic responses of a generic direct-injection single-cylinder diesel engine in order to predict the instantaneous engine speed and torque, as shown in Figures 1.5 and 1.6. The models are based on an analysis of all the major internal forces of the engine and the dynamometer. The addition of the dynamometer model permitted for analysis of the engine's behavior under loading. A more comprehensive model incorporated the friction force of the piston assembly, the bearings, the valve train, and the pumps, as shown in Figure 1.6. The

second proposed model includes not only the friction components but also takes into consideration the effect of temperature variation on the viscosity of the oil. The third model is established based on the second one by considering more factors, such as fuel supply and air as well as fuel burning rate. The model, validated using experimentally measured cylinder pressure and instantaneous engine speed, could be used as an effective simulation tool for evaluating the diesel engine control system design and dynamic analysis.

Jacob et al. [11] introduced a family of non-parametric models using the radial basis function (RBF) networks. These may be applied for reconstructing the cylinder pressure based on easy-to-obtain measurements of instantaneous crankshaft angular velocity and cylinder head vibration. The conventional parametric models of the cylinder pressure in engines have been derived from the angular momentum of the reciprocating components [6]. Assuming steady state operating condition and rigid crankshaft system, the motion of the engine crankshaft is described on the basis of various torques, including those due to gas pressure, inertial forces, friction and external load.

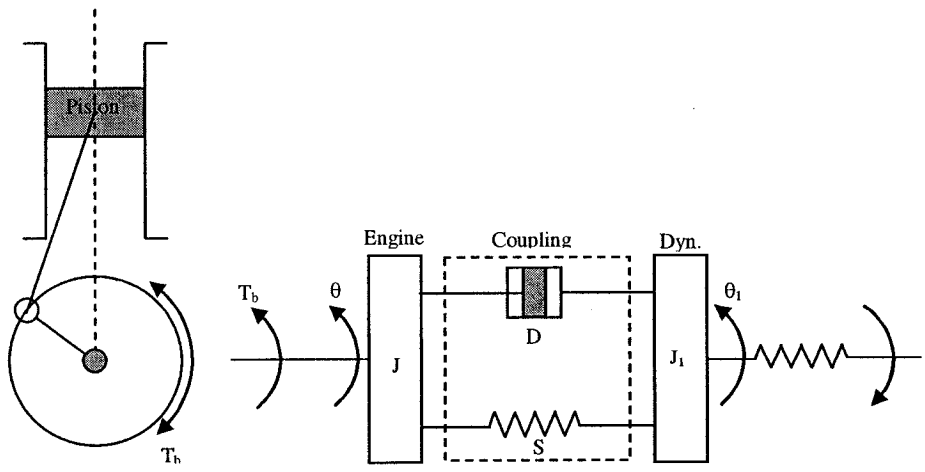

Figure 1.5: Engine and dynamometer model [16].

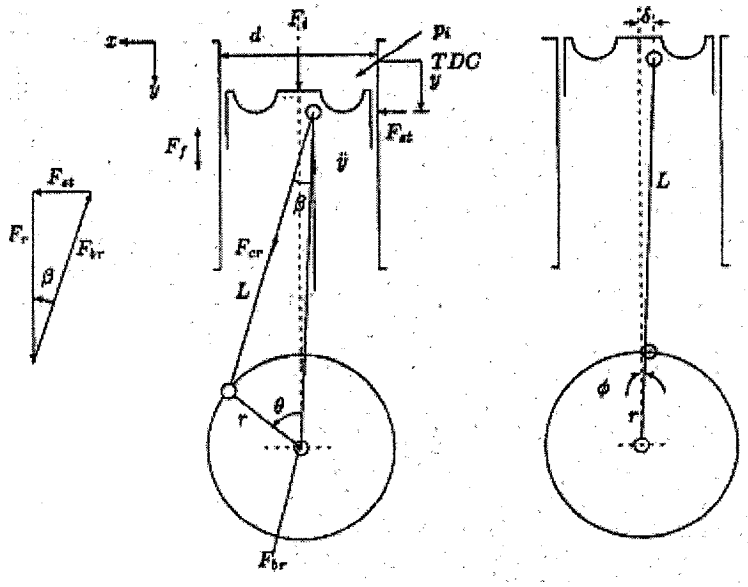

Figure 1.6: Schematics of models illustrating forces and motions of the piston-crank mechanism [17].

Combustion pressure

It has been widely reported that the engine vibration responses are directly related to variations in the gas pressure. Different approaches have been proposed to identify relationships between the gas pressure and the engine vibration. Du et al. [26] presented an approach to reconstruct the gas pressure in the internal combustion engine using radial basis function (RBF) networks. The relationship between the cylinder pressure and the engine cylinder head vibration was analyzed. The validation of this approach to derive cylinder pressure from the vibration signals is demonstrated for a two-cylinder and four-stroke direct injection diesel engine over a wide range of speed and load settings. The non-linear variations in the gas pressure with the engine vibration and the signal noise resulted in poor accuracy of the estimation approach.

Kao and Moskwa [27] demonstrated that engine cylinder pressure has long been a useful mean to determine the engine vibration response. A need to accurately characterize

the engine cylinder pressure was thus emphasized. A nonlinear sliding observer approach was used to estimate the rapidly changing engine cylinder pressure for both steady-state and transient operations. The simulated cylinder pressures under varying engine speeds were obtained through analysis of a detailed cylinder-by-cylinder model using a fourth-order Runge-Kutta method. The tuning of the observer design was accomplished for a one cylinder case and later extended to a six-cylinder engine [27]. Except for the errors around the top dead center, the observed cylinder pressure was considered to be accurate in relation of the actual values. The observed variations in the cylinder pressure, reported in this study, could thus be applied for engine vibration analysis, and performance evaluations and designing of engine mounts.

1.2.2 Engine Mount

The vehicle engine mounting system generally consists of an engine (vibration source) and several mounts inserted between the engine block and the vehicle structure. The primary functions of the engine mounting system are to support the weight of the engine and to reduce the transmission of engine vibration to the chassis. The design of the engine mount system thus requires considerations of the static and dynamic forces. Apart from these, an engine mount system is designed to accommodate the motions of the engine block with respect to the chassis and to provide acceptable service life [28].

The engine mount system has to comply with numerous constraints that are contradictory, which poses considerable design challenges [29]. Modern engine mounting systems have been successfully used to isolate the driver and passenger from both the noise and vibration generated by the engine. A need for further improvement in the

performance of engine mounting systems, however, still exists, because modern car designs tend towards lighter car bodies and smaller engines. The need for higher power to weight ratio often imposes adverse effects on the vibratory behavior, and generally yields higher vibration and noise level [8]. Different types of engine mounts, ranging from simple elastomeric to complex hydraulic, and from passive to active, have been widely investigated to enhance the noise and vibration isolation performance.

Elastomeric Mounts

Simple elastomeric mounts are widely used within the engine mounting systems. These are designed to support the load and to provide necessary stiffness characteristics in all the directions to achieve vibration isolation [29-31]. Such mounts are mostly modeled as a parallel combination of either linear or nonlinear spring and a damping element [30]. Such mounts offer advantages in view of their compact configurations, lower cost and undemanding maintenance. The elastomeric mount can be represented by the familiar Voigt model, which consists of a spring and a viscous damper, as shown in Figure 1.7 [44]. The stiffness properties of the elastic mounts exhibit nonlinear variations with excitation frequency, static load and deflection. The dynamic stiffness of an elastomeric mount at higher frequencies is generally higher than its stiffness at lower frequencies [50]. This characteristic makes it difficult to design a mount system that satisfies all of the design requirements under a wide range of operating conditions. A high stiffness or high damping elastomeric mount can yield a low shake level at low frequencies, but its performance at high frequencies could be poor. On the other hand, low stiffness and low damping mounts yield low noise levels, but induce high shake levels [8]. Despite such inherent performance limitations, such mounts have been

successfully and widely used for engine mounts for many decades due to their compact design, low cost, and long service life. Some typical ealstomeric mounts are shown in Figure 1.8 and Figure 1.9[28].

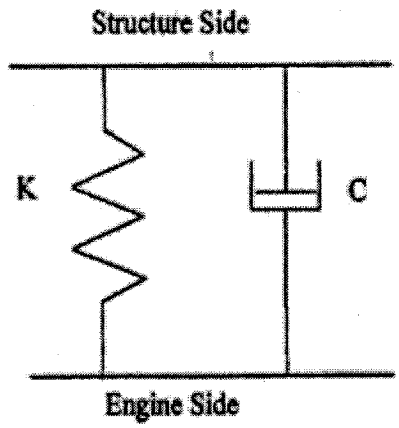

Figure 1.7: Mechanical model for elastomeric mount [44].

Current trends toward light weight, front wheel drive vehicles and smaller size engines with low idle speeds could cause lower frequency vibration of the chassis, closer to the comfort and perception range of the occupant. Elastomeric mounts with potential to provide isolation of lower frequencies vibration are thus desirable. Furthermore, nonlinear force-deflection properties could yield variations in the natural frequency with changes in the speed. Rivin [29] investigated nonlinear characteristics of an elastomeric mount and concluded that of the engine mount could be obtained in a broad load range. The study used materials with high internal damping with highly amplitude-dependent damping and stiffness properties to achieve variable stiffness properties. Many different methods have also evolved for characterizing the elastomeric mounts. While the majority of the studies characterize the mounts through static-force-deflection properties, a few studies have investigated the rate dependent stiffness properties [29, 30]. Richards et al.

[30] proposed experimental methods involving single and multi-degree-of-freedom configurations and different types of excitations. The static stiffness experiments are conducted to measure time-invariant load-deflection curves and the influences from a rubber durometer. Kim et al [31] developed a bush type engine mount using the method of parameter optimization. A commercial non-linear finite element program is used to determine the design that satisfies the stiffness requirements of engine mounts.

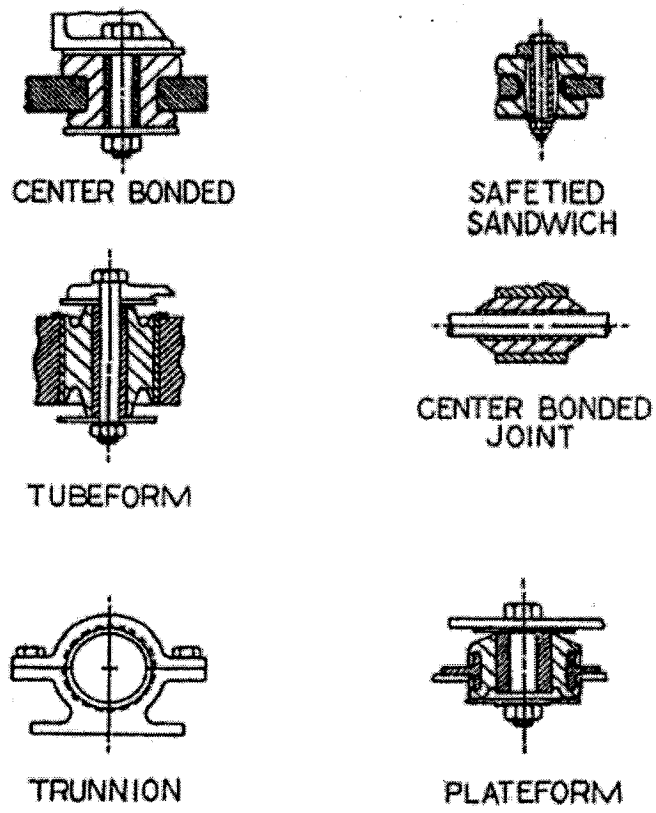

Figure 1.8: Typical elastomeric mounts [28].

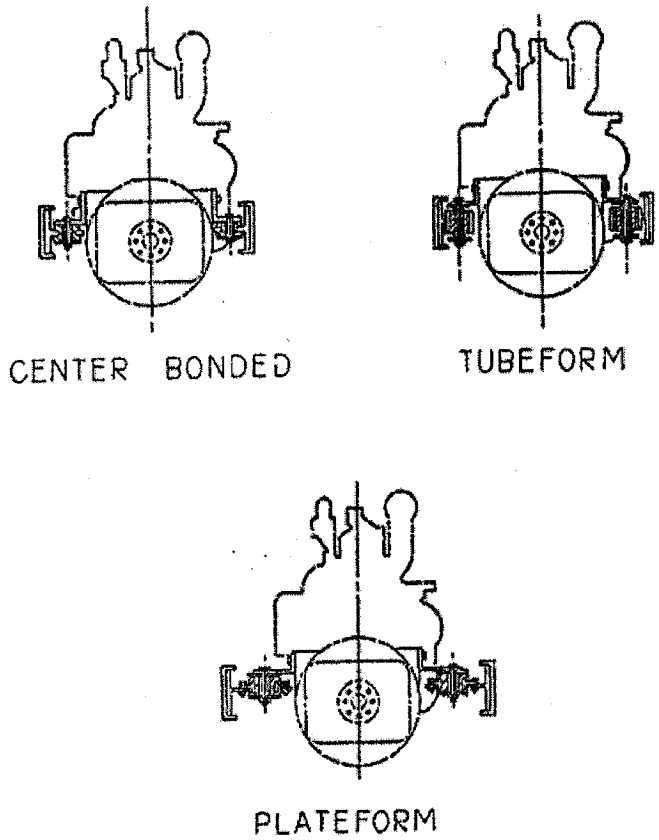

Figure 1.9: Typical rear mounts installations [28].

Hydraulic Mounts

A range of hydraulic mounts have been developed to realize enhanced variable damping properties. These mounts could be classified in three different categories on the basis of primary principles, such as, passive, semi-active, and active. Since the early 1980's, various types of passive hydraulic mounts have been developed to reduce engine vibration and noise transmitted to the operator cabin. Hydraulic mounts are currently being employed in several vehicle models [40]. The hydraulic mounts offer many desirable properties: (i) variable damping properties through fixed or variable orifices and inertia track [41, 43]; (ii) superior dynamic properties to achieve lower resonant transmission and good isolation vibration at higher frequencies, and thereby improved

ride and acoustic comfort [40, 42]; and (iii) compact design performs the required performance through variable projected piston area of the top chamber [41].

It has been reported that significant improvements in ride comfort and noise levels can be achieved by using the hydraulic mounts instead of the conventional elastomeric mounts [32-33]. Corcoran et al. [33] presented a comparison of performance characteristics of both the hydraulic and elastomeric mounts for a V-6 gasoline rear-wheel drive passenger car engine. The results of the study revealed that the hydraulic mounts presented a superior advantage in reducing the transmitted vibration in the lower frequency range (less than 20 Hz), while the noise level decreased as much as 5 dBA for a smooth road maneuvering. The study also showed that the acceleration levels at the seat tracks were significantly reduced when operated on a simulated bumpy road. Superior resonance control capability of the hydraulic mounts was further demonstrated at the engine-mounting system's natural frequency of 11.3 Hz. The superior performance of hydraulic mounts was also demonstrated by Bernuchon [32] through experiments. The study employed hydraulic shakers to excite the vehicle's front wheels in the frequency range of 2-20 Hz with an amplitude of 1.5 mm. The measurements clearly showed that the hydraulic mounts could reduce the acceleration levels at the seat rail considerably, while the car noise level was reduced by 5 to 6 dBA on an open road.

A wide range of designs and design concepts have evolved to realize variable damping and stiffness properties of passive hydraulic mounts. These developments could be further grouped in three categories on the basis of the design concept and construction: simple orifice, inertia track, and inertia track with decoupler [8, 41, 43]. A hydraulic mount with a simple orifice is schematically shown in Figure 1.10. The simple orifice

type hydraulic mounts provide nonlinear damping force approximately related the square of the velocity. The damping force tends to increase at higher frequencies and thus limits the vibration attenuation performance at higher frequencies. The inertia track mounts with and without decoupler offer variable damping to achieve both resonance control and improved vibration isolation. Damping caused by inertia track is considered to be more effective due to its long channel [36, 37, 41].

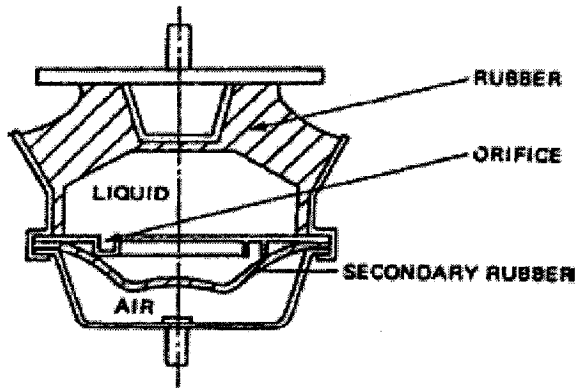

Figure 1.10: Simple hydraulic mount [43].

Flower [43] analyzed the performance characteristics of all three types of hydraulic mounts for power trains, including a hydraulic mount with simple orifice, a hydraulic mount with inertia track and a hydraulic mount with inertia track and decoupler. The study concluded that mounts with an inertia track help to yield high damping at a low frequency, to achieve lower resonant transmissibility, while it yields relatively poor isolation performance at higher frequencies. Mounts with an inertia track with a de-coupler revealed superior vibration isolation performance, and relatively low dynamic stiffness under lower magnitudes of excitation. A typical hydraulic mount with inertia track and decoupler is shown in Figure 1.11 [39].

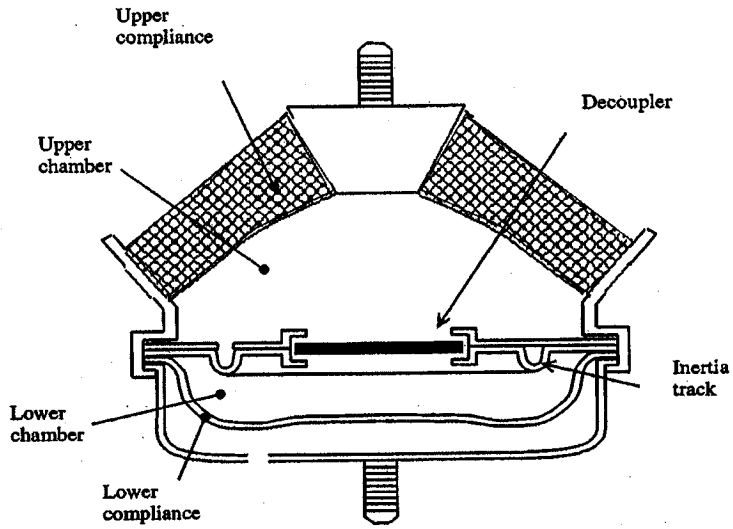

Figure 1.11: Hydraulic mount with inertia track and decoupler [39].

The hydraulic mounts comprise two fluid chambers made of compliant elastomeric materials. The properties of the elastomeric enclosures coupled with fluid flows through orifice and dynamics of the inertia track yield highly nonlinear stiffness and damping properties. A wide range of analytical models, including single-DOF and multi-DOF, and varying complexities associated with short and long orifice flows have been developed [32-33, 35-36, 41, 47]. Matthew [35] developed a linear two-DOF model of a hydraulic mount to study the significance of the inertia track. The proposed model was validated using the experimental data for the mount. The study showed that under small forcing amplitudes (<0.3mm), the fluid is free to move between the upper and lower chambers of the mount through the decoupler. The decoupler is thus suspended in the fluid and offers very little resistance to flow. For large amplitude (>0.3mm) vibrations, the pumping action of the top chamber forces the decoupler to bottom against its seat and thereby terminates the flow through the decoupler channel. In this case, the fluid flow is forced

through the inertia track, which results in a sharp increase in the magnitude of dynamic stiffness at low frequencies.

A number of nonlinear analytical models of the automotive hydraulic mounts have been reported during the last two decades [36-39, 41, 50]. Through analyses of the nonlinear models, Kim and Singh [36-37] concluded that highly nonlinear dynamic properties of hydraulic mounts are significantly frequency-dependent and highly sensitive to the deflection amplitudes. The study employed experimental and analytical approaches to characterize the nonlinear properties of a generic hydraulic mount with an inertia track without a decoupler [37]. This study was the first one to propose a low-frequency lumped-parameter mathematical model of the hydraulic mount, considered valid in the 1-50 Hz frequency range and based on the measured nonlinear system parameters, such as the steady-state inertia track fluid resistance and fluid chambers compliance.

Ahmed et al. [38] developed and analyzed nonlinear analytical models of hydraulic mounts with short and long orifices, as well as with flexible chambers. The simulation results demonstrated the influence of oscillatory flows on the dynamic characteristics of the mounts. The study further presented the influence of variations in the diameter of the short orifice, varied between 0 to 5mm on the dynamic properties. The effect of additional bleeder orifice flows on the dynamic performance is specifically explored to enhance the shock as well as vibration attenuation performance of the hydraulic engine mounts. Geisberger et al. [39] presented a new approach in non-linear modeling of hydraulic mounts following the models reported by Kim and Singh [36-37] and other studies. Continuous algebraic functions were developed to model the decoupler cage contact and its effects on the dynamic responses of the hydraulic mount. The model

further incorporated the decoupler leakage flows. An experimental apparatus was developed to isolate the mount components for identifying their parameters, over the full range of loading conditions (frequency and amplitude). The model predicted the hydraulic mount behavior with the error being less than 5%.

The vast majority of the studies have investigated the dynamic properties of engine mounts, assuming negligible coupling with the vehicle system. Only a few studies have investigated the dynamic responses of the mounts in conjunction with a vehicle dynamic model. Kim and Singh [36] examined the dynamic performance of hydraulic mounts coupled with a simple single-DOF vehicle model, as shown in Figure 1.12 . The study developed a mathematical model of the hydraulic mount with an inertia track and integrated it to a single-DOF vehicle model with linear suspension properties. The study demonstrated that this nonlinear model can reasonably represent the frequency variant dynamic properties of the inertia track mount in the frequency range up to 20 Hz. Experiments were also performed to identity the performance features and limitations of the conventional hydraulic mounts.

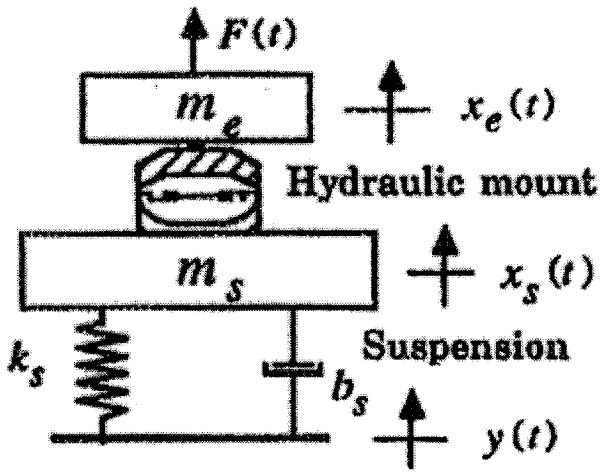

Figure 1.12: A simple vehicle model with hydraulic engine mounts [36].

A number of studies have also investigated semi-active hydraulic mounts, which consist of a passive controllable element [8]; Electro-Rheological (ER) fluids have been employed to achieve rapid variations in the damping properties [46-48]. ER fluids offer rapid variations in the fluid viscosity when an electric field is applied. Such fluids have thus been applied for semi-active vibration control, which is usually adapted to dissipate the vibration energy by changing the dynamic properties, such as damping, of the engine mount [46]. The semi-active engine mounts are mostly based on hydraulic fluid, either through modulation of the flow resistance or by varying the viscous properties of the fluid. The designs provide high damping during the low frequency shock excitation. The structure of the semi-active mount with ER fluid is similar to that of a conventional passive hydraulic mount, except that the hydraulic is replaced by an ER fluid. The mount also comprises electrodes to establish a controllable magnetic field and thus the damping properties. The ER fluids, however, require high voltage to achieve rapid variation in the fluid viscosity.

The dynamic responses of most semi-active hydraulic engine mount systems are very sensitive to the system parameters. The reported works have established that semi-active engine mounting systems are used mainly to improve the system performance in the low frequency range. Only fully active engine mounts can be used to tune the performance at a high frequency. Active mounts use the addition of energy to realize vibration reductions over traditional passive mounts [50]. A mechanical model of a hydraulic active mount is shown in Figure 1.13, where an active dynamic force (F) generated by an actuator is used to add or remove energy in response to a command signal based upon the response and excitation variables [51, 54, 55].

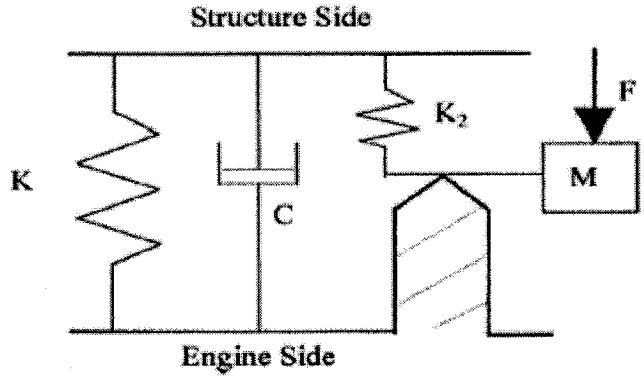

Figure 1.13: Mechanical model for active hydraulic mount [50].

A number of concepts in active mounts have evolved over the past few decades; these include hydraulic as well as elastomeric active mounts. Elastomeric mounts are used to achieve variable stiffness properties control algorithms to realize high stiffness under low frequency excitations (1-50Hz) and low stiffness at higher frequencies have been proposed to achieve enhanced vibration isolation [49]. Active hydraulic mounts, on the other hand, are mostly formulated to achieve variable damping and stiffness behavior. Such mounts are tuned to achieve high damping in the vicinity of the engine bounce frequency for resonance control and relatively low stiffness under high frequency excitation [49, 50]

Many different active mount configurations together with the actuation technologies, and sensor and controller designs, have been thoroughly reviewed by Swanson et al. [50-51]. Nakaji et al. [51] implemented an active mount system in a sport-utility vehicle with a transversally mounted 2.5L four-cylinder turbo-diesel engine to test its effectiveness in reducing the engine vibration. The study concluded that the floor vibration and the booming noise can be significantly reduced when active control is applied. Despite the superior performance potentials of active engine mounting systems, their

implementations have been limited to cases, where the high cost and complexity of an active mount is justifiable.

1.2.3 Engine Mounts Design

The performance characteristics of an engine mounting system, generally consisting of three to four mounts, depends not only on the performance and properties of the individual mounts, but also on the orientation of different mounts within the complete system. The load distribution over different engine mounts, and the locations of the mounts, determine the pitch and roll oscillation centers for the engine mass and thus the nature of vibration transmitted to the chassis. The design of an engine mount system generally includes the selection of stiffness coefficients, load distribution, location and orientation of the individual mounts. The stiffness properties of individual mounts are chosen in relation to the distribution of the engine weight and the corresponding static deflections of the mounts. The vast majority of the studies have employed nonlinear modeling and optimization techniques to identify optimal stiffness and damping properties of individual mounts with little or no consideration of the orientations within a multi-DOF engine system [55, 57-60, 62]. The mounting configuration of the mounts within the total system plays an important role in identifying the optimal properties of the mounts. Only minimal efforts, however, have been made to identify optimal locations of the mounts for a particular engine [61]. The identification of a near optimum initial mounting configuration is not an easy task due to the complex nature of the engine's inertia properties and packaging constraints imposed on the mount locations by the manufacturability considerations.

In almost all the studies, the engine is modeled as a six degree-of-freedom rigid body to freely translate and rotate about the three independent Cartesian axes as shown in Figure 1.1 [61]. It is reasonable to model the engine as a rigid body because its natural frequency is much higher than the mounting system's. Ashrafiuon [57] pointed out that it is standard practice for better isolation of the engine's vibration if the engine mounts are installed in the orientation, at which their line of action converges around the center of mass. This theory was used by Geck [61] and is shown in Figure 1.14.

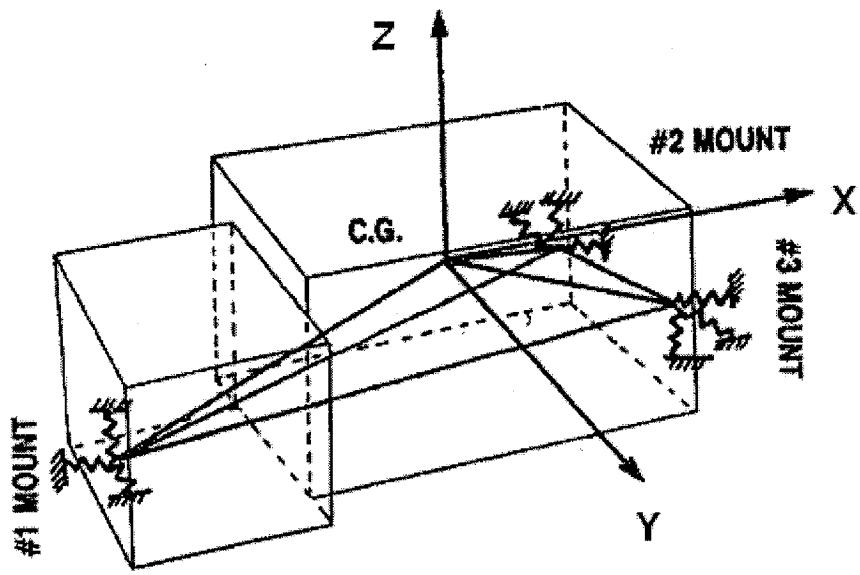

Figure 1.14: Engine model [61].

The foundation is usually modeled as a rigid body [59-61]. The reasons for excluding the vibration of the foundation [58] are: (a) the displacement on the body side of the engine mount is small compared to the engine side so that the engine and mounting system can be treated outside the context of a full vehicle; (b) it is difficult due to its complexity to fully optimize the mount system in the context of a full vehicle. The flexibility foundation model has also been reported in previous papers [56-58]. The

results show that coupling effects are enormous for low frequency modes of foundation and that high frequency modes have no coupling effect.

The primary work of the optimization is defining the objective function, which is considered different in each of the literatures. One is to tune the natural frequency of the engine mounting system to some desired range to avoid resonance and to improve the isolation of vibration and noise and shock excitation [63, 56]; another one is to minimize the dynamic force transmitted from the engine to the body [64, 65]. The second method is considered more effective because it can directly realize the design goal considered as the isolation of engine vibration. The constraints on the design variables must be determined once the objective is established [8]. Two kinds of constraints are used in the engine mount optimization. One is the constraint that directly keeps the design variables within lower and upper limits, such as how the mount location and the orientation are limited by the available engine compartment space. Another one is an indirect constraint like the maximum allowable deflection for the engine's center of gravity or the desirable natural frequency range.

The optimization methods have been explored by many researchers in the field of engine mount system design. However, some limitations still exist in the present work. For example, only elastomeric engine mounts, linear stiffness and damping were considered. The hydraulic mount is rarely used in optimization of engine mount systems. A few works [57] mentioned hydraulic mount optimization modeled with linear frequency dependent damping properties. The nonlinear stiffness and damping in elastomeric mounts, and the complex characteristics of hydraulic mounts such as nonlinear frequency and amplitude dependent stiffness and damping have not been

considered. As pointed out by Rivin [29], there is a great variation in mount stiffness, total engine weight, the position of Center of Gravity of the engine and the moment of inertia in actual vehicles; these variations will greatly affect the results of optimization of engine mounting systems and lead to limitations for their practical use.

1.3 Scope of Dissertation Investigation

From what has been discussed above, the primary functions of an engine mounting system are not only to support the weight of the engine, but also to supply the performance requirements for isolating engine vibrations caused by engine disturbances in a complete speed range. Meanwhile, the handling of vibration resources and engine excitation force shown in both forms of gas pressure and inertia force, will cause considerable discrepancy in the solution. A great quantity of research has described the fundamentals of engine vibration by using different engine dynamic models that focus on torsional vibration. However, few models are related to the mechanism of the transmittal of the engine excitation forces. Specifically, the engine combustion pressure is considered as the system input given in the form of measured numerical signals.

Although the vibration isolation performance of an engine mounting system can be dependably assessed through experiments in the vehicle, this approach will result in high expenses and time limits. The effective optimal methodology is expected to solve the design problem of the engine mounting system with an analytical system model as well as an engine mount model. Much research has been done in the area of engine mounting system design and optimization. The effectiveness of optimization work requires modeling of the properties of the engine mounting system, which consists of three or four engine mounts supported at selected locations and orientations. Furthermore, different

types of engine mounts, from conventional elastomeric to hydraulic, from passive to active mounts, have been proposed in the published studies, which are selected to be used in the modeling of engine mounting system. Nevertheless only a few prior studies have analyzed the effect of hydraulic mount nonlinearities on the dynamic response of a vehicle model.

In the optimization approach, most of the methods reviewed in the literature only focus on the linear rubber mount. In this thesis, the well designed three-DOF engine mount system with three nonlinear elastomeric mounts is optimized. The most commonly used optimization algorithm called Sequential Quadratic Programming (SQP) is expected to achieve a satisfactory solution with the more accurate model used. Nonlinear constraints include the stiffness and damping of the mounts, and the individual engine mount locations and orientations are employed as variables in the optimization processes. In addition, the comparison work between rubber mounts and hydraulic mounts is achieved by measuring their performance differences simulated on a vehicle. As a consequence of the complexity of the hydraulic mount characteristics, the performance of the hydraulic mount system is compared by using the optimal elastomeric mount location.

1.4 Objectives of the Dissertation Research

The overall objective of this dissertation research is to develop a simulation methodology for identifying optimal locations of engine mounts and optimal design of engine mounting system. This will be achieved by analyzing the influence of the engine mounting system with respect to the isolation of vibrations.

The specific objectives of the study are:

(i) Identify engine excitation forces and moments considered as inputs to the engine mounting system, through systematic considerations of the combustion process, and kinematic and dynamic motion of the rotating and reciprocating components.

(ii) Develop nonlinear analytical models of an elastomeric and a hydraulic mount, through consideration of their nonlinearity, especially nonlinear compliance of hydraulic mount and its influence to the chamber volume change and chamber pressure.

(iii) Characterize static and dynamic properties of the elastomeric and the hydraulic mounts from previous publications.

(iv) Derive a multi-DOF engine mounting system model for different engine mounts, such as rubber mounts and hydraulic mounts, incorporating the bounce, roll and pitch motion of the engine block.

(v) Formulate and solve an optimization problem with appropriate constrains for minimizing the total transmitted forces and moments in the entire frequency range of 1-200Hz.

(vi) Compare the performance characteristics of the hydraulic mounts with those of the rubber mount in MDOF by employing it in the optimal location generated in the optimization solution of the rubber mount system model.

1.5 Organization of the Thesis

The thesis is divided into seven chapters. Chapter 2 of the thesis establishes the engine dynamic model with a force analysis of the engine cylinder and reciprocating parts; the engine excitation force is identified. An analytical elastomeric mount and

highly nonlinear flexible chamber hydraulic mount model are developed based on the reported work. The characteristics of the mount with the internal detailed parameters, typically for a hydraulic mount are performed. The nonlinear equations of motion are solved to characterize the damping properties. Chapter 3 presents models of the characteristics of an optimized nonlinear elastomeric mount, and a flexible chamber hydraulic mount with one and two short orifices.

The analytical model for the engine mounting system is developed in Chapter 4 for both elastomeric and hydraulic mounts. The detailed derivation of the differential equation is completed for static and dynamic motion of the system. Chapter 5 primarily deals with the performance of the engine mounting system with the model developed in Chapter 4. The performance of the mount in terms of vibration isolation is presented in the form of transmissibility in the frequency domain. The displacement, acceleration and transmitted forces are also simulated in the time domain.

Chapter 6 presents the optimization methodology for the optimum placement of the elastomeric mount established in Chapter 4. The objective function and its weighting factors are decided to success the optimization program with nonlinear multi-constrains.

Chapter 7 of the thesis concludes the present investigation with highlights of the findings in the considered models. It also presents a list of recommendations for future work.

CHAPTER 2

ENGINE EXCITATION FORCES

2.1 General

The vibration responses of I.C. engines are most significantly dependent upon the nature of excitation forces and moments. The principal disturbances in an engine arise from variations in the gas pressure forces, and unbalance forces and moment due to the reciprocating mechanism. The analyses of engine vibration and design/selection of engine mounts thus necessitates total characterization of the disturbance forces and moments. A vast number of studies have analyzed engine mounts under idealized vibration excitations [52-65]. The design parameters and optimal designs derived from such studies thus may not be directly applicable for real engines. The characterization of the gas pressure forces and unbalance forces thus form the essential task in design and analysis of engine mounts. The characterization of the disturbing forces, however, requires the treatment and understanding of the gas pressure variation, combustion process and the variable inertia aspects of the engine components [6, 7,10].

In this chapter, the combustion process and the dynamics of a four-cylinder internal combustion engine are examined in an attempt to develop an understanding of the excitation forces. The principal goals are to construct a rational parameter model for the dynamics of the rotating and reciprocating assemblies as well as cylinder block components, and to characterize the engine's self-excitation forces to serve as primary excitations to the engine mounting system. A relationship between the cylinder pressure, net engine torque, and acceleration of the crankshaft is formulated, while the equivalent vertical excitation force is derived from the analyses of the rotating and reciprocating

subsystems. The roll excitation torque is further analyzed through formulation and analysis of a torsional vibration model. The excitations arising from the engine are formulated in terms of three different components: (i) the unbalanced inertia forces due to reciprocating and rotating parts; (ii) the torque developed by gas pressure and unbalanced inertia force and the corresponding roll excitations; and (iii) the pitch torque generated by the unbalanced inertia force about the axis perpendicular to the crank in a lateral direction.

2.2 Sources of Engine Vibration

It has been acknowledged that the engine is the primary vibration source along with external disturbance forces to the vehicle. The firing cycle from each cylinder and the moving masses resulting from the firing cycle impart dynamic forces and moments to the internal combustion engine block which in turn may be transmitted through the engine mounts into the frame. For this reason, the characterization of engine disturbances forms one of the most important tasks for developing effective mounts for isolating the transmitted force from engine to the vehicle frame. On the basis of the reported studies, the dynamic disturbances for an internal combustion engine could be grouped in three categories:

(i) Firing pulse, due to the explosion of the fuel in the cylinder, causes a moment to act on the block about an axis parallel to the crank [28, 3, 4].

(ii) Inertia forces and torques caused by rotating and reciprocating parts, namely the piston, connecting rod, and crank, where the direction of the inertia forces are both parallel to the piston axis and perpendicular to the crank and piston axis. The inertia torque acts about an axis which is parallel to the crankshaft.

For multi-cylinder engines, this inertia torque acts about axes that are parallel to the piston axes and perpendicular to the piston and crank axes [28, 5, 9].

(iii) Friction and pumping losses form the third source, which is attributed to piston and ring sliding friction, and the pumping action of the engine [6]. These losses have traditionally been lumped together due to the difficulty in separating the effects of one from the other. Frictional losses in particular are the subject of considerable research efforts [15-17] at present. The friction losses are neglected in this study, since they are small compared to the torque generated by the process combustion [6,9].

An analysis of the dynamics of the internal combustion engine can be found in many textbooks and research articles [1-29]. Considering the case of a three degree-of-freedom (DOF) engine model, the system disturbances will cause engine bounce, roll and pitch vibration. The detailed three DOF engine model under the support of engine mounts will be established in Chapter 4.

2.2.1 Unbalance Force

The forces acting on the principal moving parts of a reciprocating engine are the gas pressure forces, the inertial forces of the reciprocating parts, and the inertia and centrifugal forces of the rotating parts [5]. The principal reciprocating parts of an engine are included in the piston assembly. The upper part of the connecting rod is assumed to have a reciprocating motion, its weight being added to the weight of the piston assembly [5]. The crank end of a connecting rod undergoes a rotating motion, while its weight is lumped with the weight of the crank pin assembly. The rotating parts will counterbalance

in both the static and dynamic conditions by either adding or reducing the mass appropriately on the crankshaft [5].

Figure 2.1 shows the engine balancing in the first, second and fourth harmonics for a four cylinder engine. The first harmonic is inherently balanced (Figure 2.1b). When cranks 1 and 4 are at the top dead center (Figure 2.1c), all the weights representing the second harmonic for all cranks will be located at the top dead center, resulting in unbalanced force. Thus, the unbalanced second harmonic causes a vertical vibration with a frequency twice that of the engine speed. The fourth harmonic (Figure 2.1d) and all higher even harmonics act as the second harmonic but have a higher frequency and exert less force [1,3,4]. they can usually be neglected in the calculation of the unbalanced force.

For the multi-cylinder engine, the components of the unbalanced engine disturbance depend on the number and arrangement of the engine cylinders. The four-cylinder, in-line, and four-stroke engine has a vertical inertia force which acts on the engine block in addition to the oscillatory torque about the crankshaft. The frequency of fundamental disturbances occurs at the second order of the engine speed. The frequency range is 20-200Hz for an engine speed range of 600-6000rpm [8]. The function of unbalanced force will be derived in the next section.

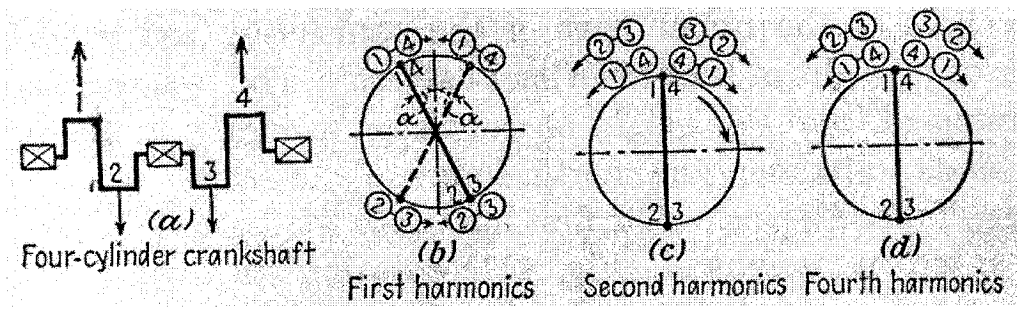

Figure 2.1: A schematic of the crank shaft and reciprocating cylinders illustrating the balancing property of the engine [5].

2.2.2 Inertia Force

The inertia forces occur in the vertical and horizontal directions [28]. The primary component of the vertical force is equal to the inertia action of the combined rotating and reciprocating masses as if they were moving up and down harmonically at the crankshaft frequency and amplitude. The secondary vertical component is equal to the inertia action of the reciprocating mass moving up and down with twice the crankshaft frequency. The horizontal inertial force has a primary component due only to the rotating mass. The position of the piston depends on the crank position and the connecting-rod-crank ratio as demonstrated in Figure 2.2. The distance z_1, describing the piston position from the top dead center (TDC) corresponding to a crank angle of θ, measured from the same dead center, is given by:

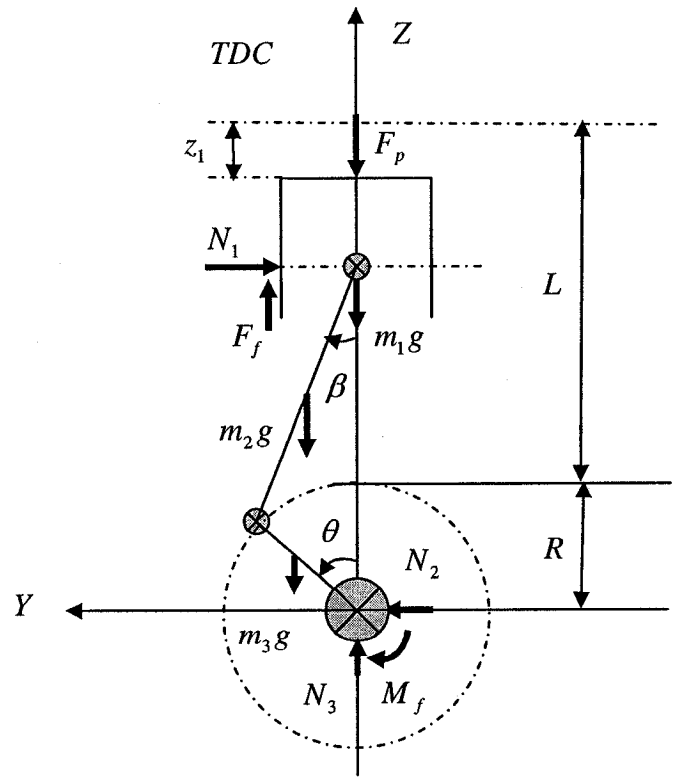

Figure 2.2: Kinematic relationship of the piston-crank motions.

$$z_1^{\downarrow} = R + L - L\cos\beta - R\cos\theta \tag{2.1}$$

where L is the length of the connecting-rod, R is the crank throw, and β is the connecting-rod angle to the line-of-stroke. From geometry, $L\sin\beta = R\sin\theta$; $\sin\beta = \frac{R\sin\theta}{L}$; and

$$L\cos\beta = L\sqrt{1-\sin^2\beta} = L\sqrt{1-\left(\frac{R\sin\theta}{L}\right)^2} \tag{2.2}$$

Substitute Equation (2.4) into Equation (2.1) yields:

$$z_1^{\downarrow} = R\left[(1-\cos\theta)+\frac{L}{R}\left(1-\sqrt{1-\left(\frac{R\sin\theta}{L}\right)^2}\right)\right] \tag{2.3}$$

Adding $R^4\sin^4\theta/4L^4$ to the terms under the radical to complete the square, results in the approximate relation of the form:

$$z_1^{\downarrow} = R\left[(1-\cos\theta)+\frac{R}{4L}(1-\cos 2\theta)\right] \tag{2.4}$$

The time derivative of (2.4) yields the piston velocity $\dot{z}_1$, as:

$$\dot{z}_1^{\downarrow} = \omega R\left(\sin\theta+\frac{R}{2L}\sin 2\theta\right) \tag{2.5}$$

where ω is the constant angular velocity of the crank ($\omega = \dot{\theta}$). The piston acceleration, as it moves downward from the TDC, can thus be expressed as:

$$\ddot{z}_1^{\downarrow} = \omega^2 R\left(\cos\theta+\frac{R}{L}\cos 2\theta\right) \tag{2.6}$$

The downward inertia force $F_i^{\downarrow}$ due to the reciprocating motion for the individual ith cylinder, is given by Tylor [4], which equals the equivalent mass times the vertical acceleration of the piston:

$$F_i^{\downarrow} = m_{eqz}\ddot{z}_1^{\downarrow} \tag{2.7}$$

where m_{eqz} is the equivalent mass of the reciprocating and rotating parts constituted by the piston, connecting rod and crankshaft mechanism.

Upon substituting for $\ddot{z}_1$ into equation 2.7, the unbalanced inertia force can be completed as:

$$F_i^{\downarrow}(\theta) = m_{eqz}\omega^2 R(\cos\theta + \frac{R}{L}\cos 2\theta) \tag{2.8}$$

The upward inertia force is derived in a similar manner, and given by:

$$F_i^{\uparrow}(\theta) = F_i^{\downarrow}(\theta + \pi) = m_{eqz}\omega^2 R(\frac{R}{L}\cos 2\theta - \cos\theta) \tag{2.9}$$

The total inertia force is obtained by summing the forces due to the four cylinders with appropriate consideration of the phase [6].

$$F(\theta) = F_i^{\uparrow}(\theta) + F_i^{\uparrow}(\theta + \pi) + F_i^{\downarrow}(\theta) + F_i^{\downarrow}(\theta + \pi) = 2(F^{\downarrow} + F^{\uparrow}) \tag{2.10}$$

Equation (2.10) to yield the total unbalanced inertia force for a four-stroke, four-cylinder inline engine as:

$$F = \frac{4m_{eqz}\omega^2 R^2}{L}\cos 2\omega t \tag{2.11}$$

The above formulation of the total unbalanced inertia force has been applied in many studies to study the effectiveness of the engine mounts [66, 67].

2.2.3 Net Torque

The gas pressure and inertia forces result in a net force on the piston that is reduced by the shearing force of the oil film between the piston assembly and the cylinder wall.

The net result is a force acting along the connecting rod that resolves itself into a turning effort or torque on the crankshaft [5]. The net torque is generated due to the resultant force, which is the algebraic summation of the gas pressure and inertia force. The gas pressure in the internal combustion engine process varies from below atmospheric to above 1000 psia in some cases [5]. The gas pressure force acting against the piston acts along the same line as the vertical inertia force. Consequently, the gas pressure and inertia forces may be combined algebraically to determine the net force acting along the center-line of the cylinder [3].

The net force F_e is exerted in a direction along the cylinder axis, as illustrated in Figure 2.3. The angular position of the connecting rod causes the net force to be divided into two components: a component (P_s) producing piston thrust against the cylinder wall and the component (F_q) acting along the axis of the connecting rod. The tangential force component F_t acting at the crankpin is determined by resolving the force F_q along the rod into two components, one acting tangentially to the crank circle at the crankpin, and the other acting radially at the crankpin. The tangential force F_t would yield the desired drive torque.

From Figure 2.3, it is evident that the relationship between the net force F_e and net torque T_e is a function of the engine geometry. A precise derivation of the functional relationship between net force and net torque is presented below. The net torque may be expressed as a function of the geometry in the following manner:

$$T_e(\theta) = F_e g(\theta) \tag{2.12}$$

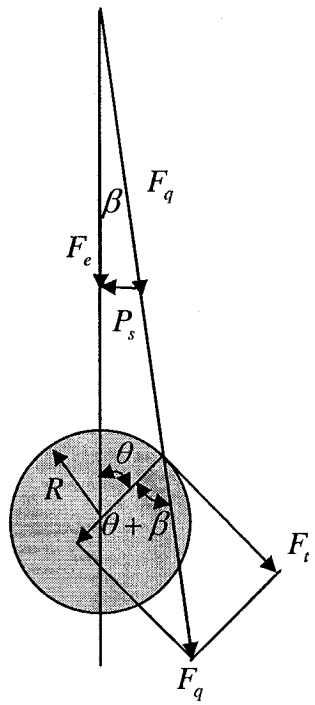

Figure 2.3: Resolution of the net force [5].

where F_e represents the net force formed by both gas pressure and inertia force, and $g(\theta)$ is the function of the geometry relationship between net force and net torque, such that:

$$g(\theta)=\frac{R\sin(\theta+\beta)}{\cos\beta} \tag{2.13}$$

which can be further expressed as:

$$g(\theta)=R(\sin\theta+\cos\theta\tan\beta) \tag{2.14}$$

where,

$$\tan\beta=\frac{2RL\sin\theta}{2L^2-R^2\sin^2\theta} \tag{2.15}$$

Equation (2.15) is obtained similarly as the derivation of Equation (2.4) by adding $\frac{R^4\sin^4\theta}{4L^4}$ to the terms under the radical to complete the square to get an approximate

solution. The geometric relationship between the net force and the net torque is thus expressed as:

$$g(\theta) = R(\sin\theta + \frac{2RL\cos\theta\sin\theta}{2L^2 - R^2\sin^2\theta}) \tag{2.16}$$

The above function for individual pistons would require the appropriate coordination of the phase angles between the pistons. The net torques developed during downward and upward motions of the piston can be expressed as:

$$T^{\downarrow}{}_e(\theta) = F_e \frac{R\sin(\theta+\beta)}{\cos\beta}. \tag{2.17}$$

$$T^{\uparrow}{}_e(\theta) = F_e \frac{R\sin(\theta-\beta)}{\cos\beta} \tag{2.18}$$

2.3 Engine Excitation Force and Moments

The analyses of vertical excitation force, and roll and pitch moment excitations due to engine require the kinematic and dynamic analyses of reciprocating parts and cylinder block. The excitation forces and moments are primarily generated by the motions of the reciprocating parts, which are then transmitted to the chassis of the vehicle through the cylinder block. Figure 2.4 illustrates a model representation of the rotating and reciprocating component, and the cylinder block. The analysis of this model is presented in the following subsections to derive the excitation forces and moments.

2.3.1 Vertical Excitation Force

The vertical excitation force is considered the same as the unbalanced inertia force. The differential equations of motion for the model are derived to quantity the dynamic relationships between the excitation force and the motion. Figure 2.4(a) shows the motion

of the reciprocating parts consisting of the piston displacement relative to the engine block, and the displacements of the crank and the connecting rod. The engine block forces and displacement with respect to the vehicle chassis are shown in Figure 2.4(b). The index $i=1$ to 3 represents respectively the masses and motions of the piston, connecting rod and crank throw. Thus, the inertia forces for the three masses can be expressed as:

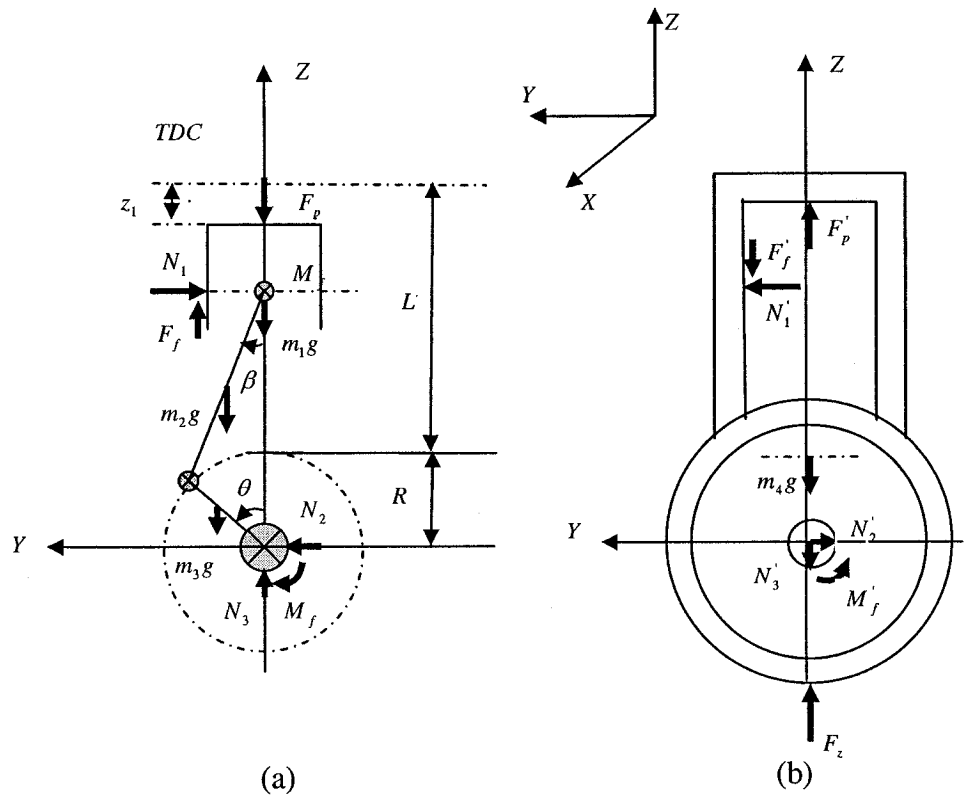

Figure 2.4: Kinematic and dynamic model of reciprocating component and the block.

$$\sum_{i=1}^{3} m_i \ddot{z}_{ai} = \sum_{i=1}^{3} m_i \ddot{z}_i + \sum_{i=1}^{3} m_i \ddot{z} \tag{2.19}$$

where z_{ai} is the absolute displacement, z_i is the relative displacement of the motion components, and z is the displacement of the cylinder block, where all displacements are

in the vertical direction. The equation of motion of the reciprocating and rotating parts in the vertical direction is:

$$\sum_{i=1}^{3} m_i \ddot{z}_{ai} = -F_p + F_f + N_3 - \sum_{i=1}^{3} m_i g = \sum_{i=1}^{3} m_i (\ddot{z}_i + \ddot{z}) \tag{2.20}$$

where F_p is the gas pressure force acting on the piston, F_f is the friction force between the piston and the cylinder block, and N_3 is the support force from the cylinder block transferred to crankshaft. The equation of motion for the cylinder block can be expressed as:

$$m_4 \ddot{z} = F_z + F_p^{'} - F_f^{'} - N_3^{'} - m_4 g \tag{2.21}$$

where F_z is the total support force of the engine mounts in the vertical direction, $F_p^{'}$ is the reaction gas pressure force to the cylinder block, $F_f^{'}$ is the reaction friction force between the piston and the cylinder block, $N_3^{'}$ is the reaction force from the crankshaft to the cylinder block, and m_4 is the mass due to the cylinder block.

Since the forces $F_p^{'}$, $F_f^{'}$ and $N_3^{'}$ are, respectively, the reaction forces of F_p, F_f and N_3, the following equally holds: $F_p^{'} = -F_p$, $F_f^{'} = -F_f$, $N_3^{'} = -N_3$. Combining Equations (2.20) and (2.21), yields the equation of motion for the entire engine in the vertical direction:

$$m\ddot{z} = F_z - mg - \sum_{i=1}^{3} m_i \ddot{z}_i \tag{2.22}$$

where,

$$m = \sum_{i=1}^{4} m_i = m_1 + m_2 + m_3 + m_4 \tag{2.23}$$

The term, $\sum_{i=1}^{3} m_i \ddot{z}_i$ in Equation (2.21) and (2.22) forms the excitation force and is expressed as:

$$\sum_{i=1}^{3} m_i \ddot{z}_i = F_{ez} \tag{2.24}$$

It is noted that the excitation force in the vertical direction is the same as the unbalanced inertia force as evident from Equation (2.7), such that:

$$F_{ez} = m_{eqz} \ddot{z}_1 \tag{2.25}$$

Equation (2.24) and (2.25) yield:

$$\sum_{i=1}^{3} m_i \ddot{z}_i = m_{eqz} \ddot{z}_1 \tag{2.26}$$

Furthermore, the bounce excitation force F_{ez} is related to the engine speed as observed in Equation (2.11). The vertical excitation force is thus identical to the unbalanced inertia force F_i Equation (2.11). The identification of equivalent mass m_{eqz} due to reciprocating components, however, is a formidable task. The reported experimental data are thus examined for this purpose and discussed in section 4 [67].

2.3.2 Roll Excitation Moment

As the engine cycle progresses, three different forces act on the connecting rod and ultimately produce a torque on the crankshaft [7]. These are the gas pressure, inertia and friction forces, which collectively produce the periodically varying rotational torque on the crank. The magnitude of the friction force, however, is known to be relatively small [56], its contribution to the net force is thus considered negligible in this study. The

engine torque, arising from the combined effects of the varying gas pressure in the cylinders and the motions of the reciprocating masses, is evaluated as the principle cause of roll vibration. A detailed study of the gas pressure force and the inertia torques is presented below.

Engine fluctuating torque

For the engine, the main source of excitation is the torque fluctuations arising from the four-stroke operation. Irregular ignition or misfiring can also lead to comprehensive magnitudes of vibration, but these factors will not be treated in this study because they represent faulty conditions. The torque delivered by the engine is not constant in magnitude, but it comprises a series of pulses corresponding to the stroke of each cylinder. Figure 2.5 shows the torque variations against the crank angle for a typical four-stroke, four-cylinder engine [7]. The flywheel inertial acts to smoothen the torque output which consists of a steady-state component superimposed with torque variations.

The torque produced from the gas pressure of an internal combustion engine exhibits periodic variations corresponding to every complete working cycle. For a four-stroke single cylinder engine, the fundamental period of oscillation is given by two revolutions of the crankshaft (4π radians) resulting in a period of $\frac{4\pi}{\omega}$, where ω is the angular velocity of the crankshaft. Therefore, the torque due to gas pressure M_g can be represented by a Fourier series consisting of a steady component M_0 and an oscillatory component. The steady part determines the useful mean output power from the engine, but does not excite the torsional vibration modes of the engine assembly. The steady component is thus omitted from the vibration analysis. Many studies have employed the

Fourier series representation of the dynamic or oscillatory component for analyses of torsional vibration behavior of the engines [11, 12, 16, 18, 65].

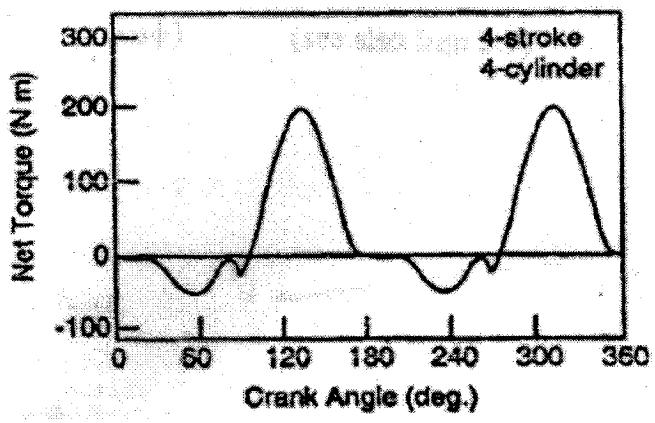

Figure 2.5: Typical torque variations at the output of a four-stroke engine [7].

The gas torque M_g due to the gas pressure arises from the combustion pressure. Let M_i represent the torque due to the effective reciprocating mass and piston motion, M_f be the torque due to friction and the pumping action of the engine, and M_1 be the external load torque. The engine excitation torque may then be considered as the difference of the external load torque (M_1) and the net torque. For the engine mount system, shown in Figure 2.6, the torque M_s generated by the engine mount forces is also considered in addition to the excitation torque, to study the roll motion of the block. The equation of motion describing the roll motion of the engine can be expressed as:

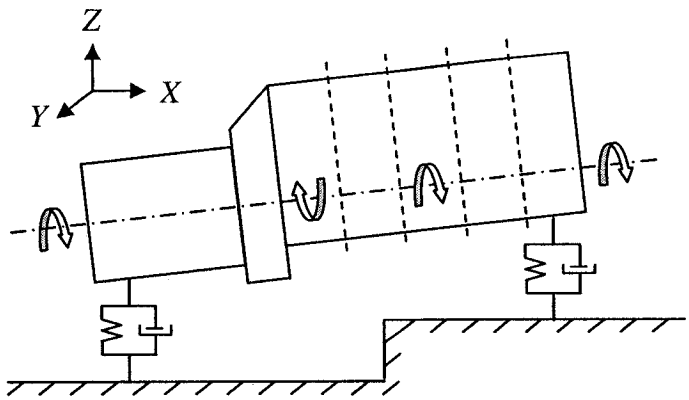

Figure 2.6: Pitch plane representation of the engine mounting system.

$$J_x\ddot{\theta} = M_{ex} - M_s \tag{2.27}$$

where J_x is the roll mass moment of inertia of the engine assembly about an axis passing through the crankshaft, and M_{ex} is the net excitation torque, given by:

$$M_{ex} = M_g - M_i - M_f - M_1 \tag{2.28}$$

The torque due to friction and pumping losses is considered to be relatively small and thus disregarded in this study. The effective inertial torque M_i is determined from the inertia force F_i derived in Equation (2.11), and $M_g - M_1$ is considered as the dynamic or oscillatory torque, which contributes to the roll motion of the engine.

Roll excitation moment

The roll moment excitation of the engine is generated by the gas pressure and the inertia forces, where the torque due to gas pressure forces is referred to as the indicated torque. The foremost source of engine vibration arises from the gas pressure forces, generated by the conversion of the chemical energy to the thermal and subsequently to the mechanical energy during the combustion process [5, 6]. Following the relationship in Equation (2.12), the gas torque can be expressed as:

$$M_g(\theta) = F_p g(\theta) \tag{2.29}$$

where the gas pressure force F_p is related to the gas pressure and the effective area, such that:

$$F_p = P(\theta)A \tag{2.30}$$

where $P(\theta)$ is the uniform gas pressure acting on area A of the piston, corresponding to crank angle θ. It has been reported that the gas torque attributed to vibration excitation is usually in the range of 1-5% of the indicated torque [5]. The magnitude of the roll moment excitation in this study is thus assumed as 5% of the total gas torque, such that:

$$M_p = 0.05M_g \tag{2.31}$$

where M_p is the magnitude of the roll moment excitation. The 5% value selected in this study would relate to the upper bound, as suggested in [5].

Apart from the component of above indicated torque, another component also plays a very important role in determining the net torque applied to the crankshaft. This component is due to the reciprocating action of the piston and of the upper position of the connecting rod, which are constantly being accelerated upward or downward. The torque caused by inertia force can be expressed in a similar manner, as:

$$M_i = Fg(\theta) \tag{2.32}$$

The fluctuating component of the torque at the crankshaft is the sum of the gas pressure torque and the reciprocating masses inertia torque [65]. Consequently, the total excitation torque that forms the roll excitation applied to the cylinder block is the reaction torque to the total fluctuating torque applied to the crankshaft. The torque generated by

the gas pressure and the inertia force, and thus the roll excitation which can be attained by the same geometry relationship described in the form of $g(\theta)$, is given as:

$$M_{ex} = M_i + M_p = (F + 0.05F_p)g(\theta) \tag{2.33}$$

substituting Equations (2.11), (2.16) and (2.30) into (2.33), yields following expression for the roll moment excitation:

$$M_{ex} = [\frac{4R^2 M_{eqz}}{L}\omega^2 \cos 2\theta + 0.05P_i(\theta)A]R(\sin\theta + \frac{RL\sin 2\theta}{2L^2 - R^2\sin^2\theta}) \tag{2.34}$$

2.3.3 Pitch Excitation Moment

Pitch excitation torque is commonly considered to be caused by the unbalanced inertia force for an inline four-cylinder engine. The excitation torques can be obtained from the amplitudes of inertia forces due to each cylinder, and the distances between each cylinder center to the center of gravity of the engine parallel to the crankshaft [66]. This relationship is shown in Figure 2.7, where F_f and F_{re} are the support forces from the front and rear engine mounts. The total pitch excitation torque is the resultant of the torque due to each cylinder. The firing order for a four-cylinder engine is usually chosen as 1-3-4-2. The inertia forces due to each cylinder are considered together with the corresponding phase in accordance with the known firing order. The analysis of the pitch excitation torque thus involves consideration of inertia forces due to each cylinder. The inertia force generated from the cylinder #1, where the force is directed downward, is computed from Equation (2.8):

$$F_1^{\downarrow} = Rm_{eq}\omega^2(\cos\theta + \frac{R}{L}\cos 2\theta) \tag{2.35}$$

The inertia force due to cylinder #3, directed upward, is derived in a similar manner, as:

$$F_3^{\uparrow} = F_{1(\theta+\pi)} = Rm_{eq}\omega^2(\frac{R}{L}\cos 2\theta - \cos\theta) \tag{2.36}$$

The inertia force due to cylinders #4 and #2, directed downward and upward, respectively, are given by:

$$F_4^{\downarrow} = F_{1(\theta+2\pi)} = Rm_{eq}\omega^2(\cos\theta + \frac{R}{L}\cos 2\theta) \tag{2.37}$$

$$F_2^{\uparrow} = F_{1(\theta+3\pi)} = Rm_{eq}\omega^2(\frac{R}{L}\cos 2\theta - \cos\theta) \tag{2.38}$$

In the above equations, F_1, F_2, F_3 and F_4 are the inertia forces generated from the four cylinders respectively. The superscript arrow represents the direction of the inertia force as either upward or downward.

In order to simplify the calculations, it is assumed that the c.g. is located at the central axis of the fourth cylinder [63]. The total pitch excitation torque from the inertia forces is thus computed from:

$$M_{ey} = -3d_cF_1 + 2d_cF_2 + F_3d_c \tag{2.39}$$

where M_{ey} is the pitch excitation torque acting on the engine, and d_c is the distance between the center lines of two adjoining cylinders.

Upon substituting for inertia forces due to individual cylinders from Equation (2.35) to (2.37), the pitch moment excitation is derived as:

$$M_{ey} = -6d_cRm_{eq}\omega^2\cos\theta \tag{2.40}$$

The above formulation for the pitch excitation agrees with that reported in [66], although this reported study utilizes a different approach based on total inertia forces as shown in Equation (2.11).

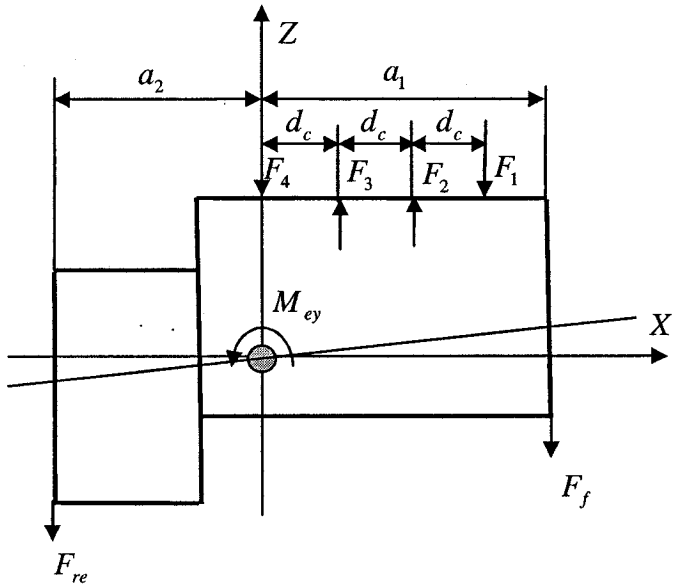

Figure 2.7: Force analysis of engine pitch motion.

2.4 Gas Pressure

The analysis of the roll excitation necessitates characterization of the gas pressure, as it is evident from Equation (2.34). The gas pressure is known to vary considerably depending on the engine and cylinder sizes, injection system, and various thermal factors. The characterization of the gas pressure variation is thus a relatively complex task. Many studies have attempted to characterize the variations in the gas pressure in the cylinders through measurements [10-12,26]. The reported results reveal considerable differences that are attributable to different engines and cylinder designs employed in different studies, and variation in the test conditions. It is thus vital to characterize the gas pressure variation for a particular engine under consideration, and typical operating conditions.

The majority of the studies on vibration analyses of engines and engine mounts either do not consider the variations in the gas pressure or consider an idealized gas pressure force in terms of selected harmonics [7, 9]. It has been reported that the predicted vibration amplitudes can only serve as estimates [11]. The gas pressure variations within the cylinders need to be determined under different operating speeds and load conditions by installing a pressure transducer inside the combustion chamber. In this study, the data reported by Minghui et al. [27], for a four–cylinder diesel engine is considered to describe the gas pressure by discretized values as a function of the crank angle.

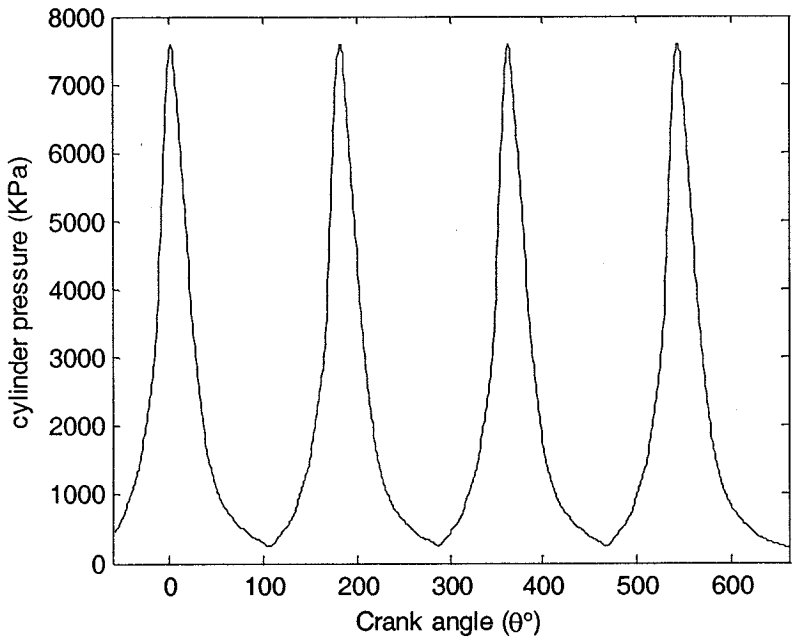

Figure 2.8: variations in the cylinders pressure of a four cylinder engine.

Figure 2.8 illustrates the measured variations in the cylinder pressure corresponding to the crankshaft rotating speed of 3000rpm, which is considered as the optimal operating condition [27]. The measured data was discretized and fitted by an interpolation approach. The result will be applied as inputs in the simulation of engine mount system in Chapter 5.

2.5 Summary

In this chapter, the engine as a vibration source is analyzed on the basis of kinematics and dynamics of its components and the gas pressure variation. The engine model is formulated for the purpose of evaluating the engine excitation force along the vertical direction, and roll and pitch moments. The unbalanced inertia force caused by engine reciprocating and rotating parts is analyzed to derive the vertical component of the excitation force in the engine mounting system. The net torque, generated from net force produced by the gas pressure and inertia forces, is derived using the geometry relationship. The variation in the gas pressure is characterized on the basis of the data reported in a published study. The measured pressure is characterized as a function of the crankshaft angle, and is expressed in the time domain to compute the roll moment excitation. The excitation forces and moments derived in this chapter are applied to the total engine mount model in the subsequent chapters.

CHAPTER 3

MODELING OF RUBBER & HYDRAULIC MOUNT

3.1 General

Besides supporting the static weight of the engine and restraining it from large movements, the primary function of the engine mount is to isolate the vehicle structure from the engine disturbance forces. An IC engine, especially the popular four-cylinder engine, is a highly vibro-active unit and the attenuation of its vibration is required over a broad frequency band up to 200 Hz. The growing trend for lighter car bodies and more powerful engines imposes more complex requirements for engine mounts in terms of their noise and vibration isolation performance. A vast number of engine mounts have been developed to enhance the noise and vibration isolation performance. These include the passive, semi-active and active engine mounts [33-50]. The rubber and hydraulic mounts are commonly applied in the modern automobile designs [29-31]. Even though semi-active and active mounts have achieved successful applications with enhanced performances, the high cost and complex maintenance associated with such mounts prohibits their general applications [50-51, 54-55]. The passive rubber and hydraulic mounts thus remain the common and meritorious choice.

In this chapter, the elastomeric and hydraulic engine mounts are considered for model development and analyses. The nonlinear static and dynamic properties of both, the elastomeric and hydraulic mounts, are described and systematically applied to develop the analytical models for analyzing their vibration isolation performance.

3.2 Characterization of a elastomeric Mount

The elastomeric mounts are most commonly used in the engine mounting systems due to their low cost and more or less maintenance free design. The visco-elastic properties of such mounts strongly depend upon the material and the geometric properties of the elastomer. The elastomeric mounts in general yield nonlinear force-deflection characteristics, and light damping. The design of such mounts involves appropriate considerations of the static load supported by a mount and the nature of disturbance forces (magnitude and frequency contents) arising from the engine. Figure 3.1 illustrates a schematic of a bush type rubber mount proposed for applications in the automobile engines. The geometry of the engine mount was proposed to satisfy the stiffness requirements for typical automobile engines [31].

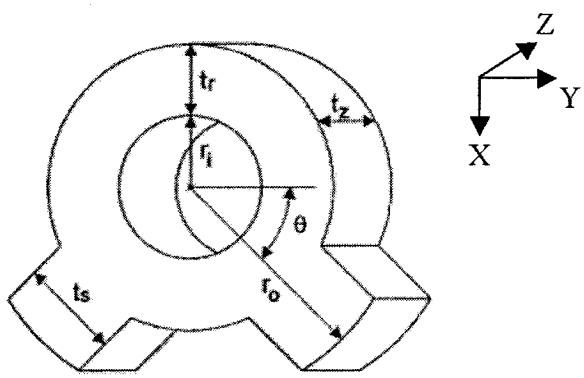

Figure 3.1: Schematic diagram of bush type engine mounts [31].

The proposed rubber mount exhibits highly nonlinear force deflection properties and is chosen for vibration isolation performance analysis, when considered either as a single mount or as a multiple mount arrangement within the total engine-mount system. The mount is considered to be loaded along the x-axis. The force-deflection data, described in

[31], are used to describe the mount force as a polynomial function in deflection along the x-axis, such that:

$$F_k = k_1 x + k_2 x^2 + k_3 x^3 \tag{3.1}$$

where, F_k is the static force developed by the mount due to deflection x, and k_1, k_2 and k_3 are stiffness coefficients.

For the given force-deflection data [31], the stiffness coefficients are identified as: $k_1 = 160N/mm$, $k_2 = -24N/mm^2$ and $k_3 = 1.4N/mm^3$. Figure 3.2 illustrates a comparison of the force-deflection characteristics derived from the polynomial function with the measured data. The polynomial model yields reasonably good representation of the measured data, except in the vicinity of $x = -5mm$ and $x = 15mm$, where the mount stiffness changes significantly. The force-deflection characteristics reveal low spring constant in the vicinity of the operating point, to be determined from the static load supported by the mount. This property would yield improved vibration isolation at frequencies of predominant engine vibration. The mount also exhibits strongly stiffening and softening properties under high magnitude deflections in compression and extension, respectively.

It should be noted that an engine mounting system employs a combination of three to four mounts to support the engine load and to provide the isolation from the engine disturbance forces. The distribution of the static engine load in the mounts would thus affect the static deflection of each mount and thus the stiffness near the static equilibrium or the operating point.

For a single equivalent mount, the static deflection of the mount can be derived upon solving the polynomial function, described in Equation (3.1), such that:

$$F_{st} = k_1 x_{st} + k_2 x_{st}^2 + k_3 x_{st}^3 \tag{3.2}$$

For a typical engine mass of 139.5 kg [67], the above model yields a static deflection, $x_{st} = 0.014m$.

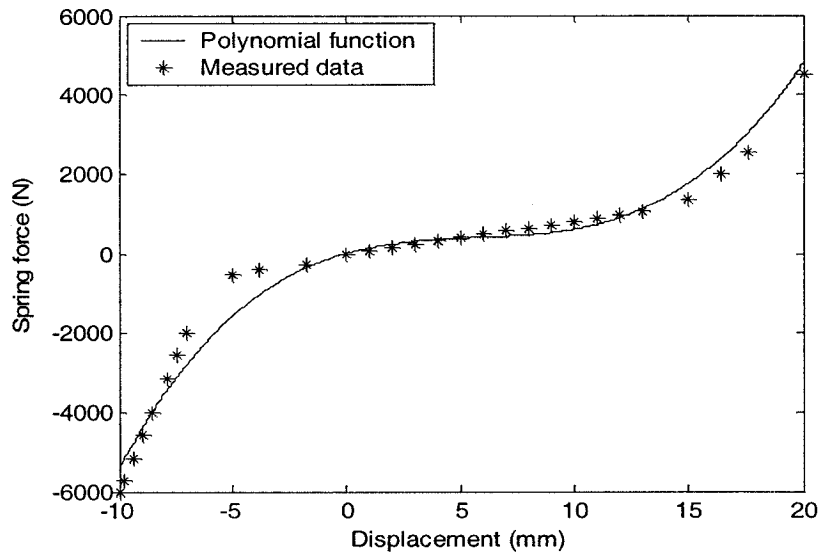

Figure 3.2: Comparison of force-displacement characteristics of the elastomeric mount, derived from the polynomial function, with the measured data [31].

3.3 Dynamic Properties –SDOF analysis

The dynamic properties of the elastomeric mount could be conveniently evaluated through consideration of a single degree-of-freedom (DOF) system, as illustrated in Figure 3.3. In the model, the mass m represents the engine mass supported by the mount, and the nonlinear stiffness and damping coefficients are represented by $k(x)$ and c, respectively. The dynamic response of the engine mount may be conveniently derived under base excitation of harmonic nature, $x_1(t) = X_1 \sin \omega t$. The equation of motion for the engine mass, constrained to move along the x-axis alone, can be expressed as:

$$m\ddot{x}_2 = F_k + F_c - mg \tag{3.3}$$

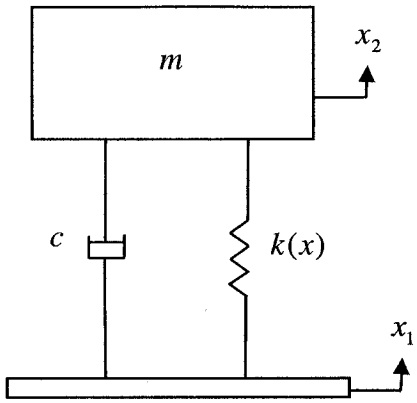

Figure 3.3: A single-DOF engine mount model.

where F_k and F_c are the stiffness and damping forces due to the rubber mount, x_2 is the engine mass displacement and g is acceleration due to gravity. Defining the relative motion across the mount, $x = x_1 - x_2 + x_{st}$, and applying the nonlinear force model of the mount, defined in Equation (3.1), the mass acceleration can be expressed as

$$\ddot{x}_2 = \frac{1}{m}(k_1 x + k_2 x^2 + k_3 x^3 + F_c - mg) \tag{3.4}$$

Assuming linear damping due to the mount, the damping force of the rubber mount is expressed as $F_c = c\dot{x}$, where c is the viscous damping coefficient. Figure 3.4, as an example, illustrates the time-histories of the engine mass displacement, velocity and acceleration, when subject to 1mm excitation at the base ($X_1 = 1$ mm) at a frequency of 10 Hz. A damping coefficient of $1000 Ns/m$ is assumed for the analysis. The results show asymmetric displacement and acceleration responses due to nonlinear mount stiffness. The displacement and acceleration response amplitudes are larger in compression, when compared to those in extension. This is attributed to differences in hardening and softening force-displacement characteristics, as shown in Figure 3.2.

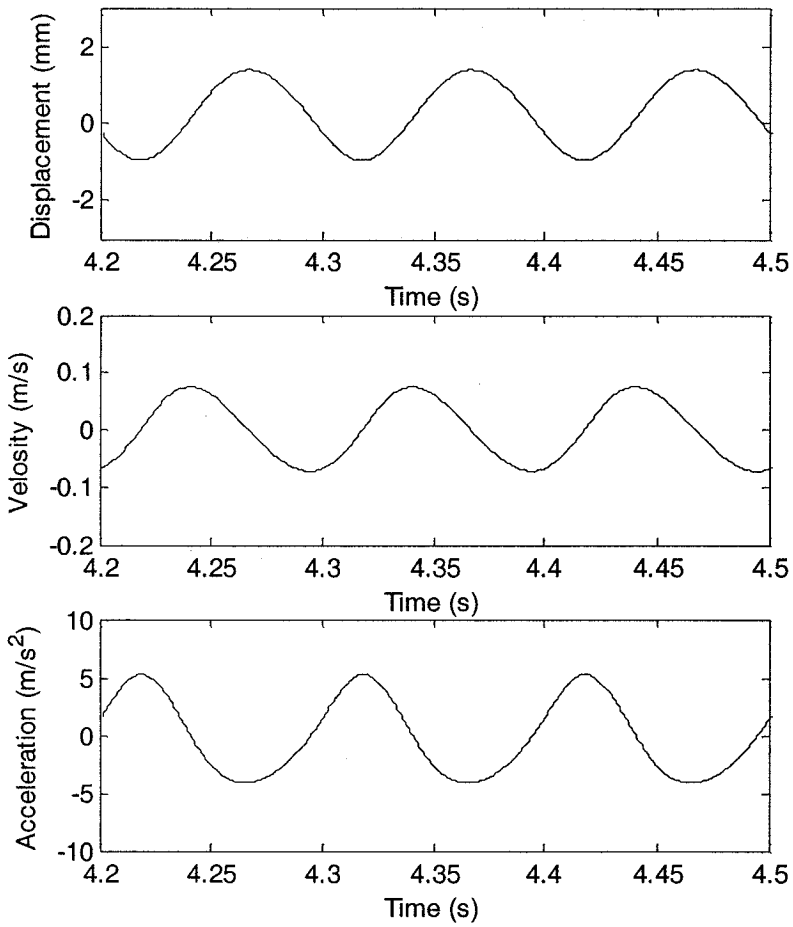

Figure 3.4: Time histories of displacement, velocity and acceleration responses of the engine mass, derived from the single-DOF model subject to harmonic excitation at 10 Hz.

Transmitted Force

The performance characteristics of the engine mount can be better assessed in terms of the force transmitted to the chassis. A simple single-DOF model may be employed to study the fundamental force-transmission characteristics of the nonlinear elastomeric mount, as illustrated in Figure 3.5. Let $F_0(t)$ represent the unbalance force arising from the engine, as described in Chapter 2. $F_T(t)$ represents the force transmitted to the chassis,

which is assumed to be fixed. The governing equation of motion for the engine mass can be expressed as:

$$m\ddot{x}_2 = F_0 + mg - F_k - F_c \tag{3.5}$$

where $F_k = k_1(x_2 + x_{st}) + k_2(x_2 + x_{st})^2 + k_3(x_2 + x_{st})^3$ and $F_c = c\dot{x}_2$.

The total force transmitted to the chassis structure, can be expressed as:

$$F_T = F_k + F_c - mg \tag{3.6}$$

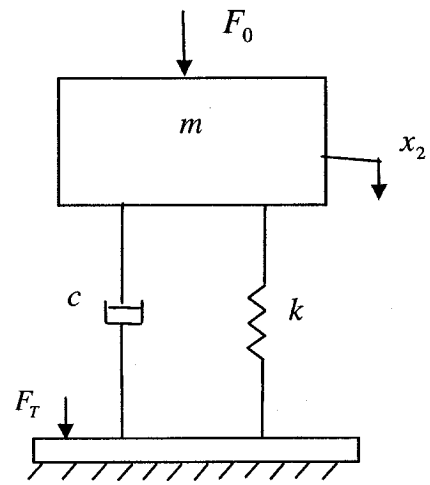

Figure 3.5: Single-DOF representation of the engine mass and mount subject to unbalance excitation force.

In the above formulation, the unbalance inertial force, expressed in Equation (2.11), is applied as the excitation force. The magnitudes of the transmitted force play an important role in the vibration analysis of the chassis structure. Owing to the nonlinear behavior, as evident in Figure 3.4, the force transmission of the mount can be effectively evaluated in terms of the root mean square (RMS) value of the force. The RMS value of transmitted force F_T is defined as:

$$F_{Trms} = \sqrt{\frac{1}{T_1}\int_0^{T_1} F_T^2(t)dt} \tag{3.7}$$

where T_1 is the observation period, and F_{Trms} is the RMS force corresponding to frequency. The RMS value of the transmitted force may also be estimated from the discrete values of the force, such that:

$$F_{Trms} = \sqrt{\frac{1}{n}\sum_{i=1}^{n} F_T{}^2(i)} \tag{3.8}$$

where n is the number of force data points used to calculate the RMS value, and i refers to discrete value of the time. The RMS value of the excitation force can also be computed in a similar manner:

$$F_{0rms}(f) = \sqrt{\frac{1}{n}\sum_{i=1}^{n} F_0{}^2(i)} \tag{3.9}$$

The force transmissibility T of an engine mount is then described as the ratio of the RMS value of the transmitted force to that of the unbalance excitation force at each frequency:

$$T(f) = \frac{F_{Trms}(f)}{F_{0rms}(f)} \tag{3.10}$$

The excitation force described in Equation (2.11), is a second harmonic force, which implies that the excitation predominantly occurs at a frequency f_e, which is twice the frequency f_s corresponding to the engine speed:

$$f_e = 2f_s = \frac{n_s}{30} \tag{3.11}$$

where n_s is the engine speed.

Equation (3.5) is solved under excitation arising from the engine unbalance force F_0, described in Equation (2.11), while the engine speed is varied from 100 to 6000 rpm in increments of 100 rpm. The unbalance excitation force is computed using a crankshaft radius (R) of 0.0337 m, a connecting rod length (L) of 0.1285m and equivalent mass (m_{eq}) of 0.7kg, while the total engine mass is held the same as 139.5 kg. Figure 3.6 illustrates the RMS values of the engine mass displacement, velocity and acceleration responses as a function of the engine rpm. The RMS values of the excitation and transmitted forces, together with the force transmissibility, are presented in Figure 3.7.

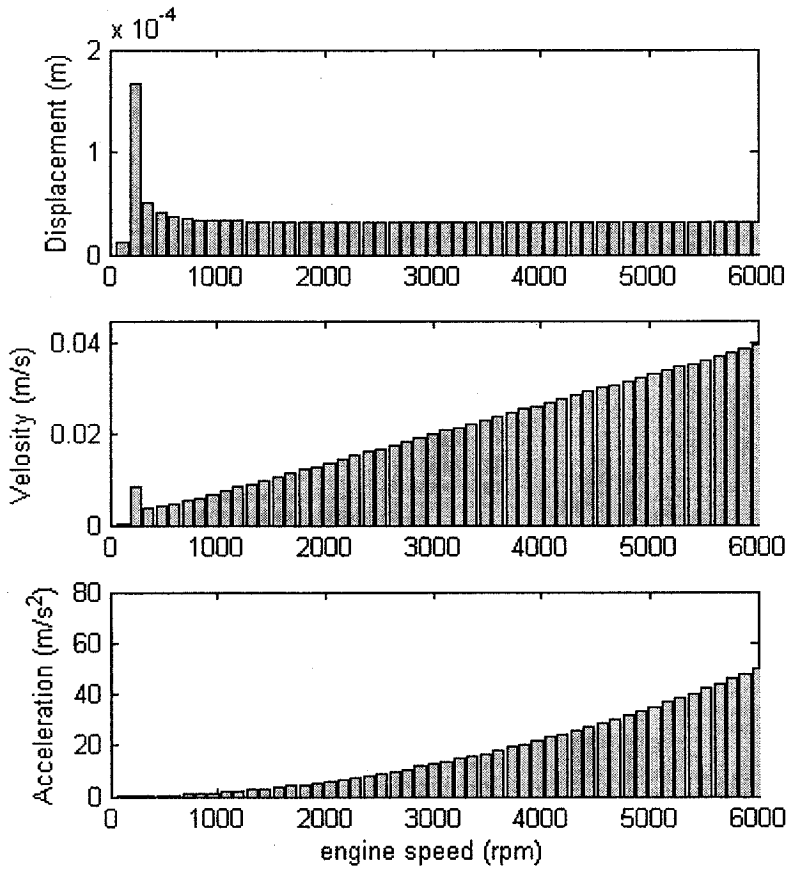

Figure 3.6: RMS displacement, velocity and acceleration responses of the engine mass as a function of the engine speed.

The results show peak values of the engine mass displacement and transmitted force near 210 rpm, which corresponds to excitation frequency of 7 Hz and the resonance of the elastomeric mount. The force transmissibility corresponding to this speed approaches as high as 4.6, suggesting higher degree of vibration and force transmission to the chassis. The engine mount, however, provides effective attenuation of force at speeds above 300 rpm, while the RMS acceleration of the engine mass approaches significantly higher levels at higher rpm.

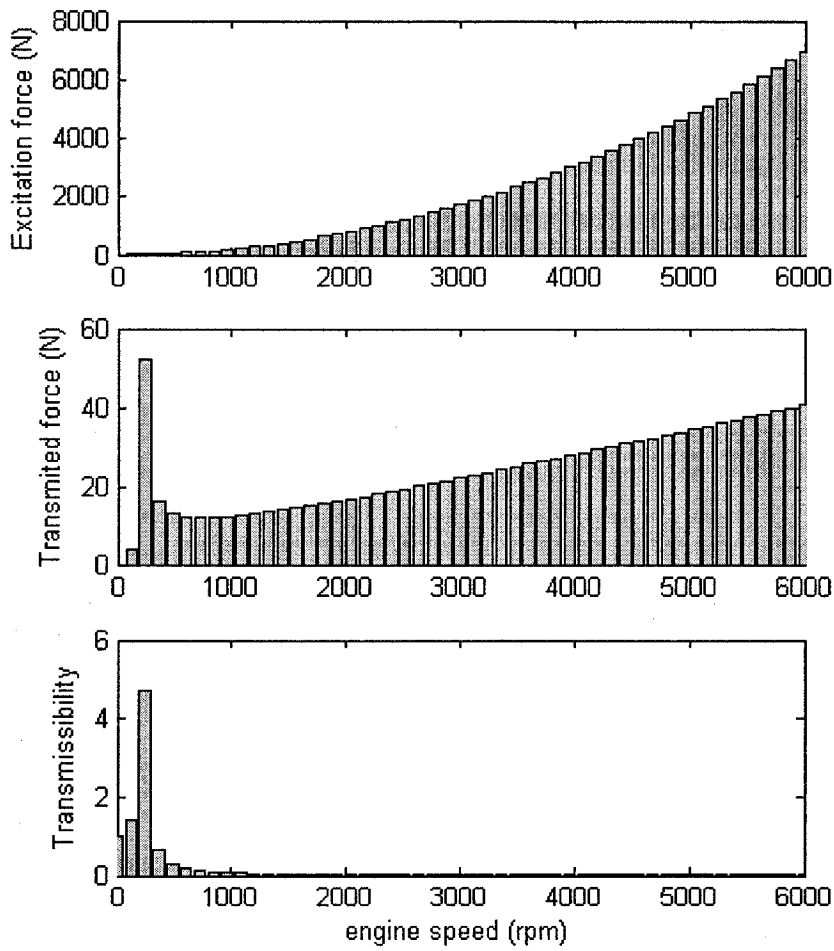

Figure 3.7: RMS excitation and transmitted forces, and force transmissibility as a function of the engine speed.

3.4 Characterization of a Hydraulic Engine Mount

Although elastomeric mounts serve as simple and low cost means to achieve attenuation of vibration and transmitted force, their performance is limited due to fixed stiffness characteristics and light damping property of the elastomer. Alternatively, a number of hydraulic engine mounts have been developed to realize higher damping and variable stiffness properties [35-37, 40-42]. Such mounts with flexible chambers are known to represent a fundamental improvement over the conventional elastomer mounts [42]. Hydraulic mounts can offer high damping under large motions induced by engine shake and low dynamic stiffness [8]. Moreover, the flexible chambers coupled with flow modulations through an orifice or damper valve can offer variable stiffness and damping properties, as opposed to the rubber mounts, which exhibit static and dynamic properties practically invariant with the excitation amplitude and frequency over a wide frequency range. It has been suggested that despite their variable properties, the hydraulic mounts are less effective in isolating forces and motion in the high frequency range [42].

3.4.1 Development of the Analytical Model

The damping properties of a hydraulic mount mostly derive from hydraulic flows through an orifice. The hydraulic flows within a mount may occur through short or relatively long orifices. The short orifice mounts are considered desirable due to their simple and compact construction [41]. Moreover, such mounts do not employ any moving parts. A simple passive hydraulic mount comprising a short orifice and compliant chambers is thus considered for the analysis. Figure 3.8 illustrates a schematic of such a mount. The mount comprises two hydraulic chambers, coupled through a short

cylindrical orifice. Both the upper and lower chambers are made of flexible rubber material to permit the flows from one chamber to the other and to provide the desired flexibility of the total mount. The flows to and from the chambers, and thus the damping property depends upon the geometry of the orifice. The top chamber consists of elastic material such as rubber, shaped like a conical frustum. An analytical model of the mount is developed assuming incompressible fluid, and identical cross-sectional areas of the top and bottom chamber projections. The flow through the orifice is assumed to be of turbulent nature, which does not seem to be amenable to accurate analysis. Therefore, a lumped-parameter modeling approach is considered to be more appropriate for representing the dynamic responses of the hydraulic mount [37]. The rubber material of the top chamber of the hydraulic mount serves as the spring to support the engine load and to act as an isolator. It also acts as a piston, and therefore the need for moving parts, as required for a rigid wall orifice damper, is eliminated. The bottom chamber of the mount is often designed with relatively higher compliance and acts as a reservoir for the fluid. The application of an external excitation causes the deformations of the top chamber, which causes the fluid to flow through the orifice to produce a damping effect. The upper and lower chambers of the mount are typically filled with a glycol fluid mixture of anti-freeze and distilled water due to its relatively low sensitivity to temperature variations.

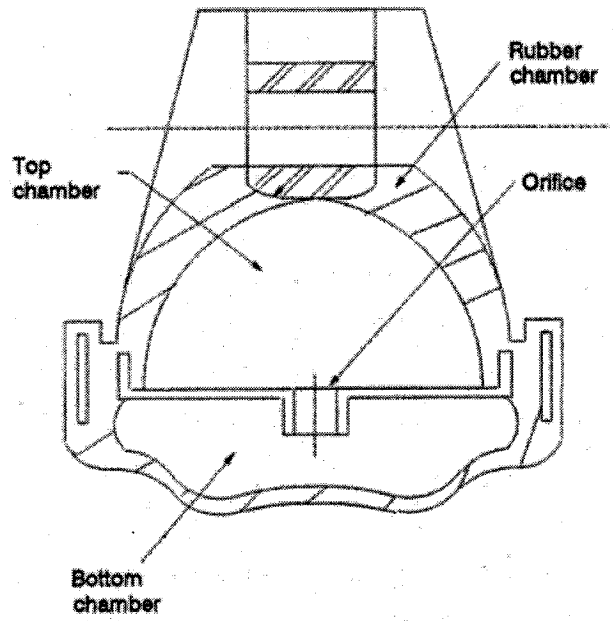

Figure 3.8: Schematic diagram of an orifice type hydraulic mount with flexible chambers [41].

In the model formulation, the fundamental equation of continuity is considered to determine the fluid flow characteristics. Fluid flow through the orifice Q_0, top chamber pressure P_T, bottom chamber pressure P_B, piston area A_{TP} and orifice diameter D_0, are considered as the primary variables for the mathematical formulation. The flow through the short orifice can be related to the pressure differential across the orifice in the following manner:

$$Q_0 = A_0 C_D \sqrt{\frac{2|P_T(t) - P_B(t)|}{\rho}} \operatorname{sgn}(P_B - P_T) \tag{3.12}$$

where C_D is the discharge coefficient for the orifice and the 'sgn' function determines the flow direction, where a positive flow refers to the flow from the bottom to the upper chamber. A_0 is the short orifice area, and P_T and P_B are the pressure states in the top and bottom chambers, respectively, The discharge coefficient C_D is a function of the orifice

diameter D_0 and the Reynolds number R_e of the flow. It has been shown that the C_D can assume values ranging from 0.13 up to 0.816, depending primarily on the Reynolds number [77]:

$$R_e = \frac{\rho Q_0 D_0}{\mu A_0} \tag{3.13}$$

where μ is the kinematic viscosity of the fluid.

The effective chamber compliance may be defined as the increase in the chamber volume per unit rise in the chamber pressure [41], such that:

$$C_v = \frac{dV}{dP} \tag{3.14}$$

The compliance of the rubber chamber is known to be considerably higher than that of the fluid. The fluid is thus assumed to be incompressible. The compliance properties of the chambers however may vary in either linear or nonlinear manner. Two different compliance models are thus formulated under static as well as dynamic loading.

3.4.2 Static Equilibrium

The hydraulic pressure developed within the two chambers under the application of a static load depends on the static mass, spring stiffness of the rubber, chamber compliance and equivalent piston area of the damper. Since linear and nonlinear compliances are considered for the investigation, two sets of equations will govern the static equilibrium condition of the mount.

Linear Chamber Compliance

Assuming that the pressure variations in a particular chamber occur as a linear function of the volume change, caused by a static deflection, the top and bottom chamber pressures, P_T and P_B , can be written as:

$$P_T(t) = \Delta V_T(t) / C_{VT} + P_{AT} \tag{3.15}$$

$$P_B(t) = \Delta V_B(t) / C_{VB} + P_{AT} \tag{3.16}$$

where, ΔV_T , ΔV_B are the volume changes of the top and bottom chambers, respectively, due to an increase in the fluid pressure or application of a static load. C_{VT} and C_{VB} are constants representing the linear compliance of the top and bottom chambers, respectively, and P_{AT} is the atmospheric pressure.

In static equilibrium the fluid pressures in the top and bottom chambers approach the static pressure, P_{ST} , such that:

$$P_T = P_B = P_{ST} \tag{3.17}$$

Equations (3.15) to (3.17) yield following relationship between the compliance and volume change of the top and bottom chambers:

$$V_{BST} = V_{TST} C_{VB} / C_{VT} \tag{3.18}$$

where V_{TST} and V_{BST} are the volume changes of the top and bottom chambers, respectively, under a static load.

Based on the assumption that the projected cross-sectional areas of the top and bottom chambers are equal, the static load is given by:

$$F_{ST} = K_{ST} X_{ST} + A_{TP} (P_{ST} - P_{AT}) \tag{3.19}$$

where K_{ST} and X_{ST} are the constant stiffness coefficient of the rubber material and static deflection of the mount, and A_{TP} is the projected area of the top chamber, which is identical to that of the bottom chamber A_{BP}.

The definition of the chamber compliance, given in Equation (3.14), yields following relationships between the static volume and change in the top chamber pressure:

$$C_{VT} = V_{TST} / (P_{ST} - P_{AT}) \tag{3.20}$$

$$P_{ST} - P_{AT} = V_{TST} / C_{VT} \tag{3.21}$$

Furthermore, the static deflection of the mount can be obtained from the total change in the chambers volume, as:

$$X_{ST} = -(V_{TST} + V_{BST}) / A_{TP} \tag{3.22}$$

Upon substituting for V_{BST} from Equation (3.18), the static deflection may be expressed as a function of the linear compliance ratio and static volume of the top chamber alone:

$$X_{ST} = -(1 + C_{VB} / C_{VT}) V_{TST} / A_{TP} \tag{3.23}$$

Equations (3.19), (3.21) and (3.23) yield the following expression for the static force:

$$F_{ST} = K_{ST}(1 + C_{VB} / C_{VT}) V_{TST} / A_{TP} + A_{TP}(V_{TST} / C_{VT}) \tag{3.24}$$

Equation (3.24) can be solved for a given preload to compute the volume change of the top chamber (V_{TST}) caused by the pressure change from initial atmospheric pressure to static pressure. The application of volume change in equation (3.15) would then yield the static pressure P_{ST}. The volume change of the bottom chamber caused by pressure change from atmospheric pressure to static pressure V_{BST}, can be derived from Equation (3.18). The static deflection of the mount is then computed from equation (3.23).

Equations (3.15) to (3.24) are solved for static load of mg and diameter of top chamber projection (D_1) of 70 mm. The solutions resulted in $V_{TST} = 1.0347cc$, $V_{TST} = 10.347cc$, $P_{ST} = 204.77kPa$ and $X_{ST} = -0.003m$.

It should be noted that the top chamber volume change V_{TST} is positive, when a compressive static load is applied and negative during expansion. The static pressure P_{ST} and volume change of the bottom chamber V_{BST} also remain positive, when the bottom chamber is expanded. Both these parameters do not approach negative values. Table 3.1 summarizes the parameters used in the analysis of the linear compliance model, as reported in [41].

Table 3.1: Simulation parameters of the hydraulic mount with linear compliance

$D_1(mm)$	$D_0(mm)$	$m(kg)$	$A_{TP}(m^2)$
70.0	4.5	125	0.00385
$C_{VT}(m^5/N)$	$C_{VB}(m^5/N)$	$K_{ST}(kN/m)$	$P_{AT}(kPa)$
1×10^{-11}	1×10^{-10}	200	101.3

Figure 3.9 shows the variations of the top and bottom chambers volume changes, and the static pressure increment as a function of the static load. The figure also illustrates the static deflection of the mount under varying static loads. It is apparent that volume change primarily occurs in the bottom chamber, which is attributed to its high compliance, as evident in Table 3.1. Owing to the linear compliance, the static deflection and pressure increase linearly with the static load, while effective stiffness of the mount is considerably larger than that of the rubber material (K_{ST}).

Nonlinear Chamber Compliance

It has been reported that the top and bottom chambers of a hydraulic mount exhibit nonlinear compliant properties [37, 40-42]. Kim [37] performed experiments to characterize the chamber pressures and the corresponding changes in top and bottom chamber volumes under different static loads. The study revealed nonlinear variations in the static chamber pressures with varying chamber volume. The experimental data was used to characterize the chamber pressures by regression functions in volume decrements, expressed as:

$$P_T = P_{AT} + \sum_{i=1}^{3} C_{Ti} \Delta V_T^{\alpha_i} \quad ; \text{for } \Delta V_T > 0 \tag{3.25}$$

$$P_B = P_{AT} + \sum_{i=1}^{3} C_{Bi} \Delta V_B^{\beta_i} \quad ; \text{for } \Delta V_B > 0 \tag{3.26}$$

where C_{Ti} and C_{Bi} are the regression coefficients for the top and bottom chambers pressures, ΔV_T and ΔV_B define the change in volume with respect to the free volume, and α_i and β_i are the corresponding exponents. The volume change in the above regression models is expressed in cm^3, while the pressure is in kPa.

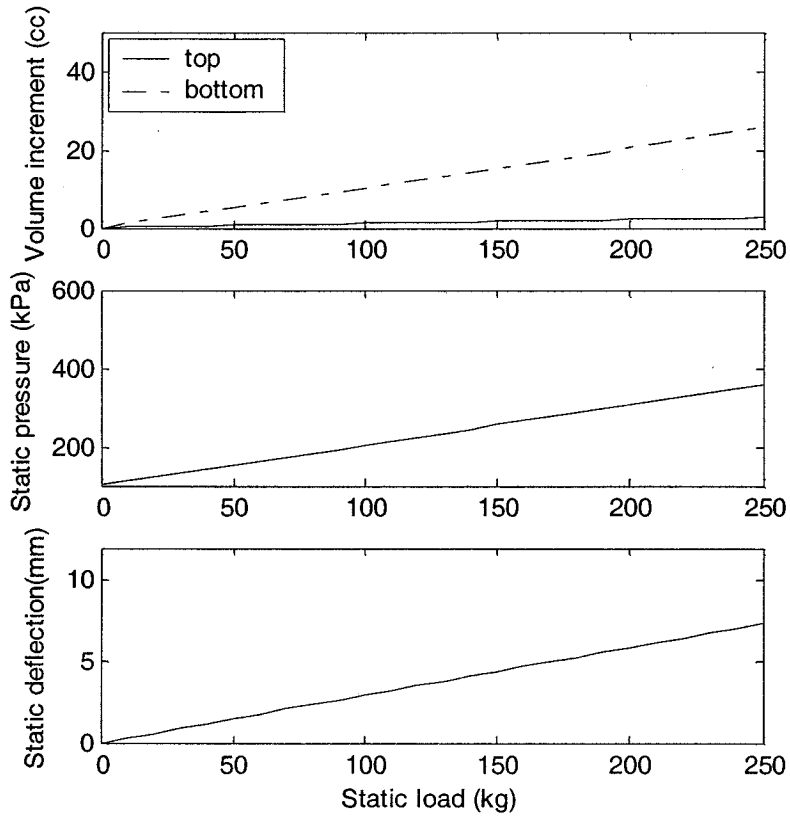

Figure 3.9: Effect of static load on the variations in the chamber volumes and pressures, and static deflection of the mount.

The high compliance of the bottom chamber does not permit its pressure to drop below the atmospheric pressure. Furthermore, the high compliance yields considerably larger change in the bottom chamber volume when compared to that of the top chamber. This is also evident in Figure 3.9, when linear compliant properties are considered. The static deflection of the mount is mostly attributed to the volume change of the bottom chamber. This is also attributed to high compliance of the bottom chamber, such that $V_{TST} << V_{BST}$ and $V_{BST} \cong V_{BST} + V_{TST}$. The static deflection of the mount is thus mostly related to the volume change of the lower compliant chamber.

$$X_{ST} \cong -V_{BST} / A_{TP} \tag{3.27}$$

Considering that the pressures in both chambers approach identical values under static equilibrium, the static force of the mount can be derived from Equation (3.19), the static pressure of top and bottom chambers can be derived from Equations (3.25) and (3.26) such that:

$$F_{ST} = K_{ST}(\frac{V_{BST}}{A_{TP}}) + A_{TP}\left[\sum_{i=1}^{3} C_{Bi} V_{BST}^{\beta_i}\right] \tag{3.28}$$

$$P_{ST} = P_{AT} + \sum_{i=1}^{3} C_{Ti} V_{TST}^{\alpha_i} = P_{AT} + \sum_{i=1}^{3} C_{Bi} V_{BST}^{\beta_i} \tag{3.29}$$

Table 3.2 summarizes the regression coefficients of the hydraulic mount (Figure 3.8) with $D_1 = 70\,\text{mm}$. Application of static load due to assumed engine mass of 125kg and solution of above equations yields:

$V_{TST} = 0.7561 cm^3$, $V_{BST} = 22.8512 cm^3$, $P_{ST} = 111.3547 kPa$ and $X_{ST} = -0.0061 m$.

Table 3.2: Regression model constants of the hydraulic mount [41]

Constant	Value	Constant	Value
C_{T1}	-6.4	C_{B1}	5.26×10^{-3}
C_{T2}	29.2	C_{B2}	-8.9×10^{-8}
C_{T3}	0	C_{B3}	1.41×10^{-8}
α_1	1.0	β_1	2.5
α_2	7/6	β_2	6.0
α_3	0	β_3	6.5

Equations (3.27) to (3.29) are solved, using the regression models constants, summarizes in Table 3.2, to determine the variations in the volume changes in the top and bottom chambers, the static equilibrium pressure and the mount deflection, under varying static loads. Figure 3.10 illustrates the variations in the volume change, and static

pressure and deflection, as a function of the static load. The results show nonlinear variations in both the volumes and the pressure with the static load. The results also show that the bottom chamber volume change is significantly larger than that of the top chamber, while the static pressure tends to grow rapidly under loads above 200kg. A comparison of Figure 3.9 and Figure 3.10 reveals relatively higher static stiffness of the mount, when nonlinear compliant properties are considered. This is mostly attributed to the progressively hardening property of the compliant hydraulic chambers, as evident from the static pressure variations, the results shown in Figure 3.10 revealed good agreement, which is exactly the same with those presented in [41].

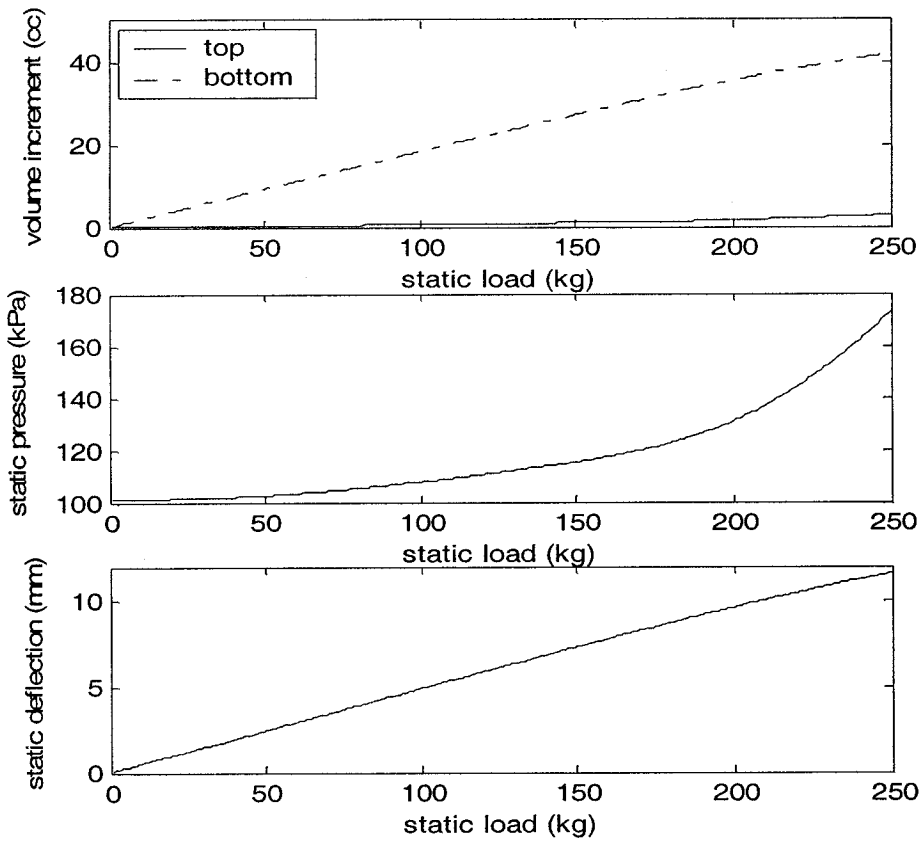

Figure 3.10: Effect of static load on the volume change, static pressure and static deflection responses of the mount with nonlinear compliant properties.

3.4.3 Dynamic Properties of Hydraulic Mount

The dynamic properties of the hydraulic mount with either linear or nonlinear chamber compliance could be derived using a simple single-DOF model, as shown in Figure 3.11. In the model, m represents the engine mass and F is the total force developed by the mount when subjected to a base excitation $x_1(t)$. The total force developed by a hydraulic mount comprises a restoring force component due to the elastomeric material, damping force due to the elastomeric material, and a component due to pressure change, which also incorporates the variable damping force attributed to orifice flows. The equation of motion for the single-DOF isolator is derived on the basis of Equation (3.19) and linear damping coefficient of the rubber material, such that:

$$m\ddot{x}_2 = -Kx - C\dot{x} + A_{TP}(P_T - P_{AT}) - mg \tag{3.30}$$

where $x = x_2 - x_1 - x_{st}$, C is linear damping coefficient of the rubber material and K is the constant dynamic stiffness coefficient of the rubber material, which is larger than the static value (K_{ST}) applied in Equation (3.19) [41].

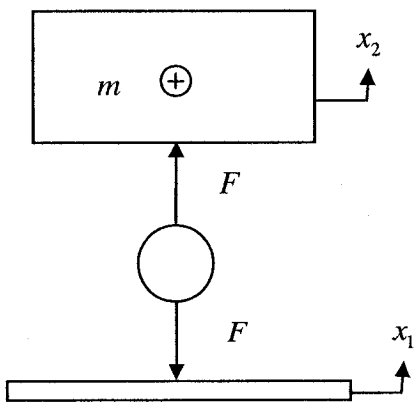

Figure 3.11: A single-DOF model of the engine mass supported on a hydraulic mount.

The equation of motion of the isolator may be rewritten with respect to the static equilibrium, in the following form:

$$m\ddot{x}_2 = -K(x_2 - x_1) - C(\dot{x}_2 - \dot{x}_1) - A_{TP}(P_{ST} - P_T) \tag{3.31}$$

where P_{ST} is the fluid pressure in the top and bottom chambers corresponding to static equilibrium position.

Both the static and instantaneous top chamber pressures are derived from the hydraulic flow through the orifice, and compliant properties of the chambers. Assuming linear compliance of the top and bottom chambers, the flow through the orifice can be derived from the continuity equation:

$$Q_0 = A_{TP}\dot{x} + C_{VT}\dot{P}_T \tag{3.32}$$

The flow through the orifice also determines the variations in the bottom chamber fluid pressure, such that:

$$Q_0 = -C_{VB}\dot{P}_B \tag{3.33}$$

Assuming turbulent flow through the orifice, the flow rate Q_0 is expressed in Equation (3.12). The fluid pressures in the top and bottom chambers can thus be expressed by the following expression for linear compliant properties:

$$C_{VT}\dot{P}_T = -A_{TP}\dot{x} + A_0 C_D \sqrt{\frac{2|P_T - P_B|}{\rho}}\,\mathrm{sgn}(P_B - P_T) \tag{3.34}$$

$$C_{VB}\dot{P}_B = -A_0 C_D \sqrt{\frac{2|P_T - P_B|}{\rho}}\,\mathrm{sgn}(P_B - P_T) \tag{3.35}$$

The dynamic force developed by the mount and thus the force transmitted to the base can be simply derived from:

$$F_T = -K(x_2 - x_1) - C(\dot{x}_2 - \dot{x}_1) - A_{TP}(P_{ST} - P_T) \tag{3.36}$$

The instantaneous hydraulic damping force is obtained by:

$$F_D = A_{TP}(P_T - P_B) \tag{3.37}$$

The variations in the top and bottom chamber pressures are evaluated for harmonic base excitation ($X_1 = 1mm$ and $f = 10Hz$), and the parameters described in Table 3.3. The fluid density ρ is taken as $1059kg/m^3$, while the discharge coefficient as 0.806. Equations (3.31), (3.34) and (3.35) are solved with the initial conditions: $P_T(0) = P_B(0) = P_{ST}$; $\Delta V_T(0) = V_{TST}$; $\Delta V_B(0) = V_{BST}$.

Table 3.3: Parameters of hydraulic mount with linear compliance (dynamic)

$D_1(mm)$	$D_0(mm)$	$m(kg)$	$K(kN/m)$	$C(Ns/m)$
70.0	4.5	125	280	180
$C_{VT}(m^5/N)$	$C_{VB}(m^5/N)$	C_D	$\rho(kg/m^3)$	$P_{AT}(kPa)$
1×10^{-11}	1×10^{-10}	0.806	1059	101.3

Figure 3.12 illustrates the time histories of fluid pressure in the top and bottom chambers and the mass deflection. The results show that the chambers pressures vary around the static pressure, $P_{ST} = 204.77kPa$. The steady-state amplitude of the top chamber pressure is considerably larger than that of the bottom chamber pressure, which is attributed to the large compliance of the bottom chamber. The peak magnitude of the engine mass displacement with linear compliance of the hydraulic mount approaches near 2 mm, suggesting amplification of the base excitation at 10 Hz.

Nonlinear Chamber Compliance

In the nonlinear case, compliances are assumed to be a function of chamber pressure and chamber volume change. The top chamber pressure P_T is a function of the top chamber volume change as expressed in Equation (3.25) with regression coefficients

shown in Table 3.2. When $\Delta V_T > 0$, the top chamber is compressed. Here, P_T is measured in Pascal and ΔV_T is measured in cubic millimeter. When $\Delta V_T < 0$, the top chamber is under extension and it is in a state of vacuum. It is assumed that an amount of entrapped air V_A contributes to the volume change following the Boyle's Law [55]

$$P_T = P_{AT} V_A / V_{TA} \text{ , for } \Delta V_T < 0 \tag{3.38}$$

$$V_{TA} = V_A + |\Delta V_T| \tag{3.39}$$

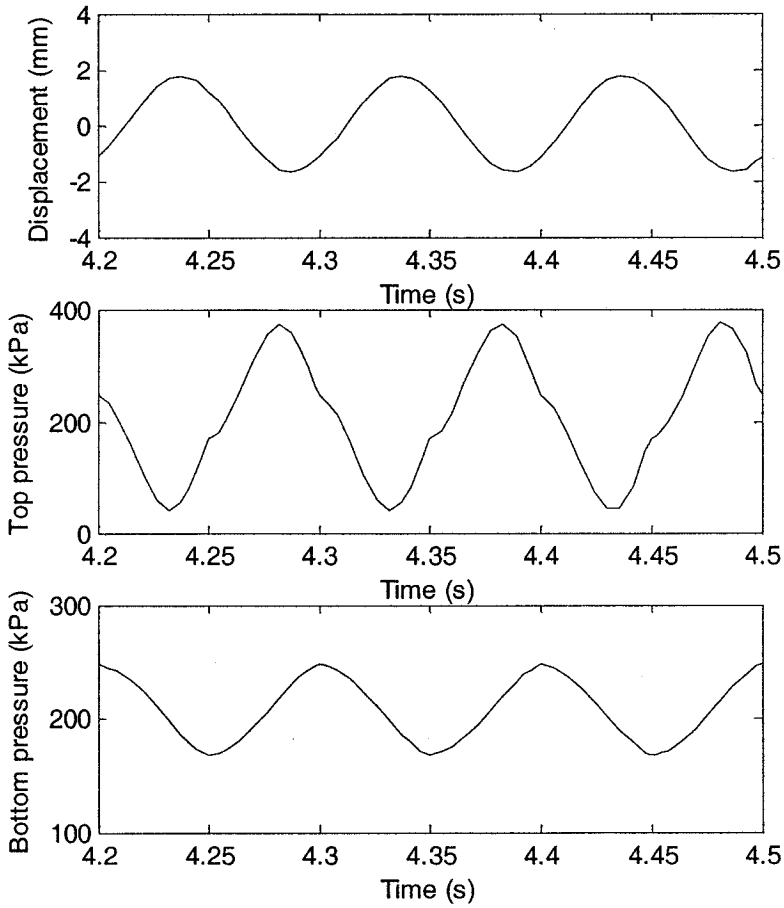

Figure 3.12: Variation in the mass displacement and chambers pressures of the hydraulic mount derived using a linear compliance model, under harmonic base excitation.

It has been suggested that a negative compliance of the top element exists when $P_T < P_{AT}$. A definite amount of air, initially dissolved in the glycol fluid, may be released and the glycol fluid may become a mixture of liquid and gas phases. Furthermore, in extreme cases, a vaporous cavitation may occur. The characterization of dynamic behavior of the mount incorporating all of the above-mentioned phenomena, expressed by a negative compliance is quite complex to measure and not amenable to accurate analytical predictions. Alternatively, the negative compliance in the model may be considered by assuming that a small amount of air volume V_A is initially entrapped within the top portion of the upper chamber. The volume change in the top chamber is thus given by:

$$\Delta V_T = V_{TO} + V_{TST} - A_{TP}(x_2 - x_1) \tag{3.40}$$

where

$$V_{TO} = \int_0^t Q_O dt \tag{3.41}$$

is the total volume of the fluid transferred from one chamber to the other chamber. The flow through the orifice is given by Equation (3.12). In Equation (3.12), the bottom chamber pressure P_B is derived as a function of the volume change ΔV_B, as expressed in Equation (3.26) with regression coefficients shown in Table 3.2. Moreover, the total volume change of the bottom chamber can be expressed as:

$$\Delta V_B = -V_{TO} + V_{BST} \tag{3.42}$$

The instantaneous fluid pressures within the top and bottom chambers (P_T and P_B), and the mass displacement x_2 can be computed by solving Equations (3.25), (3.26), (3.31), and (3.38) to (3.42). The results are obtained in both time and frequency domains

to demonstrate the damping characteristics in terms of orifice flow, chamber pressure, damping force and transmitted force. The results are described in the following subsections.

Characteristics of the mount

The analytical model of the nonlinear hydraulic mount is solved using the parameters summarized in Table 3.4, representing the dynamic and static properties, respectively. The above parameters are selected from the data reported in [37], in order to compare the results with the available experimental data. Table 3.5 lists the static deflection, the corresponding pressure and changes in fluid volumes of the top (V_{TST}) and bottom (V_{BST}) chambers, as derived from the solutions. These results show very good agreement with the experimental data reported in [37]. Figure 3.13 illustrates the variation in the top and bottom chambers volumes, as derived from Equations (3.25) and (3.26), (3.38) and (3.39). The results clearly show that the bottom chamber volume undergoes significant variations, while the corresponding change in the top chamber volume is quite small. This is attributed to relatively higher compliance of the bottom chamber, as observed from Figure 3.10 for the mount with linear compliance. Furthermore, the bottom chamber volume asymptotically approaches a steady value under higher fluid pressures. The static equilibrium response results are also shown in Figure 3.13, which show good agreement with the simulation results presented in Table 3.5.

Table 3.4: Simulation Parameters of hydraulic mount with nonlinear compliance(dynamic)

$D_1(mm)$	$D_0(mm)$	$m(kg)$	$K(kN/m)$	$C(Ns/m)$
80.0	5.9	122.5	280	180
$\mu(N.s/m^2)$	$V_A(cc)$	C_D	$\rho(kg/m^3)$	$P_{AT}(kPa)$
3.6×10^{-6}	4.5	0.806	1059	101.3

Table 3.5: Static equilibrium responses of hydraulic mount with nonlinear compliance

$D_1(mm)$	$V_{TST}(cc)$	$V_{BST}(cc)$	$P_{ST}(kPa)$	$X_{ST}(m)$
80.0	0.9850	28.2441	116.4597	-0.0058

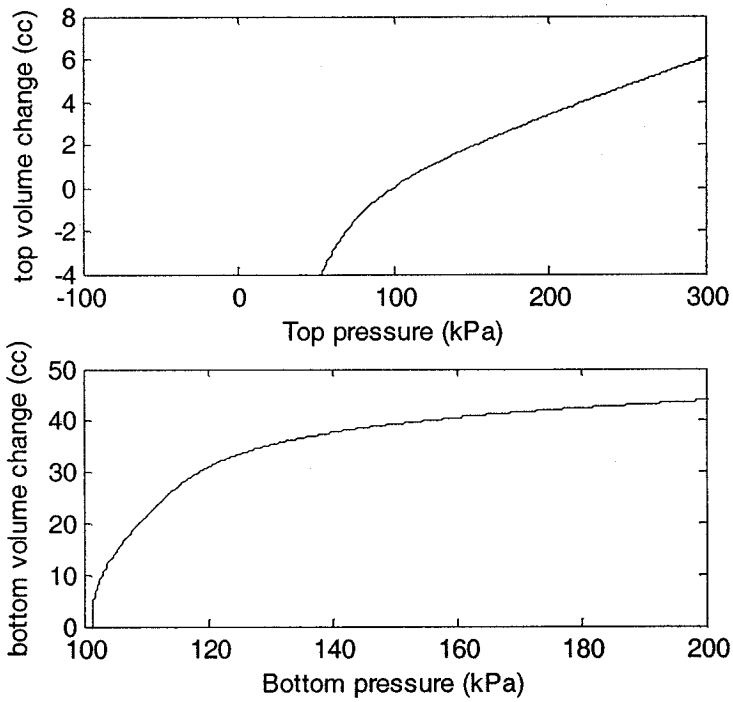

Figure 3.13: Increments in the top and bottom chamber volumes with fluid pressure, illustrating nonlinear compliance.

The equations of motion derived for the hydraulic mount with nonlinear compliance are solved using Runge-Kutta ode45 algorithm to determine the dynamic responses. A hydraulic mount with two flow orifices of the same cross-section area, are considered to

reduce the effective damping and thus the transmitted force in the isolation region. Figure 3.14 illustrates the variations in the fluid pressure and changes in volume of the top and bottom chambers under application of a 0.5 mm harmonic excitation at selected frequencies, namely, 7, 10 and 20 Hz. Figure 3.15 illustrates the corresponding responses in terms of transmitted force, damping force, flow rate and Reynolds's number.

The results show asymmetric variations in the top and bottom chambers volumes and fluid pressures, which is attributed to nonlinear compliance of the chambers, and relatively high compliance of the bottom chamber. The fluid pressure in the top chamber approaches as low as 80kPa at an excitation at 10Hz. This subatmosphric pressure distribution for the mount agrees quite well with the experimentally obtained data for a long orifice hydraulic mount reported in [37]. The variations in the fluid pressure in the bottom chamber, however, are quite small due to high compliance of this chamber, while the pressure remains about the static pressure of 116.46kPa, with peak to peak difference of only 16kPa at 10 Hz. The results further show a decreasing tendency for the peak to peak difference as the frequency increases from 10 Hz to 20 Hz. Figure 3.15 illustrates the relationship of the transmitted force and the hydraulic force with the flow rate and the Reynolds number. The peak magnitude of the transmitted force is observed to be quite high, as evident in Figure 3.15. The results further show peak transmitted force occurs at an excitation at 10 Hz, signifying the resonant frequency. The Reynold's number of the flow approaches high values suggesting turbulent flow during majority of the vibration cycle.

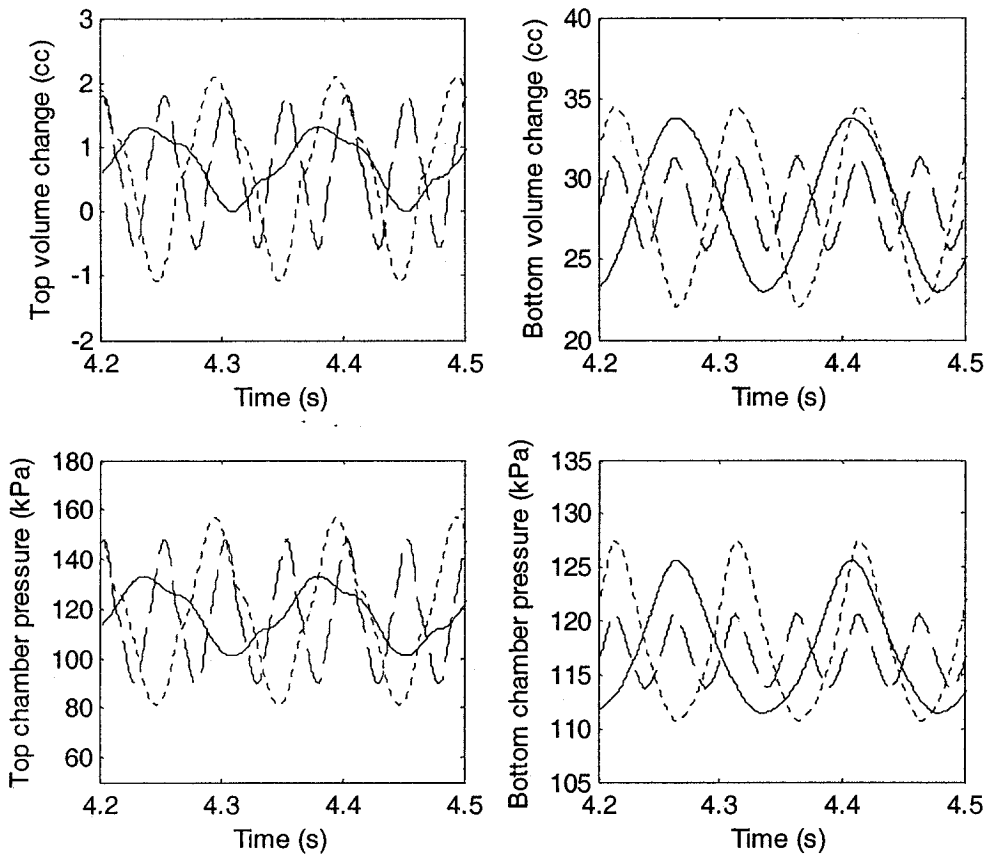

Figure 3.14: Variation in the pressure & volume of the two chambers under different frequency excitation.

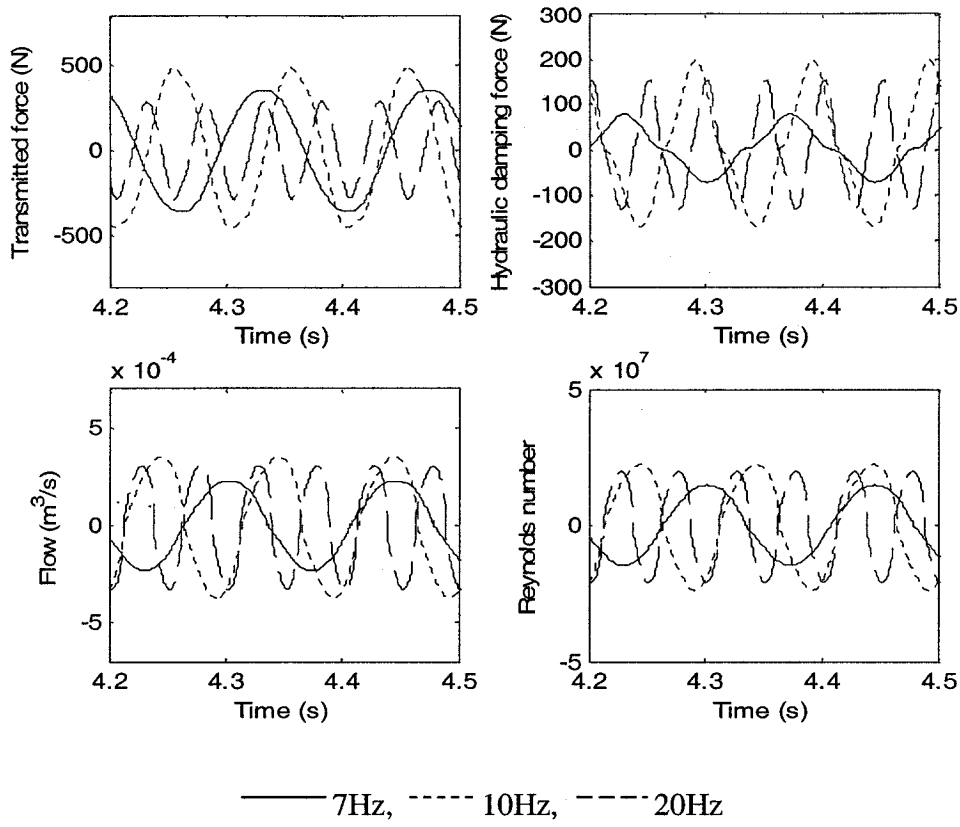

Figure 3.15: Variation in the transmitted force and hydraulic damping force, flow & Reynolds number under harmonic displacement excitations at different frequencies.

Figures 3.16 and 3.17 illustrate the effect of excitation amplitude on the response characteristics of the hydraulic mount with two short orifices, while the frequency of excitation is held as 15 Hz. The simulation results are obtained under 0.5, 0.7 and 1.0 mm displacement amplitudes. The peak volume changes and fluid pressures increase considerably with an increase in the excitation amplitude, as evident in Figure 3.16. It should be noted that the top and bottom volume changes are referred to their respective free volumes. Figure 3.17 shows that the transmitted force and the damping force increase as the excitation amplitude increases from 0.5mm to 0.7mm, and then to 1.0mm. Both the hydraulic and transmitted forces tend to be more asymmetric and non-harmonic

as the excitation amplitude increases. The asymmetric behaviour is more apparent from the hydraulic force. This tendency is attributed to the orifice flows and the nonlinear compliance. In addition, the results presented in Figure 3.17 show the variations in the flow rate and the Reynolds number. A positive flow rate refers to the flow from the bottom chamber to the top chamber, while a negative rate relates to the opposite flow. The asymmetric orifice flow rate characteristics, attributed to lower compliance of the lower chamber, show nonsinusoidal behavior due to turbulent orifice flows. For each cycle, the magnitude of maximum flow is higher in reverse flow than in the forward flow and is asymmetry increases with increase in the excitation amplitude. The degree of asymmetry in the maximum and minimum pressure corresponding to compression and extension also increases with the excitation amplitude, which is attributed to the asymmetric compliance of the top and bottom chambers.

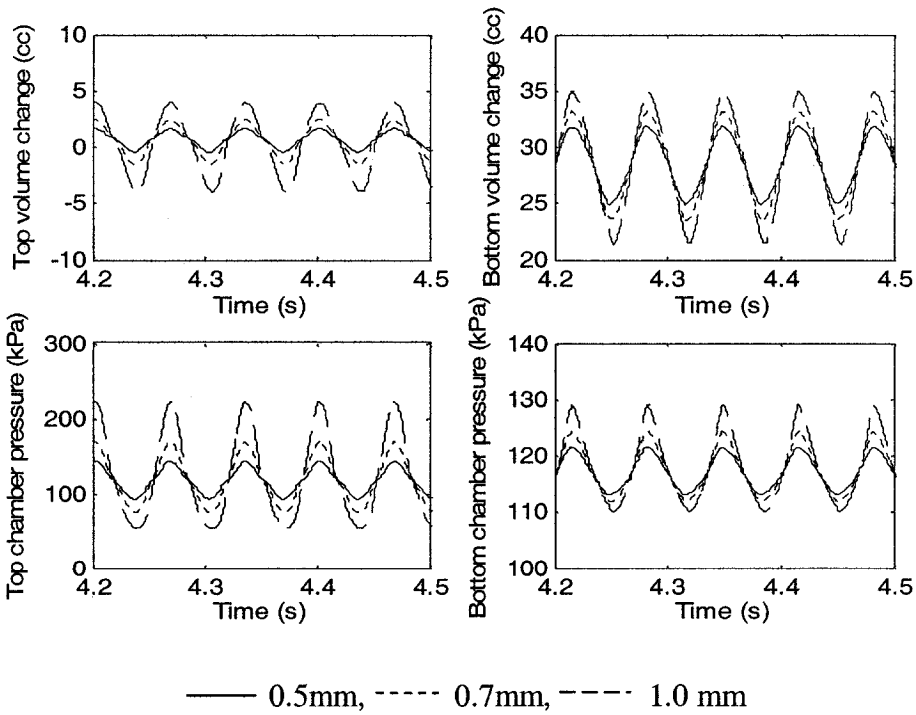

Figure 3.16: Variations in the pressure & volume of the two chambers under harmonic displacement excitations at different amplitudes.

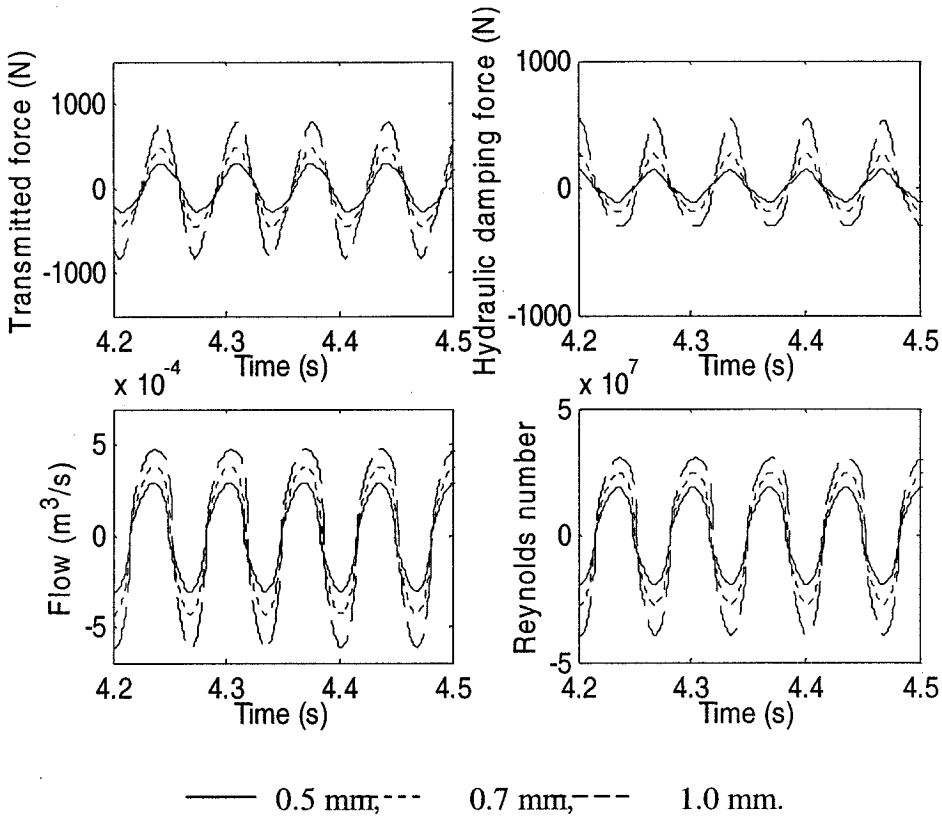

Figure 3.17: Variation in the transmitted and hydraulic forces, flow & Reynolds under harmonic displacement excitations at different amplitudes.

3.5 Summary

Two typical engine mounts consisting of elastomeric and hydraulic flows are analytically modeled and analyzed in this chapter. The characteristics of the rubber and hydraulic mounts were identified from their static and dynamic properties. Linear and nonlinear chamber compliances of the hydraulic mount were considered in the modeling and simulations.

The force-deflection characteristics of the nonlinear elastomeric mount are expressed by a third-order polynomial in deflection, while the model is formulated to study the transmitted force and vibration transmissibility under engine excitation and engine

unbalance force. From the simulation results, it is concluded that the resonance frequency is one-half of the natural frequency due to the influence of the second harmonic excitation force.

The hydraulic mount is modeled with flexible chambers through a short orifice, and the simulation results are applied to examine the model validity while assuming the single-DOF engine mounting system model. At static equilibrium, linear and nonlinear chamber compliances were employed to evaluate the static characteristics of the hydraulic mount. The influence of the static load on the static deflection, top and bottom chamber pressures and volume changes are demonstrated. The dynamic responses of hydraulic mount with linear and nonlinear compliances are also implemented in the time domain at selected excitation frequencies of 7, 10 and 20 Hz. The results suggested the presence of natural frequency close to 10 Hz at which the highest force is transmitted. The damping force tends to nonharmonic and highly asymmetric, while the degree of asymmetry increases with the increase in excitation frequency and amplitude due to the nonlinear compliance. Analytical models of the mounts are further applied in a total engine-mount system in the following chapter to study the performance behaviour of the coupled system.

CHAPTER 4

MODELING OF ENGINE MOUNTING SYSTEM

4.1 General

The performance characteristics of a vibration isolation mount rely upon its elastic and damping properties, and the load. The vast majority of studies on vibration isolation mounts have been performed assuming idealized single-DOF dynamics constrained along a single axis and subject to idealized vibration excitations [28, 32, 37, 42]. The automotive engines are invariably supported on 3 to 4 vibration isolation mounts and may cause vibration along the translational as well as rotational axes. Moreover, the mounts may be subjected to different static loads. The designs and assessments of engine mounts should thus be performed through analyses of the coupled engine-mounts system. The analyses based upon uncoupled single-DOF models can not provide the performance characteristics under vibration induced along multiple axes. A coupled engine-mounts system model permits for analyses under representative excitations arising from the unbalance due to the reciprocating components and gas forces, as described in section 2.2.

In this chapter, the coupled engine-mounts system is represented by a three-DOF dynamic system incorporating vertical, roll and pitch motions of the engine block. The purpose of a well-designed mounting system is to control the transmission of vibration caused by the firing pulses, inertial forces and the torques generated by the engine, to the vehicle chassis. The compliant characteristics of the engine mounts in the axial and shear directions cause the motions along all the three translation and rotational directions [7]. Therefore, the engine may induce forces and moments to the vehicle body in directions other than the vertical, roll and pitch axes as a result of the inherent imbalances in the

reciprocating/rotating masses. The proposed three-DOF model in this dissertation, however, is limited to the study of vibrations along the rotational direction of the driveline system and the pitch and bounce axes of the engine, which are known to be more significant [7, 9,16]. In particular, the typical nonlinear rubber and flexible chamber hydraulic mounts are applied in the three-DOF model of the engine mount system.

4.2 Model Development

The transmission and engine assembly is considered to be supported on three elastic mounts as schematically shown in Figure 4.1. Notations 'L' and 'R' represent the front left and right mounts. The figure shows the axis system with origin located at the mass center of the assembly, and two front mounts and a single rear mount. Figure 4.2 illustrates the model in the pitch plane. Each of the two front mounts is inclined in the roll plane with an angle α with respect to a horizontal axis, as shown in Figure 4.3, while the rear mount is supported centrally at the rear of the gearbox. The front mounts undergo axial and shear deformations, and the corresponding forces developed are shown in Figure 4.4.

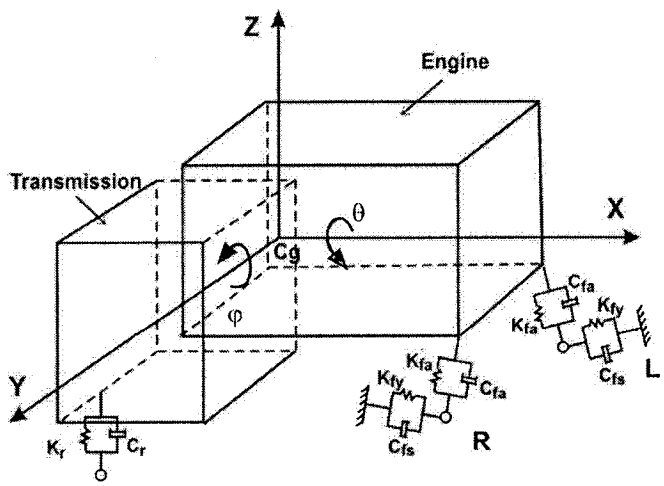

Figure 4.1: Schematic representation of the engine mounting system.

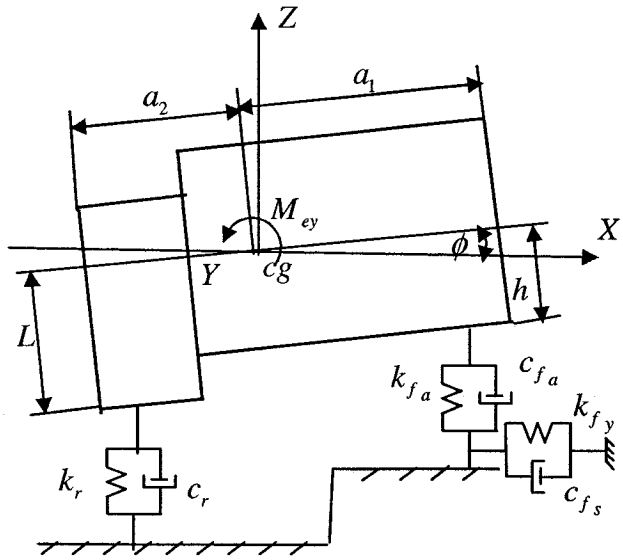

Figure 4.2: Pitch plane representation of the engine mounting system.

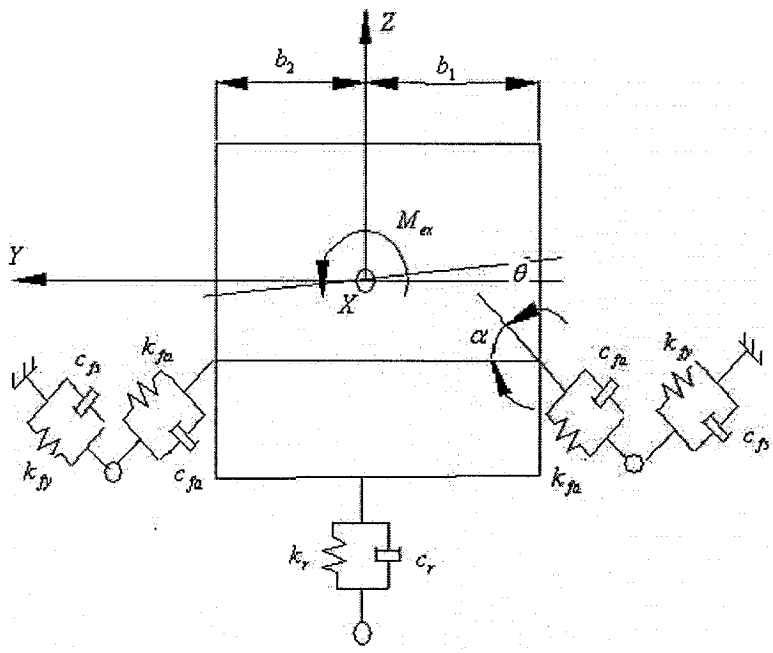

Figure 4.3: Roll plane representative of the engine mounting system model.

4.2.1 Force Analysis

The forces transmitted to the chassis due to the bounce, pitch and roll motions of the engine assembly can be studied using the model shown in Figures 4.1 to 4.3. The vertical, roll and pitch motions are defined with respect to the static equilibrium position and denoted as z, θ and φ, respectively. The static axial and shear forces of the rubber mounts are derived from the static deflections of the mounts. The dynamic forces and deflections caused by engine excitation force and moments, derived in Chapter 2 in Equations (2.11), (2.33) and (2.40), are further formulated. In Figure 4.4, the 'L', 'R', and 'Re' represent the front left, front right, and rear mounts, respectively. $z_{st}, \theta_{st}, \varphi_{st}$ represent the static deflections of the mass center in bounce, roll and pitch directions, respectively. The total deflections of the mounts along their axial direction can be expressed as:

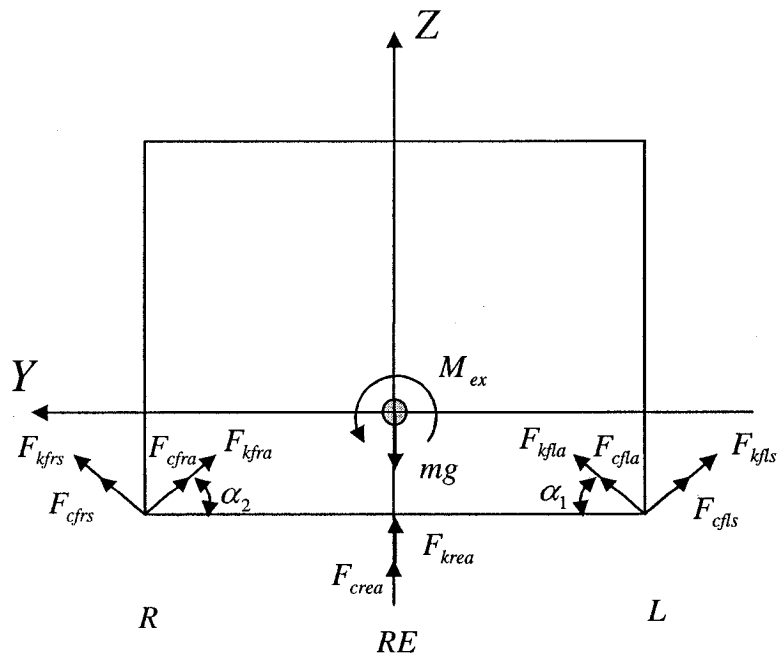

Figure 4.4: Axial and shear forces (front view).

$$\delta_{fla} = [(z_{st} - a_1\varphi_{st} - b_1\theta_{st}) - (z + b_1\theta + a_1\varphi)]\sin\alpha_1 \tag{4.1}$$

$$\delta_{fra} = [(z_{st} - a_1\varphi_{st} + b_2\theta_{st}) - (z - b_2\theta + a_1\varphi)]\sin\alpha_2 \tag{4.2}$$

$$\delta_{rea} = z_{st} + a_2\varphi_{st} - (z - a_2\varphi) \tag{4.3}$$

where δ_{fla}, δ_{fra} and δ_{rea} are the axial deflections of the front-left, front-right and rear mounts, respectively. α_1, α_2 are the inclination angles of the front-left and right mounts, with respect to a horizontal axis, as shown in Figure 4.4. In a similar manner, the deflection along the shear axis for the left and right mounts can be expressed as:

$$\delta_{fls} = [(z_{st} - a_1\varphi_{st} - b_1\theta_{st}) - (z + b_1\theta + a_1\varphi)]\cos\alpha_1 \tag{4.4}$$

$$\delta_{frs} = [(z_{st} - a_1\varphi_{st} + b_2\theta_{st}) - (z - b_2\theta + a_1\varphi)]\cos\alpha_2 \tag{4.5}$$

$$\delta_{res} = 0 \tag{4.6}$$

where δ_{fls}, δ_{frs} and δ_{res} are the shear deflections of the front-left, front-right and rear mounts, respectively. The forces shown in Figure 4.4 utilize the subscripts '*fl*'and '*fr*' for the front-left and front-right mounts, and '*re*' for the rear mount. '*c*'and '*k*' refers to damping and spring constants, '*a*'for the axial force and '*s*' for the shear force.

4.3 Engine Mounting System Model with Nonlinear Elastomeric Mount

4.3.1 Determination of Static Deflection of Rubber Mount

The rubber mounts invariably yield nonlinear force-deflection characteristics, as described in section 3.2. The static deflections of the mounts are derived on the basis of the static load distribution and the nonlinear force-deflection relationship presented in

Equation (3.1). The loads shared by each mount are determined from the static equilibrium, which yields:

$$w_f = \frac{a_2 w}{a_1 + a_2} \text{ ; and } w_r = \frac{a_1 w}{a_1 + a_2} \tag{4.7}$$

$$w_{fl} = \frac{b_2 w_f}{b_1 + b_2} \text{ ; and } w_{fr} = \frac{b_1 w_f}{b_1 + b_2} \tag{4.8}$$

where w is the weight of the engine assembly, w_f and w_r are the loads shared by the front and rear mounts, and w_{fl} and w_{fr} are the loads shared by left- and right-front mounts, respectively. The constants a_1, a_2, b_1 and b_2 define the geometry, as illustrated in Figures 4.1 to 4.4.

Denoting the total load shared by the left-and right- front mounts by $\overline{F}_{fl}$ and $\overline{F}_{fr}$, the static forces could be related to the axial and shear forces developed by the elastic mounts, such that:

$$\overline{F}_{fj} = \overline{F}_{kfja} \sin\alpha_1 + \overline{F}_{kfjs} \cos\alpha_1 ; \; j = l, r \tag{4.9}$$

where $\overline{F}_{kfja}$ and $\overline{F}_{kfjs}$ are the static forces developed by the front mount ($j = l, r$) along the axial and shear directions, respectively. The axial force developed by the mount can be derived from the force-displacement relationship defined in Equation (3.1), such that:

$$\overline{F}_{kfja} = k_{f1}\overline{\delta}_{fja} + k_{f2}\overline{\delta}^2_{fja} + k_{f3}\overline{\delta}^3_{fja} ; \; j = l, r \tag{4.10}$$

where k_{f1}, k_{f2} and k_{f3} are the stiffness coefficients of the nonlinear elastic mount, and δ_{fja} is the axial deflection of mount j ($j = l, r$).

Considering that the engines are mostly installed in the roll plane, the static roll deflection can be negligible ($\theta_{st} = 0$), when identical front mounts are used under

symmetric load distribution in the roll plane. The static deflection of the mounts may thus be simplified to:

$$\overline{\delta}_{fla} = (z_{st} - a_1\varphi_{st})\sin\alpha_1$$

$$\overline{\delta}_{fra} = (z_{st} - a_1\varphi_{st})\sin\alpha_2 \tag{4.11}$$

The static forces developed by the front left and right mounts along the shear axis are:

$$\overline{F}_{kfls} = k_y\overline{\delta}_{fls} = k_y(z_{st} - a_1\varphi_{st})\cos\alpha_1$$

$$\overline{F}_{kfrs} = k_y\overline{\delta}_{frs} = k_y(z_{st} - a_1\varphi_{st})\cos\alpha_2 \tag{4.12}$$

where $\overline{\delta}_{fls}$ and $\overline{\delta}_{frs}$ are the static deflections in the shear direction for the left- and right-front mounts. Equations (4.7) to (4.12) yield the static force equilibrium for the front-left and front-right mounts, which are derived by assuming linear stiffness coefficient k_y, such that:

$$\frac{b_2}{b_1+b_2}\times\frac{a_2 w}{a_1+a_2} = k_{f1}(z_{st} - a_1\varphi_{st})\sin^2\alpha_1 + k_{f2}(z_{st} - a_1\varphi_{st})^2\sin^3\alpha_1 + k_{f3}(z_{st} - a_1\varphi_{st})^3\sin^4\alpha_1 + k_y(z_{st} - a_1\varphi_{st})\cos^2\alpha_1 \tag{4.13}$$

$$\frac{b_1}{b_1+b_2}\times\frac{a_2 w}{a_1+a_2} = k_{f1}(z_{st} - a_1\varphi_{st})\sin^2\alpha_2 + k_{f2}(z_{st} - a_1\varphi_{st})^2\sin^3\alpha_2 + k_{f3}(z_{st} - a_1\varphi_{st})^3\sin^4\alpha_2 + k_y(z_{st} - a_1\varphi_{st})\cos^2\alpha_2 \tag{4.14}$$

The static force equilibrium for the rear mount can also be derived in a similar manner. Denoting the effective vertical force as $\overline{F}_{re}$, and applying the nonlinear force-deflection relationship, yields:

$$\overline{F}_{re} = k_{r1}(z_{st} + a_2\varphi_{st}) + k_{r2}(z_{st} + a_2\varphi_{st})^2 + k_{r3}(z_{st} + a_2\varphi_{st})^3 = \frac{a_1 w}{a_1+a_2} \tag{4.15}$$

where k_{r1}, k_{r2} and k_{r3} are the stiffness coefficients of the rear mount. Assuming symmetrical mounting of the two front mounts ($\alpha_1 = \alpha_2 = \alpha$), the total vertical load supported by the front mounts can be expressed as:

$$k_{f3}A_1^3 \sin^4\alpha + k_{f2}A_1^2 \sin^3\alpha + k_{f1}A_1 \sin^2\alpha + kyA_1 \cos^2\alpha - \frac{a_2 mg}{2(a_1 + a_2)} = 0 \tag{4.16}$$

where m is the engine assembly mass, and $A_1 = z_{st} - a_1\varphi_{st}$, is the static deflection of the mount.

The total vertical force developed by the rear mount can also be expressed in a similar manner, by letting $A_2 = z_{st} + a_2\varphi_{st}$:

$$k_{r3}A_2^{\ 3} + k_{r2}A_2^2 + k_{r1}A_2 - \frac{a_1 mg}{a_1 + a_2} = 0 \tag{4.17}$$

The static deflections A_1 and A_2 of the front and rear mounts can be determined by solving for the roots of the polynomial equations (4.16) and (4.17), respectively. The vertical and pitch static deflections of the engine assembly, z_{st} and φ_{st}, are then obtained as:

$$z_{st} = \frac{a_1A_2 + a_2A_1}{a_1 + a_2} \text{ and } \varphi_{st} = \frac{A_2 - A_1}{a_1 + a_2} \tag{4.18}$$

4.3.2 Equations of Motion of the Engine-Mount System Model

The equations of motion for the coupled engine-mount system are formulated by applying Newton's second law of motion and by considering all the support forces, and the input excitation force and moments. The coupled differential equations of motion describing the vertical roll and pitch motion of the engine assembly are expressed as:

Vertical motion

$$m\ddot{z} = F_{flz} + F_{frz} + F_{rez} - mg + \sum_{j=1}^{m} F_{ezj} \tag{4.19}$$

Roll motion

$$I_x\ddot{\theta} = M_{flx} + M_{frx} + M_{rex} + \sum_{j=1}^{m} M_{exj} \tag{4.20}$$

Pitch motion

$$I_y\ddot{\varphi} = M_{fly} + M_{fry} + M_{rey} + \sum_{j=1}^{m} M_{eyj} \tag{4.21}$$

where I_x and I_y are the roll and pitch mass moments of inertia of the engine assembly about the mass center, respectively. F_{ez}, m_{ex} and m_{ey} define the vertical excitation force, and effective roll and pitch moment excitations, respectively. F_{flz}, F_{frz} and F_{rez} are the vertical components of the compression/extension forces developed by the front-left, front-right and rear mounts, respectively. The mount forces are derived from the dynamic deflections along the axial and shear directions, such that:

$$F_{flz} = (F_{kfla} + F_{cfla})\sin\alpha_1 + (F_{kfls} + F_{cfls})\cos\alpha_1 \tag{4.22}$$

$$F_{frz} = (F_{kfra} + F_{cfra})\sin\alpha_2 + (F_{kfrs} + F_{cfrs})\cos\alpha_2 \tag{4.23}$$

where the axial and shear elastic forces are derived from

$$F_{kfja} = k_{f1}\delta_{fja} + k_{f2}\delta_{fja}^2 + k_{f3}\delta_{fja}^3 \text{ and } F_{kfjs} = k_{fy}\delta_{fjs}\ ;\ j = l, r \tag{4.24}$$

δ_{fja} and δ_{fjs} in the above equations define the deflection of mount j ($j = l, r$) along the axial and shear axes, respectively, as defined in Equation (4.1), (4.2), (4.4) and (4.5). The damping forces developed by the mounts are derived assuming linear viscous damping, such that:

$$F_{cfja} = c_{fa}\dot{\delta}_{fja} \text{ and } F_{cfjs} = c_{fs}\dot{\delta}_{fjs}\ ;\ j = l, r \tag{4.25}$$

The vertical force developed by the rear mount, in a similar manner, is expressed as a combination of the nonlinear restoring force and linear dissipative force:

$$F_{rez} = F_{krea} + F_{crea} \tag{4.26}$$

where

$$F_{krea} = k_{r1}\delta_{rea} + k_{r2}\delta_{rea}^2 + k_{r3}\delta_{rea}^3 \tag{4.27}$$

$$F_{crea} = -c_{rea}(\dot{z} - a_2\dot{\varphi}) \tag{4.28}$$

In the above equations, δ_{rea} defines the deflection of the rear mount along the axial axis, as described in Equation (4.3). The terms M_{flx} , M_{frx} and M_{rex} in Equation (4.20) are the roll moments caused by the forces developed by the front and rear mounts, respectively. While the force due to the centrally located rear mounts does not yield a roll mount ($M_{rex} = 0$), the axial and shear forces developed by the front left and right mounts yield roll moment about the x-axis, expressed as:

$$M_{flx} = F_{flz}b_1 - F_{fly}h \text{ and } M_{frx} = -F_{frz}b_2 - F_{fry}h \tag{4.29}$$

where h is the height of the front left and right mount, and F_{fly} and F_{fry} are the lateral forces caused by the front left and right mounts along the y direction, given by:

$$F_{fly} = (F_{kfla} + F_{cfla})\cos\alpha_1 - (F_{kfls} + F_{cfls})\sin\alpha_1 \tag{4.30}$$

$$F_{fry} = -(F_{kfra} + F_{cfra})\cos\alpha_2 + (F_{kfrs} + F_{cfrs})\sin\alpha_2$$

The terms M_{fly} , M_{fry} and M_{rey} in Equation (4.21), in a similar manner describe the pitch moments caused by front and rear mount forces, given by:

$$M_{fly} = F_{flz}a_1,\ M_{fry} = F_{frz}a_1 \text{ and } M_{rey} = -F_{rez}a_2 \tag{4.31}$$

The roll and pitch moment excitation in Equations (4.20) and (4.21), $\sum_{j=1}^{m} M_{exj} = M_{ex}$ and $\sum_{j=1}^{m} M_{eyj} = M_{ey}$, are described in Equations (2.33) and (2.40), respectively.

4.4 Engine Mounting System Model with Flexible Chamber Hydraulic Mounts

4.4.1 Determination of Static Deflections of the Hydraulic Mounts

The engine mounting system with hydraulic mounts is also modeled as a three-DOF dynamic system, as illustrated in Figures 4.1 to 4.3, where nonlinear hydraulic mounts replace the rubber mounts. The forces developed by the hydraulic mounts depend upon the static equilibrium pressure and thus the static deflection. It is thus essential to determine the static deflections of the mounts in order to derive the total forces. The static vertical force developed by a mount comprises three components: (i) static axial force due to the compliance of the rubber material; (ii) the shear force due to compliance of the rubber material; and (iii) the hydraulic force.

The vertical component of forces developed by the front mounts can thus be expressed as:

$$\overline{F}_{fj} = (\overline{F}_{kfja} + \overline{F}_{hfj})\sin\alpha + \overline{F}_{kfjs}\cos\alpha\ ;\ j = l, r \tag{4.32}$$

where $\overline{F}_{kfja}$ and $\overline{F}_{kfjs}$ are the static axial and shear spring forces of the rubber material of mount j ($j = l, r$), and $\overline{F}_{hfj}$ is the static hydraulic force. Assuming linear compliance due to the rubber material, the axial force developed by the mount, $\overline{F}_{kfja}$, can be expressed as:

$$\overline{F}_{kfja} = k_{fa}\overline{\delta}_{fja}\ ;\ j = l, r \tag{4.33}$$

where k_{fa} is the constant stiffness coefficient of the rubber material along the axial direction and $\overline{\delta}_{fja}$ is the axial deflection of the mount, given by:

$$\overline{\delta}_{fja} = (z_{st} - a_1\varphi_{st})\sin\alpha \tag{4.34}$$

The shear force component due to compliant rubber material can be derived from the constant lateral stiffness k_{fy} and the deflection along the shear axis, $\overline{\delta}_{fjs}$, given by:

$$\overline{F}_{kfjs} = k_{fy}\overline{\delta}_{fjs} \tag{4.35}$$

where

$$\overline{\delta}_{fjs} = (z_{st} - a_1\varphi_{st})\cos\alpha \tag{4.36}$$

The hydraulic force component developed by a front mount is related to the static chamber pressure, P_{STF} and the effective area A_{TP}, as described in Equation (3.19). The hydraulic force developed by the front mount is given by:

$$\overline{F}_{hfj} = A_{TP}(P_{STF} - P_{AT}) \tag{4.37}$$

The static force equilibrium for the front-left and right mounts can thus be expressed as:

$$\begin{aligned}\frac{b_2}{b_1+b_2}\times\frac{a_2 w}{a_1+a_2} &= [k_{fa}(z_{st} - a_1\varphi_{st})\sin\alpha_1 + A_{TP}(P_{STF} - P_{AT})]\sin\alpha_1 \\ &+ k_{fy}(z_{st} - a_1\varphi_{st})\cos^2\alpha_1\end{aligned} \tag{4.38}$$

$$\begin{aligned}\frac{b_1}{b_1+b_2}\times\frac{a_2 w}{a_1+a_2} &= [k_{fa}(z_{st} - a_1\varphi_{st})\sin\alpha_2 + A_{TP}(P_{STF} - P_{AT})]\sin\alpha_2 \\ &+ k_{fy}(z_{st} - a_1\varphi_{st})\cos^2\alpha_2\end{aligned} \tag{4.39}$$

The static force equilibrium for the rear mount can also be derived in a similar manner, by considering negligible shear force component, such that:

$$\frac{a_1 w}{a_1 + a_2} = k_{rea}(z_{st} + a_2\varphi_{st}) + A_{TP}(P_{STR} - P_{AT}) \tag{4.40}$$

where k_{rea} is the stiffness of the rubber material, $\delta_{rea} = z_{st} + a_2\varphi_{st}$ is the static deflection of the rear mount, and P_{STR} is static chamber pressure of the rear mount.

4.4.2 Equations of Motion

The differential equations of motion for the three-DOF engine mount system with compliant hydraulic mounts are derived in a manner similar to that described in section 4.3. For linear compliant properties, the static forces developed by a mount are considered to offset the static load imposed on the mount. The equations of motion are thus derived upon consideration of the dynamic force components alone, while the displacement coordinates (z , θ and φ) refer to the static equilibrium position. The equations for the roll and pitch motions are thus identical to those expressed in Equations (4.20) and (4.21), respectively, where the moments occur due to forces developed by the hydraulic mounts. The equation for the vertical motion about the static equilibrium is simplified to:

$$m\ddot{z} = F_{flz} + F_{frz} + F_{rez} + \sum_{j=1}^{m} F_{ezj} \tag{4.41}$$

where F_{flz} , F_{frz} and F_{rez} are the vertical components of the forces developed by the front-left, front-right and rear hydraulic mounts, respectively.

The vertical force developed by the front mount comprises the components due to axial and shear forces (k_{fja} and k_{fjs} ; $j = l, r$) due to rubber material, hydraulic force (F_{hfj}) and the damping forces due to rubber material (F_{cfja} and F_{cfjs} ; $j = l, r$), such that:

$$F_{fjz} = (F_{kfja} + F_{cfja} + F_{hfj})\sin\alpha + (F_{kfjs} + F_{cfjs})\cos\alpha;\ j = l, r \tag{4.42}$$

where the components are derived from the constant stiffness and damping coefficient (k_{fa} and c_{hfa}) and the dynamic deflections, δ_{fja}, given by:

$$F_{kfja} = k_{fa}\delta_{fja} \text{ and } F_{cfja} = c_{hfa}\dot{\delta}_{fja};\ j = l, r \tag{4.43}$$

where

$$\delta_{fla} = (z + b_1\theta + a_1\varphi)\sin\alpha \text{ and } \delta_{fra} = (z - b_2\theta + a_1\varphi)\sin\alpha \tag{4.44}$$

The hydraulic force component is derived from the effective area of the top chamber and the instantaneous fluid pressure in the top chamber, P_{TFj} ($j = l, r$), such that

$$F_{hfj} = A_{TP}(P_{TFj} - P_{STF}) \tag{4.45}$$

The restoring and damping forces along the shear axis (F_{kfjs} and F_{cfjs}) are derived assuming constant stiffness and damping coefficients:

$$F_{kfjs} = k_{fy}\delta_{fjs} \text{ and } F_{cfjs} = c_{hfs}\dot{\delta}_{fjs};\ j = l, r \tag{4.46}$$

$$\delta_{fls} = (z + b_1\theta + a_1\varphi)\cos\alpha \text{ and } \delta_{frs} = (z - b_2\theta + a_1\varphi)\cos\alpha \tag{4.47}$$

The dynamic vertical force developed by the rear mount is expressed in a similar manner as:

$$F_{rez} = F_{krea} + F_{crea} + F_{hre} \tag{4.48}$$

where F_{krea} and F_{crea} are the stiffness and damping forces due to the compliant mount and F_{hre} is the hydraulic force component.

Assuming constant stiffness and damping coefficients, the stiffness and damping forces are derived from:

$$F_{krea} = -k_{rea}(z - a_2\varphi) \tag{4.49}$$

$$F_{crea} = -c_{hrea}(\dot{z} - a_2\dot{\varphi}) \tag{4.50}$$

The hydraulic force developed by the rear mount is dependent upon the instantaneous fluid pressure in the top mount, P_{TRE}, and is given by:

$$F_{hre} = A_{TP}(P_{TRE} - P_{STR}) \tag{4.51}$$

where P_{STR} is the top chamber static fluid pressure.

The roll moment generated by the axial and shear forces developed by the front-left and front-right mounts can be derived from the vertical and lateral components of the forces, such that:

$$M_{flx} = F_{flz}b_1 - F_{fly}h \tag{4.52}$$

$$M_{frx} = -F_{frz}b_2 - F_{fry}h \tag{4.53}$$

where the lateral force developed by the front-left and front-right mounts can be derived from the elastic and hydraulic force components, as:

$$F_{fly} = (F_{kfla} + F_{cfla} + F_{hfl})\cos\alpha_1 - (F_{kfls} + F_{cfls})\sin\alpha_1 \tag{4.54}$$

$$F_{fry} = -(F_{kfra} + F_{cfra} + F_{hfr})\cos\alpha_2 + (F_{kfrs} + F_{cfrs})\sin\alpha_2 \tag{4.55}$$

The pitch moments developed by the forces due to three mounts about the y-axis, are derived in a manner similar to that used in section 4.3. The pitch moments due to front-left, (M_{fly}), front-right (M_{fry}) and rear (M_{rey}) mounts are expressed as:

$$M_{fly} = F_{flz}a_1, M_{fry} = F_{frz}a_1 \text{ and } M_{rey} = -F_{rez}a_2 \tag{4.56}$$

Equations (4.19) to (4.21) together with Equations (4.22) to (4.31) completely describe the forces and moments developed by nonlinear elastic mounts and thus the dynamic motions of the coupled engine-mount system with elastic mounts, Equations (4.20), (4.21) and (4.41), together with Equations (4.42) to (4.56) describe the forces and

moments developed by compliant hydraulic mount and thus the dynamic motion of the engine assembly.

4.4.3 Method of Solution

The solution of differential equations of motion for the hydraulic mounts necessitates the determination of the static characteristics of the three hydraulic mounts, specifically the static fluid pressure, under a given load distribution. Owing to the symmetric location of the front mounts in the roll plane and negligible static roll deflection, the two front mounts will have the same static deflection. The rear mount, however, undergoes different static deflection due to different static load supported by this mount and static pitch inclination of the engine assembly. The deflection of the engine mass center can be derived from the static deflections of the different mount. The dynamic response of the engine mass center is also governed by the three static and dynamic chamber pressures. The method of solution and the computational procedure for the hydraulic mount system is described below:

The static pressures of fluid within the front and rear mounts, and the static deflections (z_{st} and φ_{st}) of the engine mass center are computing using the static equilibrium equations, as described in section 3.4.2. At static equilibrium, the relationship between the chamber pressure of the front and rear mounts, P_{STj} ($j = fl, fr, re$), and volume change V_{TSTj} and V_{BSTj} ($j = fl, fr, re$), for the top and bottom chambers are derived from Equation (3.29), such that: (3.28)

$$P_{STj} = P_{AT} + \sum_{i=1}^{3} C_{Ti} V_{TSTj}^{\alpha_i} = P_{AT} + \sum_{i=1}^{3} C_{Bi} V_{BSTj}^{\beta_i} \; ; \; j = fl, fr, re \tag{4.57}$$

where the regression coefficients C_{Ti} and C_{Bi} of the hydraulic mount are shown in Table 3.2. The static forces developed by the front and rear mounts F_{STj} ($j = fl, fr, re$) are computed from Equation (3.28), and expressed as:

$$F_{STj} = K_{ST}(\frac{V_{BSTj}}{A_{TP}}) + A_{TP}\left[\sum_{i=1}^{3} C_{Bi} V_{BSTj}^{\beta_i}\right];\ j = fl, fr, re \tag{4.58}$$

Using the static equilibrium for the front-left mount and rear mount, shown in Equation (4.38) and (4.40), and by combining Equations (4.57) and (4.58), yields:

$$\frac{b_2}{b_1+b_2}\times\frac{a_2 w}{a_1+a_2} = [A_{TP}\left[\sum_{i=1}^{3} C_{Bi} V_{BSTF}^{\beta_i}\right]\times 10^3 + k_{fas}(V_{BSTF}/A_{TP})\times 10^{-6}]\sin\alpha$$
$$+ k_{fy}(V_{BSTF}/A_{TP})\times 10^{-6}\times\frac{\cos^2\alpha}{\sin\alpha} \tag{4.59}$$

$$\frac{a_1 w}{a_1+a_2} = A_{TP}\left[\sum_{i=1}^{3} C_{Bi} V_{BSTR}^{\beta_i}\right]\times 10^3 + k_{reas}(V_{BSTR}/A_{TP})\times 10^{-6} \tag{4.60}$$

The above equations are solved to compute the static volume of fluids in the bottom chambers of front and rear mounts, V_{BSTF} and V_{BSTR}. Furthermore, the static pressure of fluid in the front and rear mounts, P_{STj} ($j = fl, fr, re$), and top chamber volume changes V_{TSTj} ($j = fl, fr, re$) are derived from Equation (4.57). The deflections of the front and rear mount along the axial direction at static equilibrium, X_{STj} ($j = fl, fr, re$), are then obtained from Equation (3.22), such that:

$$X_{STj} = -(V_{TSTj} + V_{BSTj})/A_{TP};\ \ j = fl, fr, re \tag{4.61}$$

The static axial deflection of the front and rear mounts, X_{STF} and X_{STR}, can also be expressed from Equation (4.11), as:

$$(z_{st} - a_1\varphi_{st})\sin\alpha = X_{STF}$$

$$(z_{st} + a_2\varphi_{st})\sin\alpha = X_{STR} \tag{4.62}$$

The static displacement of the engine mass center z_{st} and φ_{st} are thus derivable from Equation (4.62), and given by:

$$z_{st} = \frac{a_1 X_{STR} + a_2 X_{STF}}{(a_1 + a_2)\sin\alpha}$$

$$\varphi_{st} = \frac{X_{STR} - X_{STF}}{(a_1 + a_2)\sin\alpha} \tag{4.63}$$

The instantaneous pressure of fluid in the top and bottom chambers of the front-left, front-right and rear mounts is related to the fluid volume changes. The top chamber pressure of the front-left, front-right and rear mounts, P_{Tj} ($j = fl, fr, re$), can be derived from Equation (3.25), such that:

$$P_{Tj} = P_{AT} + \sum_{i=1}^{3} C_{Ti}\Delta V_{Tj}^{\alpha_i} \text{ , for } \Delta V_{Tj} > O \text{ ; } j = fl, fr, re \tag{4.64}$$

The instantaneous pressure is further related to the entrapped air volume V_A in Equation (3.38), such that:

$$P_{Tj} = P_{AT} V_A / V_{TAj} \text{ , for } \Delta V_{Tj} < O \text{ ; } \quad j = fl, fr, re \tag{4.65}$$

The bottom chamber fluid pressure, P_{Bj} ($j = fl, fr, re$), is derived in a similar manner from Equation (3.26), as:

$$P_{Bj} = P_{AT} + \sum_{i=1}^{3} C_{Bi}\Delta V_{Bj}^{\beta_i} \text{ , for } \Delta V_{Bj} > 0 \text{ ; } \quad j = fl, fr, re \tag{4.66}$$

The total volume of the entrapped air in the fluid, V_{TAj} ($j = fl, fr, re$), is expressed as:

$$V_{TAj} = V_A + \left|\Delta V_{Tj}\right| \text{ ; } j = fl, fr, re \tag{4.67}$$

The change in the top chamber volume of the mounts, ΔV_{Tj} ($j = fl, fr, re$), is related to the static volume and the relative deflection of the mount along the axial direction:

$$\Delta V_{Tj} = V_{TOj} + V_{TSTj} - A_{TP} x_j ; \; j = fl, fr, re \tag{4.68}$$

Here, the relative displacements of the front-left, front-right and rear mounts x_j ($j = fl, fr, re$) are derived from:

$$x_{fl} = (z + b_1\theta + a_1\varphi)\sin\alpha$$

$$x_{fr} = (z - b_2\theta + a_1\varphi)\sin\alpha$$

$$x_{re} = z - a_2\varphi \tag{4.69}$$

Equation (3.42) can be applied to determine the bottom chamber volume change, ΔV_{Bj} ($j = fl, fr, re$), such that:

$$\Delta V_{Bj} = -V_{T0j} + V_{BSTj} ; \; j = fl, fr, re$$

Moreover, the total volume of fluid transferred from one chamber to the other, V_{TOj} ($j = fl, fr, re$), derived from Equation (3.41), is related to the orifice flows, Q_{0j} ($j = fl, fr, re$), given by:

$$Q_{0j} = A_0 C_D \sqrt{\frac{2|P_{Tj}(t) - P_{Bj}(t)|}{\rho}} \operatorname{sgn}(P_{Bj} - P_{Tj}) \tag{4.70}$$

The motions for bounce z , roll θ and pitch φ , as described by their respective equations of motion (4.20), (4.21) and (4.41), are finally solved in conjunction with Equations (4.42) to (4.70) to determine the bounce, roll and pitch deflections of the engine assembly. Equations (4.57) to (4.70) further define the static and dynamic characteristics of the hydraulic mounts.

4.5 Summary

A three-DOF engine mounting system model is formulated using the bounce, roll and pitch motions of the engine assembly as the generalized coordinates. The engine excitation forces, derived in Chapter 2, are applied to determine the forces and moments developed by the mounts. Two different analytical models are formulated for the nonlinear rubber mounts and flexible chamber hydraulic mounts. The static load due to the engine assembly was considered in the elastic mounts model due to the nonlinearity of the rubber mounts. For the hydraulic mounts, the three hydraulic mounts were considered to exhibit different static, as well as dynamic deflections due to differences in their chamber pressures, volume changes as well as flow rates, caused by different static loads. The simplified three-DOF engine mounting system models can provide the essential performance of characteristics in terms of the bounce, roll and pitch motions under representative excitation force. The two orifices flexible chamber hydraulic mounts are applied in the system model to derive the response characteristics that are presented in the following chapter.

CHAPTER 5

CHARACTERISTICS OF THREE-DOF ENGINE MOUNTING SYSTEM

5.1 General

Internal combustion engines are known to transmit significant levels of vibration caused by the forces due to combustion and the unbalance. A well-designed engine mounting system should effectively isolate the vibration transmitted from the engine to the chassis of the vehicle and thus the occupant [16]. The coupled engine-mounts system, analytically modeled in Chapter 4, is described by a three-DOF dynamical system comprising the vertical, roll and pitch motions of the engine assembly. The engine excitation forces arising from the firing pulses, inertial forces and the torques, described in Section 2.2, are applied for the vibration isolation analysis of the engine mount system. Two different analytical models of the engine assembly with, the nonlinear rubber mounts and flexible chamber hydraulic mounts with two orifices, are employed in the coupled three-DOF engine mount system.

In this chapter, the nonlinear static and dynamic properties of the three-DOF engine mount system with both, elastomeric and hydraulic mounts, are analyzed in order to evaluate the performance characteristics of the engine mount system. For the hydraulic mount, the performance characteristics are also illustrated in terms of intermediate physical variables, such as orifice flow, top chamber pressure and the damping force. The transmitted force, as well as the vibration transmissibility under engine excitation force and moments remains the primary performance measure.

5.2 Characterization of the Three-DOF System Model with Elatomeric Mounts

5.2.1 Static Equilibrium

The three-DOF engine mount system model combines three elastomeric or hydraulic mounts to support the engine load. The static deflection of each mount is determined from the distribution of the engine load on the mounts and the static properties of the mounts. The parameters, used in the analysis of the three-DOF system engine mount model, are summarized in Table 5.1, which are based upon engine parameters reported in [67]. The parameters of the front two mounts are identical to those described in Chapter 3, while those of the rear mount are chosen in accordance with the static load on the mount. The stiffness coefficients of the rear elastomeric mount (k_{r1}, k_{r2} and k_{r3}) and that of the rear hydraulic mount (k_{rea}), are obtained from the static engine load imposed on the rear mount, as described in Equation (4.7). The results suggest a relatively softer rear mount when compared to the effective stiffness of the two front mounts. The engine assembly thus undergoes a small magnitude of static pitch deflection.

For the elastomeric mounts, the static equilibrium responses are derived by solving for the roots of the polynomial expressions described in equations (4.16) and (4.17). The static vertical and pitch displacements of the mass center of the engine assembly are evaluated as, z_{st} =-0.0032 m and φ_{st} =0.0049 rad. The corresponding deflections of the front and rear mounts z_{stf} and z_{str} are evaluated as: -0.0017 m and -0.0049 m, respectively.

Table 5.1: Simulation parameters for three-DOF engine mounting system with elastomeric and hydraulic mounts

Parameter	Value
Engine mass, m (kg)	139.5
Mass moments of inertia, I_x and I_y (kgm^2)	3.505 and 8.473
Distance between two adjoining cylinders center lines, d_c (m)	0.100
Top area of the engine piston, A (m^2)	0.00665
Longitudinal locations of mounts, a_1 and a_2 (m)	0.300 and 0.350
Lateral locations of mounts, b_1 and b_2 (m)	0.300 and 0.300
Vertical locations of mounts, h (m)	0.200
Inclination of the front mounts in the lateral plane, α	45°
Axial stiffness coefficients of the front rubber mount, $k_{f1}(N/mm)$, $k_{f2}(N/mm^2)$ and k_{f3} (N/mm^3)	160, -24 and 1.4
Axial stiffness coefficients of the rear rubber mounts, $k_{r1}(N/mm)$, $k_{r2}(N/mm^2)$ and k_{r3} (N/mm^3)	272, -40.8 and 2.38
Shear stiffness of the front rubber mount, $k_y(kN/m)$	304
Axial damping coefficient of the front rubber mount, c_{fa} (Ns/m)	300
Axial damping coefficient of the rear rubber mount, c_{rea} (Ns/m)	300
Shear damping coefficient of the front rubber mount, c_{fs} (Ns/m)	150
Axial static stiffness of the front hydraulic mount, $k_{fas}(kN/m)$	200
Shear static stiffness of the front hydraulic mount, $k_{fys}(kN/m)$	200
Axial static stiffness of the rear hydraulic mount, $k_{reas}(kN/m)$	280
Axial stiffness of the front hydraulic mount, $k_{fa}(kN/m)$	280
Shear stiffness of the front hydraulic mount, $k_{fy}(kN/m)$	392
Axial stiffness of the rear hydraulic mount, $k_{rea}(kN/m)$	392
Axial damping coefficient of the front hydraulic mount, c_{hfa} (Ns/m)	140
Axial damping coefficient of the rear hydraulic mount, c_{hrea} (Ns/m)	140
Shear damping coefficient of the front hydraulic mount, c_{hfs} (Ns/m)	100

5.2.2 Dynamic Responses of the Engine-mount System with Elestomeric Mounts

The dynamic response charatcteristics of the three-DOF engine mount system model with elastomeric mounts are evaluated through analyses of the nonlinear differential equations of motion formulated in Section 4.3.2. The static deflections of individual mounts are considered in the dynamic simulation process due to the nonlinearity of the elastomeric mount. The stiffness properties of the rubber mounts along the shear axis are also incorporated in the analyses as described in the model. The analyses are performed under engine excitations, arising from the unbalance force/moment due to reciprocating components, and the gas forces along the bounce, roll and pitch axis. The variations in the gas pressure, described in Section 2.4, are discretized and applied to the model as a function of the crank angle. The discretized values of the gas pressure variations are obtained from the data presented in Figure 2.8, which are subsequently smoothened by using an interpolation approach.

Figure 5.1, as an example, illustrates the time-histories of the displacement responses of the engine mass, under excitations arising the discretized gas pressure and unbalance force due to reciprocating components. The results are presented for an engine speed of 3000 rpm, considered to be more frequently used speed for automotive engines. The results show oscillations at the primary frequency of 50 Hz corresponding to the chosen rpm, while the presence of secondary frequency components equal to twice the primary frequency is also observed. This second frequency component is more apparent from the vertical displacement response, which is mostly associated with the vertical unbalance force, as described in Equation (2.11). The magnitude of this particular spectral component in the roll response is relatively small due to weak coupling between the

vertical and roll motions. The results further show relatively small magnitudes of pitch and roll deflections of the engine mass.

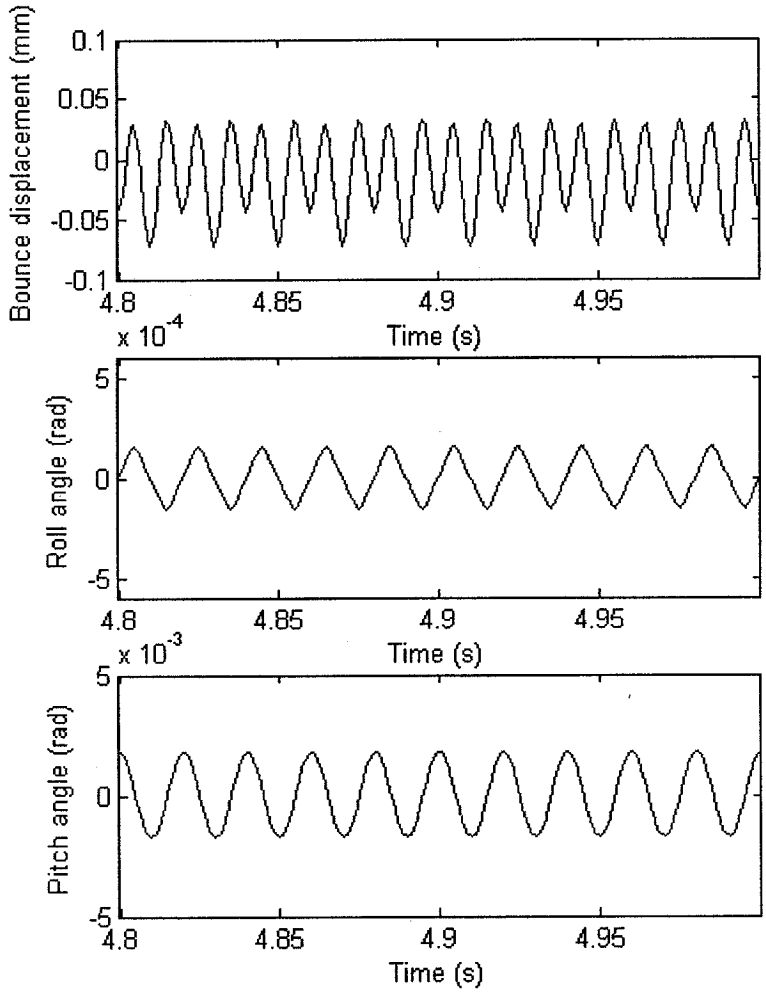

Figure 5.1: Time histories of engine mass displacement along the bounce, roll and pitch axes, under engine excitations at 3000rpm.

The responses are further evaluated over a wide speed range and expressed in terms of performance measures, namely, the transmitted force and vibration transmissibility. Owing to the asymmetric and non-harmonic responses, the magnitudes of the transmitted force and vibration are evaluated in terms of RMS quantities from Equations (3.7) to

(3.10). The dynamic properties of the elastomeric engine-mount system are evaluated over the entire range of frequencies of the related engine speed of 1-6000 rpm.

Figures 5.2, 5.3 and 5.4 illustrate the RMS magnitudes of excitation force or moment, transmitted force or moment and force/ moment transmissibility along the vertical, roll and pitch axes, respectively.

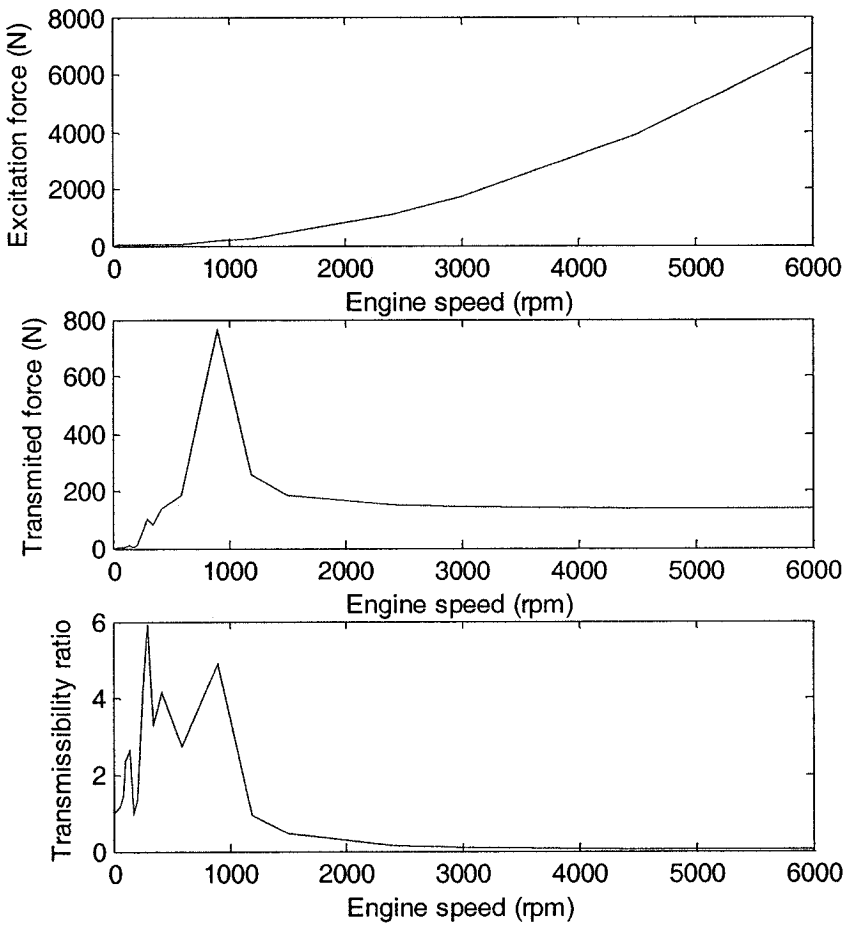

Figure 5.2: Vertical RMS excitation and transmitted forces, and force transmissibility responses of the three-DOF engine mount system model with elastomeric mounts

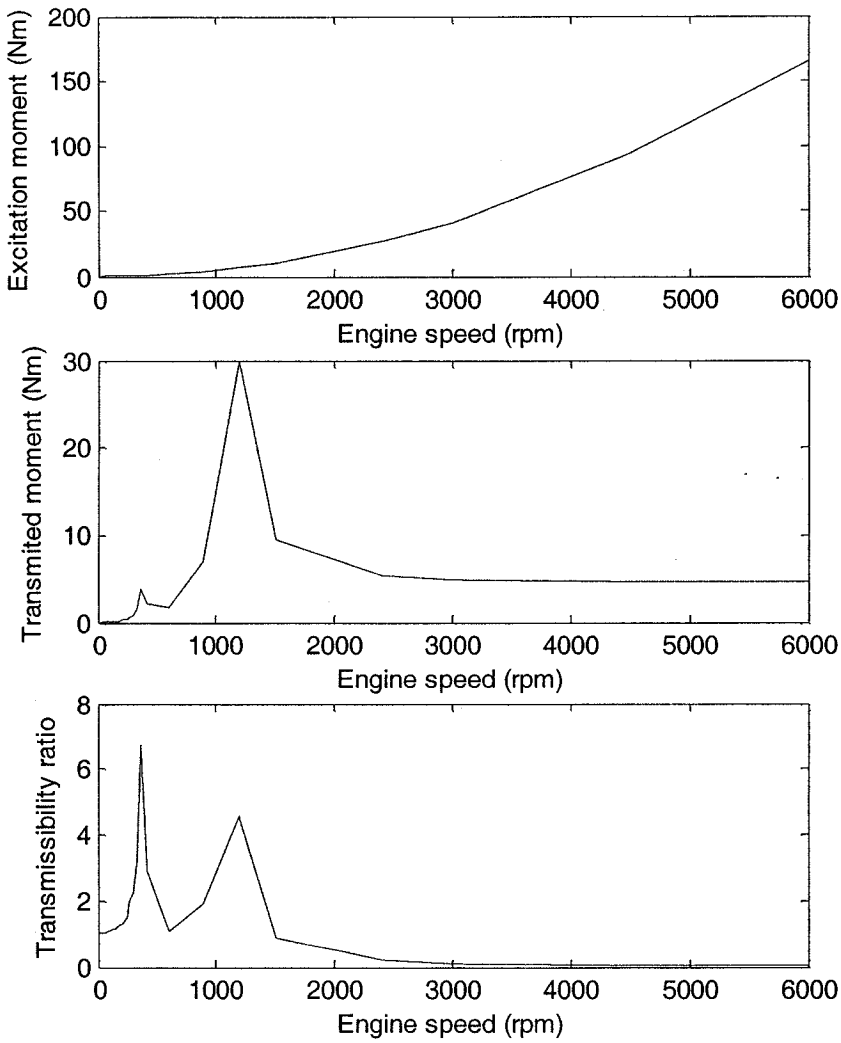

Figure 5.3: RMS values of excitation and transmitted moment along the roll axis, and the moment transmissibility of the three DOF engine-mount system model with elastomeric mounts.

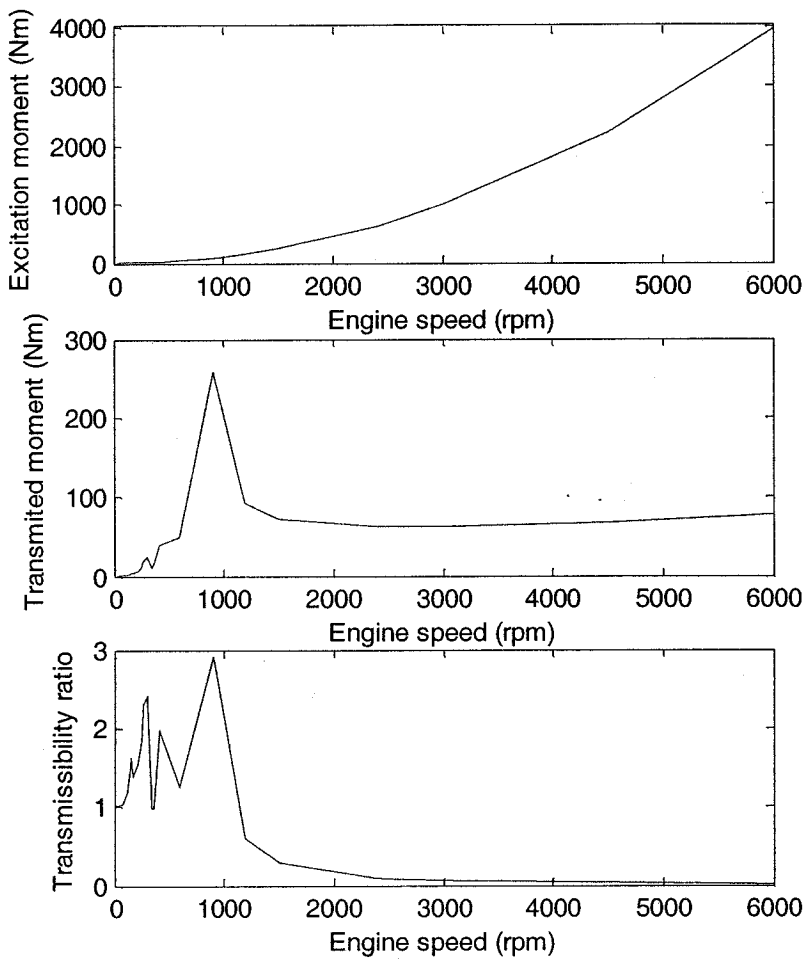

Figure 5.4: RMS values of excitation and transmitted moment along the pitch axis, and the moment transmissibility of the three-DOF engine-mount system model with elastomeric mounts.

The magnitudes of transmitted force or moment corresponding to a particular engine speed are computed from equations (4.19) to (4.21), presented in section 4.3.2. The force and moments transmitted to the chassis along the vertical, roll and pitch axes are derived from:

Vertical axis

$$F_{tz} = F_{flz} + F_{frz} + F_{rez} - mg \tag{5.1}$$

Roll axis

$$M_{tx} = M_{flx} + M_{frx} + M_{rex} \tag{5.2}$$

Pitch axis

$$M_{ty} = M_{fly} + M_{fry} + M_{rey} \tag{5.3}$$

where F_{tz}, M_{tx} and M_{ty} are the vertical force, roll moment and pitch moment transmitted to the chassis.

The steady-state force and moments are expressed in terms of their respective RMS values. The force/moment transmissibility values corresponding to different operating speeds are computed from the ratio of the RMS transmitted force/moment to the RMS excitation force/moment. The transmitted force/moment and the transmissibility ratios are the primary performance criteria for the engine mounting system, as mentioned in Chapter 2. The results show that the peak values of transmitted vertical force, and roll and pitch moments approach 760 N at 900 rpm, 30 Nm near 1200 rpm and 260 Nm near 900 rpm, respectively. The results suggest that the influence of bounce motion is most significant in view of the force transmitted to the vehicle chassis, which is mostly attributed to the engine unbalanced inertia force excitation. On the contrary, the influence of roll motion appears to be relatively small when compared with the moment caused by the pitch motion.

The excitation force and moments tend to increase in proportion to the square of the speed, suggesting major contributions due to the unbalance effects. The force transmissibility ratio reveals peaks near 300, 360 and 900 rpm, which correspond to frequencies of 10, 12 and 30 Hz, respectively. The roll moment transmissibility response,

in a similar manner reveals peaks near 360 and 1200 rpm or 12 and 40 Hz. The peak values of the pitch moment transmissibility are observed near 300, 360, 900 rpm, identical to those observed for the vertical force transmissibility. These frequencies are associated with the vertical, roll and pitch mode frequencies of the engine-mount system. The results further show that the peak transmissibility ratios approach 6, 6.8 and 2.9 in the bounce, roll and pitch axes, respectively, corresponding to natural frequency 10, 12 and 30 Hz. The results clearly show significant amplification of the force and moments in the vicinity of the resonant frequencies of the engine-mount system with elastomeric mounts.

5.3 Response Characteristics of the Three-DOF Engine-mount System with Hydraulic Mount

Owing to the pitch inclination of the engine assembly, the front and rear hydraulic mounts support different static loads and thereby yield different values of static pressures and volumes of the hydraulic chambers. The static deflections, pressures and chamber volumes of the front and rear mounts are computed using the methodology described in Section 4.4.3. Table 5.2 summarizes the static response quantities for the three-DOF engine mount system employing hydraulic mounts with two orifices. The table also summaries the static deflections of the mounts (X_{STF} and X_{STR}) and those of the engine mass center (z_{st} and φ_{st}). The results suggest slightly higher pressure and thus higher deflection of the rear mount. The resulting top chamber volume change of the front mounts is thus lower than that of the rear mount.

Table 5.2: Static response quantities of the three-DOF hydraulic mount system

P_{STF} (kPa)	P_{STR} (kPa)	V_{TSTF} (cc)	V_{BSTF} (cc)	V_{TSTR} (cc)
102.0	103.4	0.17	6.50	0.31
V_{BSTR} (cc)	X_{STF} (mm)	X_{STR} (mm)	z_{st} (mm)	φ_{st} (mm)
11.15	-0.0013	-0.0025	-0.0023	0.0021

The differential equations of motion derived for the three-DOF model, presented in Section 4.4.2, are solved to determine the dynamic responses of the individual mount and the overall engine-mount system in terms of the transmitted force and moments. Figures 5.5 to 5.7 illustrate the dynamic responses of the front and rear mounts, respectively, under engine excitations caused by unbalance force and gas pressure, at a frequency of 15 Hz. The results show only minimal change in the fluid volume of the top chamber of the three mounts, which is attributed to lower compliance of the bottom chamber, as described earlier in Section 3.4.3. The negative change in the volumes of the top chambers cause the chambers in a state of vacuum, as observed from the results attained from the single-DOF model of the mounts. Moreover, the volumes and thus the pressures of fluid in the top chambers vary in a highly asymmetric manner, where the pressure values approach as low as 92 and 89 kPa, with respect to front-left and front-right mounts. This trend of sub-atmospheric pressure for the mounts agrees quite well with the experimentally obtained pressure for a hydraulic mount reported in [37]. The peak values of the pressure of the top chambers approach near 111 and 113 kPa for the two mounts. The variations in the bottom chambers pressures are very low compared to those of the top chambers, due to the high compliance nature of the bottom chambers, where peak-to-peak difference is observed to occur in the 0.9-4.4 kPa range. The changes in the volumes of the top and bottom chambers of the rear mount, however, are observed to be larger

then those obtained for the front mounts. This is attributed to its higher effective axial stiffness. While the top chamber pressure approaches significant vacuum state (minimum pressure $\approx$65 kPa), the bottom chamber pressures remains just above the atmospheric pressure. The volume-pressure relationships of all three mounts are observed to be nonlinear, while the volume change increases with the fluid pressure.

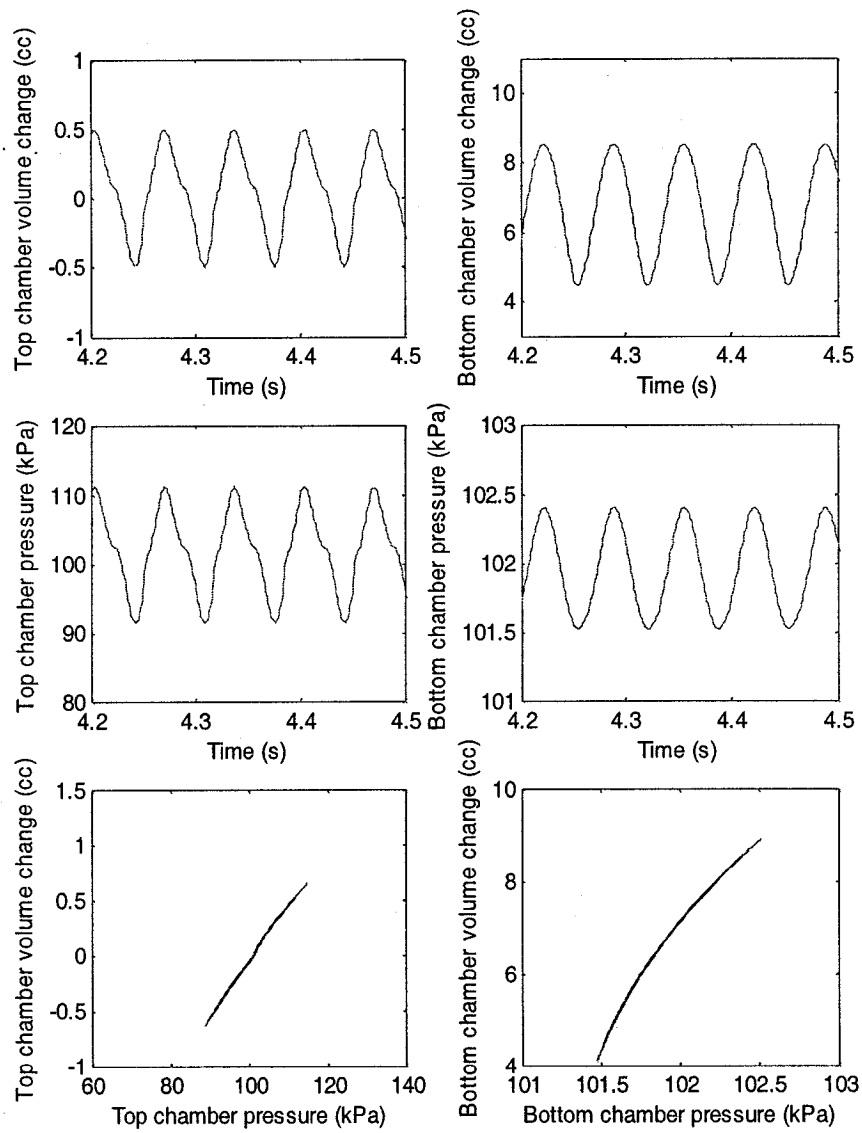

Figure 5.5: Variation in the pressure & volume of the two chambers in a three-DOF system (front left mount).

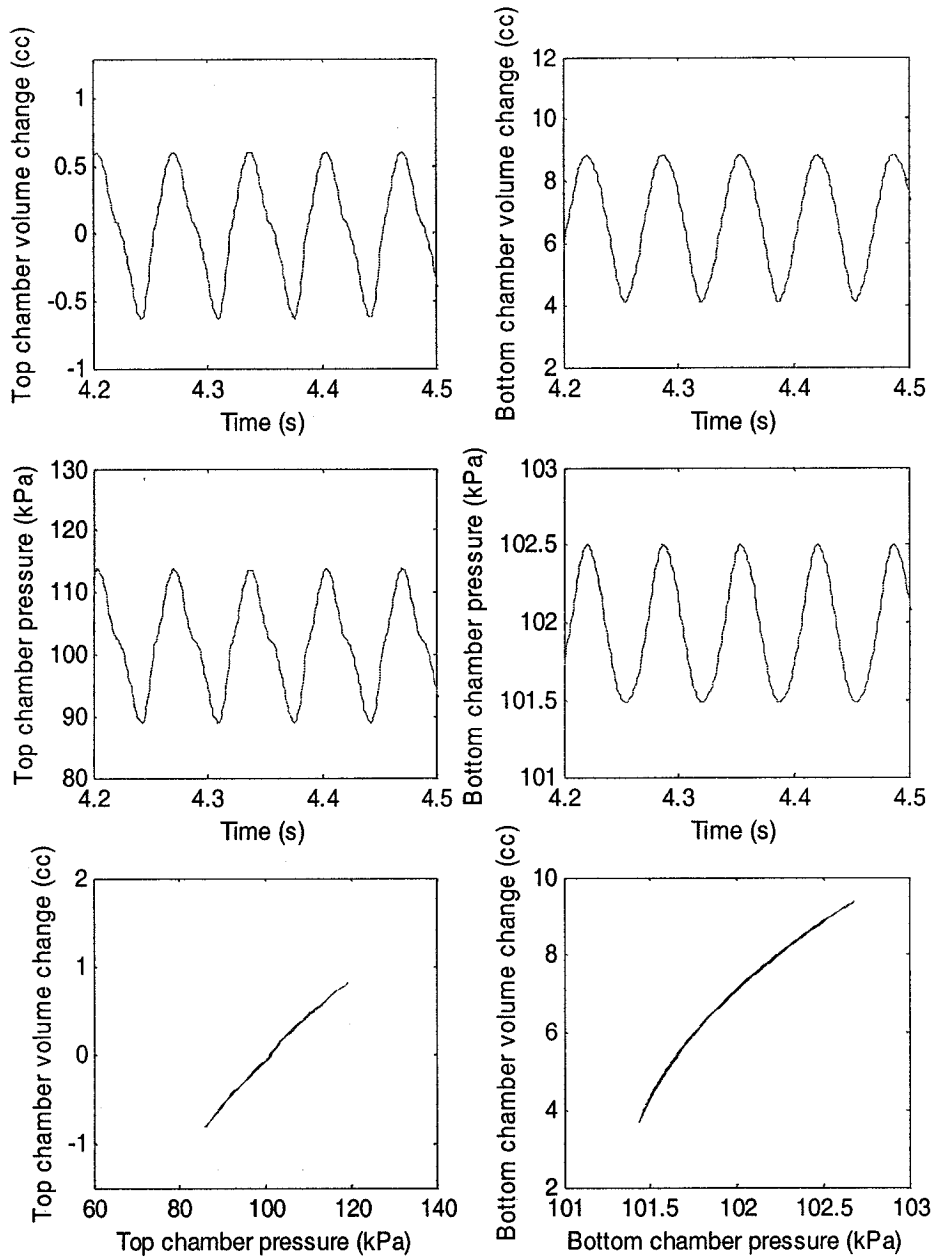

Figure 5.6: Variation in the pressure & volume of the two chambers in a three-DOF system (front right mount).

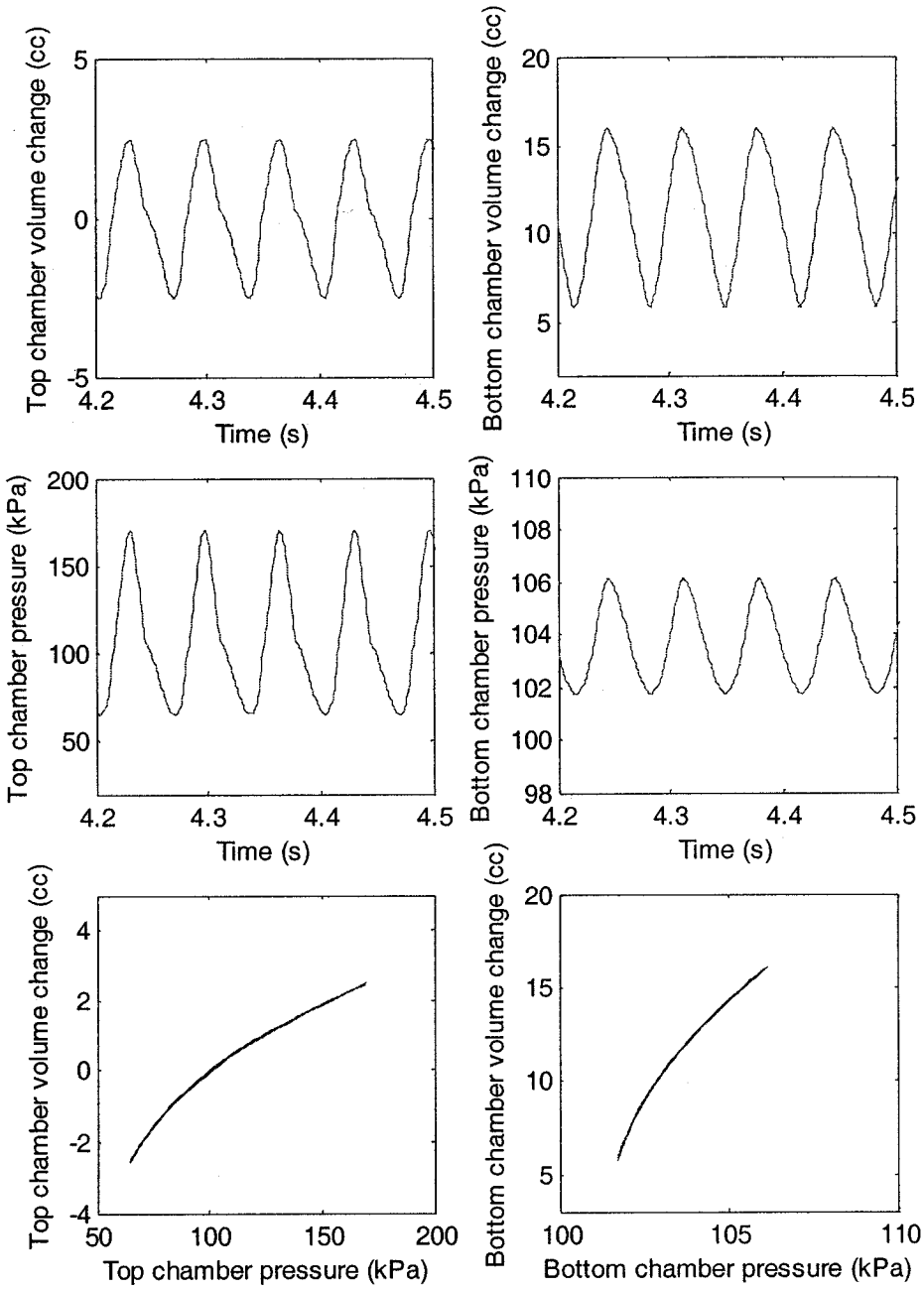

Figure 5.7: Variation in the pressure & volume of the two chambers in a three-DOF system (rear mount).

Figures 5.8 to 5.10 show the time-histories of the responses in terms of transmitted force, hydraulic damping force and flow rate for the three individual mounts. The peak

values of the transmitted forces approach peak magnitudes of 70, 90, and 550 N for front-left, front-right and rear mounts, while the corresponding hydraulic damping forces approach as 45, 50, and approximately 310 N, respectively. The variations in the damping are observed to be non-harmonic due to turbulent flows through the orifices. The considerably higher flow rates of the rear mount is attributed to high relative motion across the mount, which is most likely caused by the pitch mode oscillation of the engine mass. This tends to cause very high transmitted force at the rear mount. The figures also show the force-velocity properties of the three mounts, which show significantly higher relative velocity of the rear mount and thus the magnitude of the damping force. The results show that the damping coefficient of the mounts increases progressively with the relative velocity, while the damping coefficient is low in the vicinity of lower velocities.

The results also show that a positive flow occurs from the bottom chamber to the top chamber (reverse flow), and a negative flow occurs from the top to the bottom chamber (forward flow). The variations in the flow rate of the mounts exhibit strong differences between the front and the rear mounts, which is partly attributed to the load distribution and the orifice sizes. The asymmetric orifice flow rate characteristics show lower peak to peak changes for the two front mounts, which is attributed to relatively lower load supported by each mount. The asymmetric nature of fluid flow in the reverse and forward directions is caused by the relative compliance properties of the top and bottom chambers. The figures also illustrate that the magnitudes of the top chamber pressures and transmitted forces of the front mounts are lower, compared with the results obtained for the single-DOF system model due to the load being shared by the front and rear mounts in the three-DOF system model.

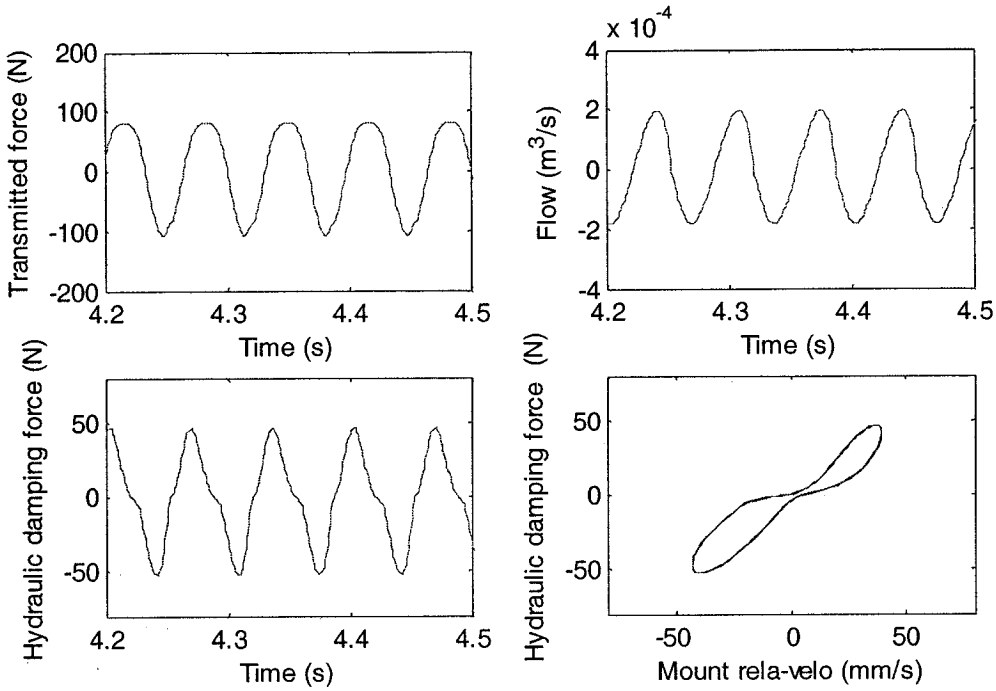

Figure 5.8: Variation in the transmitted force, hydraulic damping force and flow in a three-DOF system (front left mount).

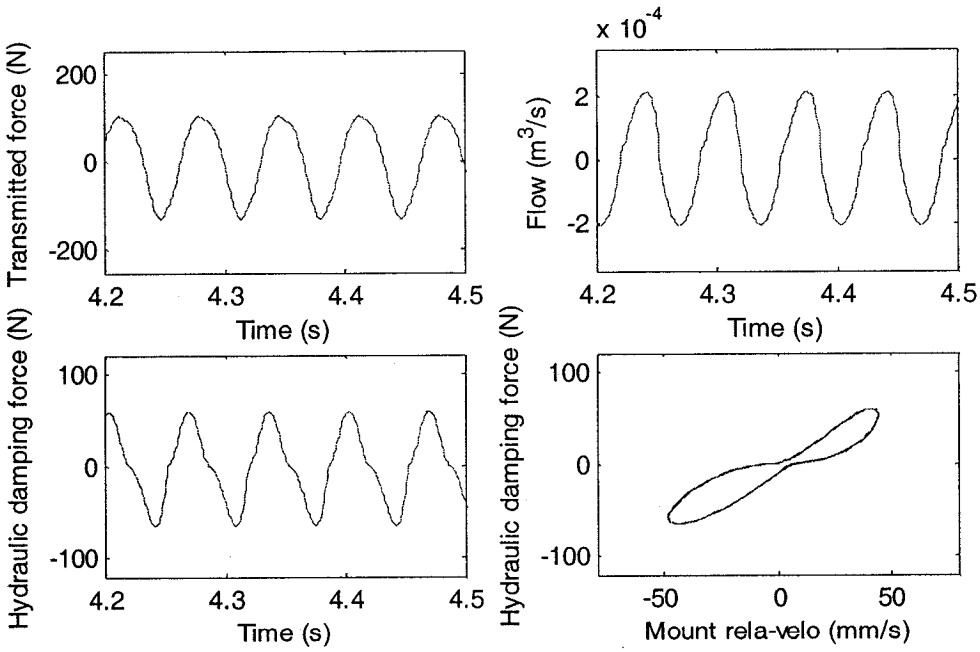

Figure 5.9: Variation in the transmitted force, hydraulic damping force and flow in a three-DOF system (front right mount).

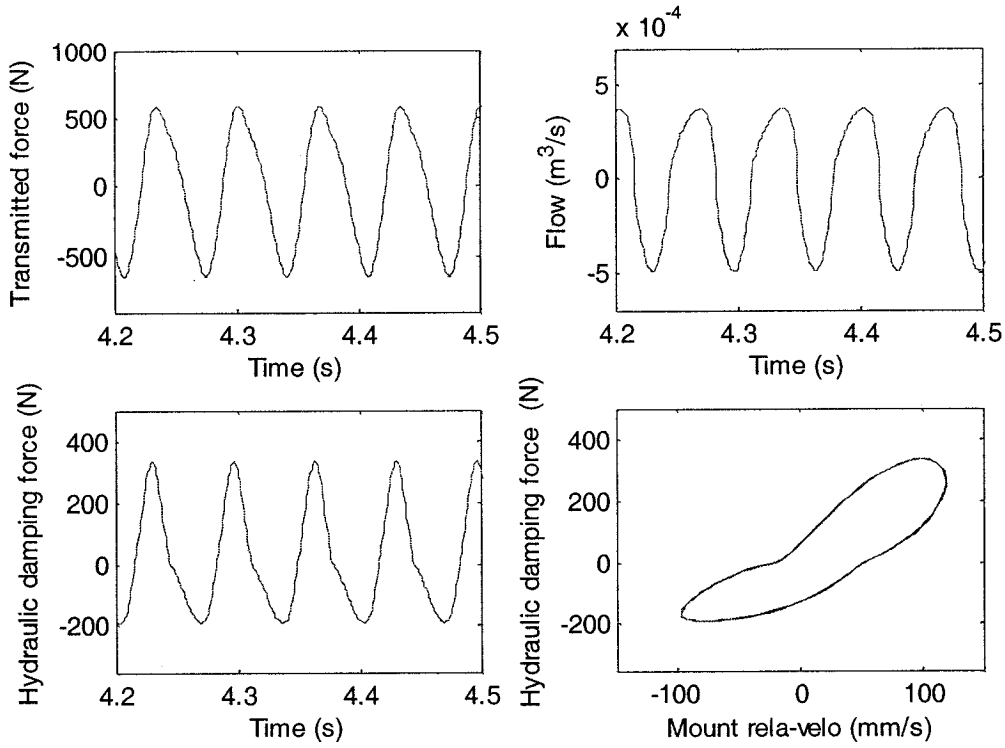

Figure 5.10: Variation in the transmitted force, hydraulic damping force and flow in a three-DOF system (rear mount).

The response characteristics of the engine-mount system with hydraulic mounts are further evaluated in terms of transmitted force/moment and the corresponding transmissibility ratios as a function of the engine speed. Figures 5.11 to 5.13 illustrate the RMS magnitudes of excitation force or moment, transmitted force or moment and transmissiblility ratio responses along the vertical, roll and pitch axes, respectively, under the excitations arising from the unbalance and the gas pressure variations. The results show significant magnitude to the transmitted force around the engine speed of 1250 rpm. The peak magnitude of this force, which approaches 500 N, is much lower to that attained with the elastomeric mounts, while the corresponding engine speed is higher than that obtained for the elastomeric mounts (near 900 rpm). This is attributed to its higher bounce and pitch mode natural frequencies. The peak value of the force

transmissibility ratio of the hydraulic mounts system occurs near 300 rpm, while its magnitude of 5.7 is slightly lower than that attained with the elastomeric mounts.

The peak values of transmitted roll and pitch moments is apparently observed to approach 3.4 and 400 Nm near 500 and 1250 rpm, while the magnitude of roll transmitted moment shows much lower than that appears in elastomeric mounts model, however, the magnitude of the pitch moment reveal quite higher than that attained from the elastomeric model. Furthermore, the peak transmissibility ratios appear as 5.2 and 2.3 in roll and pitch axes, respectively, and corresponding to the engine speeds of 130 and 1250 rpm.

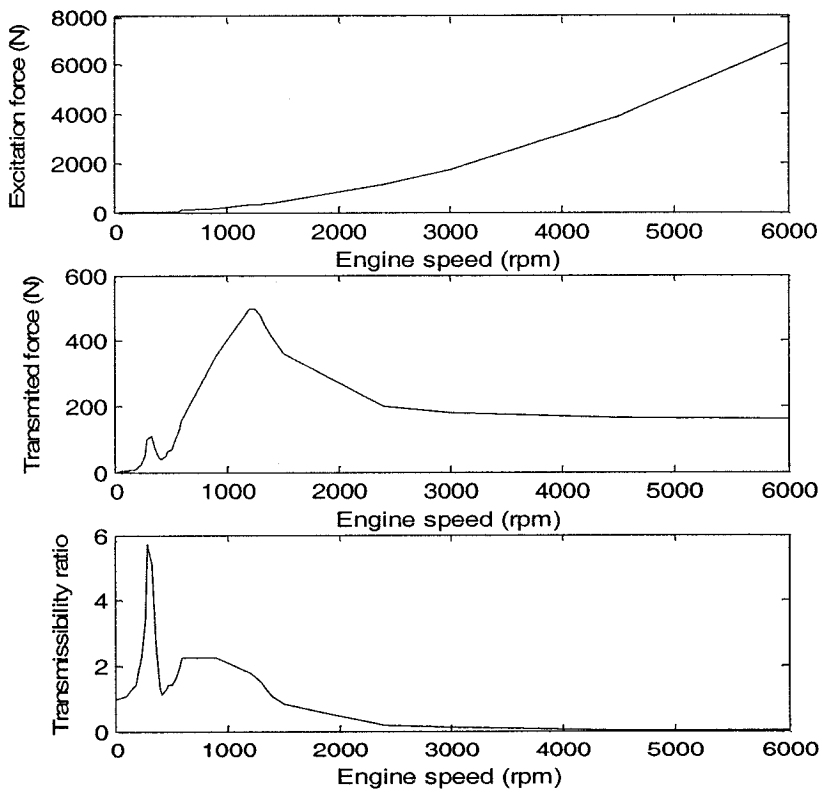

Figure 5.11: Vertical RMS excitation and transmitted forces, and force transmissibility response of the three-DOF engine-mount system model with hydraulic mounts.

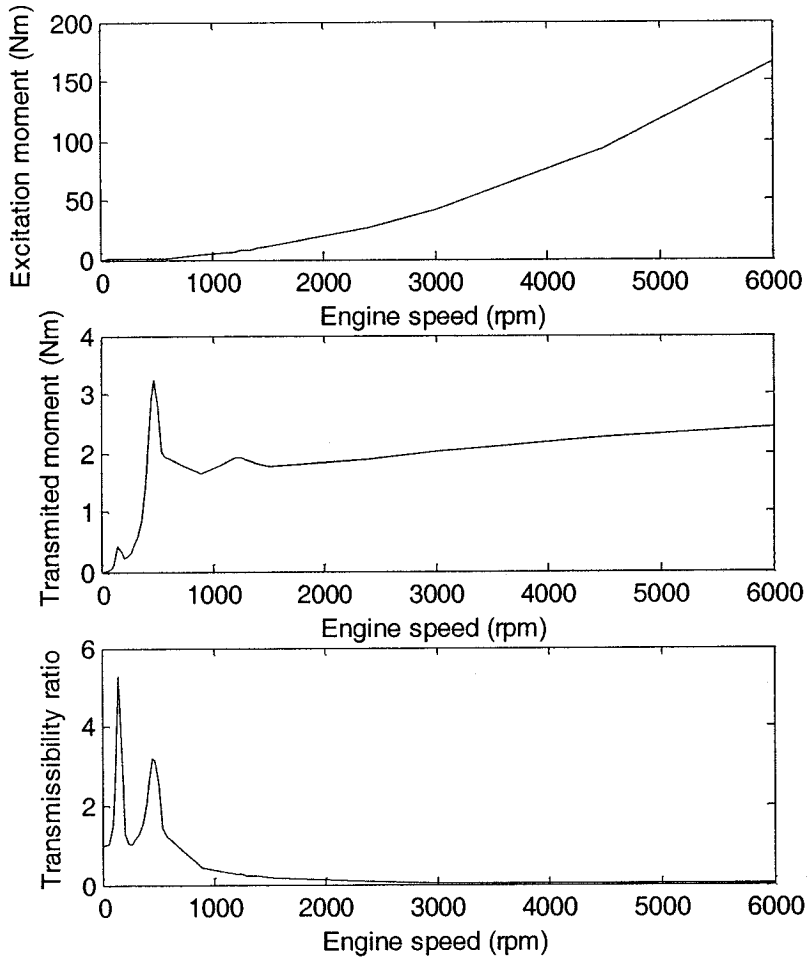

Figure 5.12: RMS values of excitation and transmitted moment, along the roll axis, and the moment transmissibility of the three-DOF engine-mount system model with hydraulic mounts.

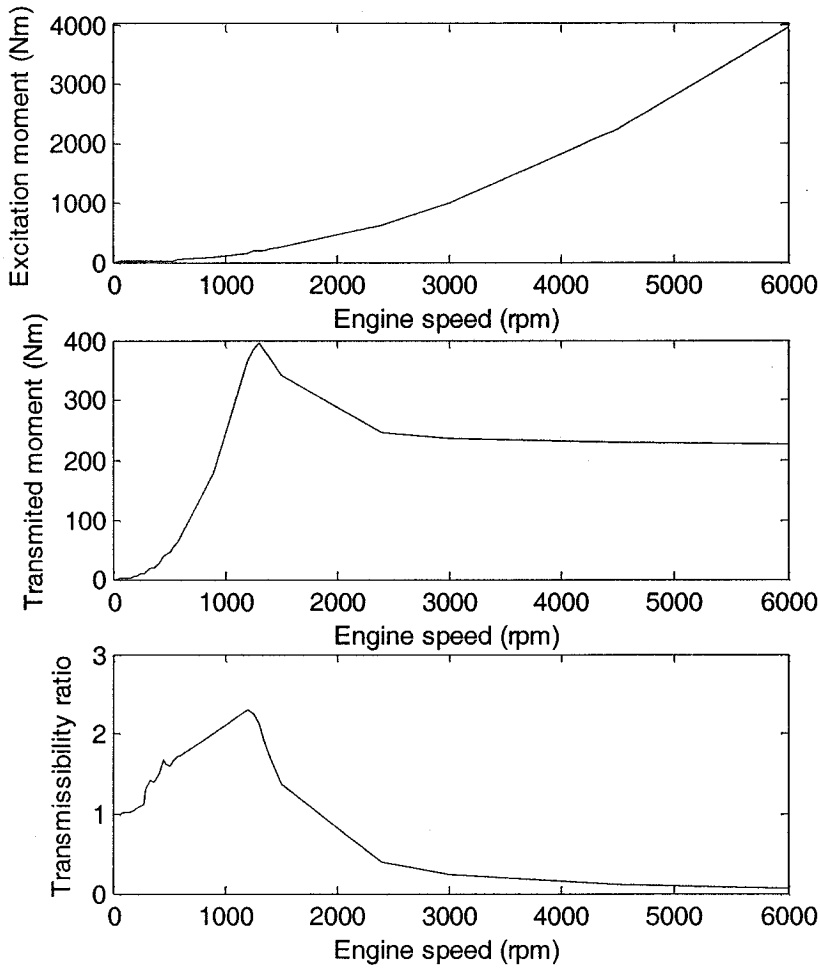

Figure 5.13: RMS values of excitation and transmitted moment, along the pitch axis, and the moment transmissibility of the three-DOF engine-mount system model with hydraulic mounts.

5.4 Summary

In this chapter, the response characteristics of the 3DOF engine mount system model, with rubber and hydraulic mounts, are evaluated under excitations. The probable natural frequencies and the modes of the two nonlinear models are identified from the forced responses, arising from the unbalance and the gas pressure variations. It is evaluated for the individual hydraulic mounts and the total engine-mount systems, and the responses

are presented in terms of the RMS transmitted forces and moments, and the transmissilibity ratio along the vertical, roll and pitch axes.

The transmissibility responses of the hydraulic mounts system in bounce, roll and pitch axes are observed to be lower than those of the rubber system. The peak values of the transmitted bounce force for the hydraulic mount model is quite lower, while the hydraulic mounts also yield improved performance in roll. The peak value of the transmitted roll moment was only 3.4 Nm, compared to 30 Nm for the elastomeric mounts system. The hydraulic mounts, however, cause excursive pitch moment, with peak magnitude of 400 Nm, which is much higher than the peak magnitude of the pitch moment caused by the elastomeric mounts. The results also show that the engine mount system with hydraulic mounts yields lower natural frequency in roll and higher natural frequency of the pitch mode. This is most likely attributed to the uneven axial stiffness of the front and rear mounts. The pitch moment and the vertical force transmissibility of the mounting system could be enhanced by adequate selection and tuning of the mounts properties. A softer elastomeric mount, however, may provide good performance at higher frequencies but could cause shock excitation caused by sudden acceleration or deceleration at low frequencies.

CHAPTER 6

OPTIMIZATION OF THE ENGINE MOUNT SYSTEM

6.1 General

The negative effects from engine vibrations such as dynamic forces and moments can be reduced by the judicious selection of the position and the characteristics of the engine mount system [67]. The performance characteristics of the three-DOF engine mount system with elastomeric and hydraulic mounts are evaluated in Chapter 5. The nonlinear properties of the coupled system, including bounce, roll and pitch motions, are analyzed under engine excitations. In this chapter, a well-known Sequential Quadratic Programming (SQP) optimization method is selected for the elastomeric mount system to minimize the transmitted force and moments from the engine to the vehicle chassis.

The objective function based on the total transmitted forces and moments in the entire frequency range of interest for all of the mounts is minimized. Weighting factors representing the rank of the effect of each force or moment are applied in the objective function. The optimization program **fmincon,** the nonlinear constrained multi-variable optimization technique, is used to determine the mount design parameters which minimize the transmitted forces in the mounts, subject to constraints on the maximum allowable deflection of the engine to static forces [64]. The design parameters considered are stiffness, damping coefficient and orientation of each individual engine mount. The characteristics of the engine mount system with hydraulic mount are finally simulated at the optimal location of the elastomeric mount system, in order to compare the performances of the two systems.

6.2 Objective Function for Elastomeric Mounts

Different objectives were considered for the current optimization work. One objective is to tune the natural frequency of the engine mounting system to some desired range to avoid resonance and to improve the isolation of vibration, noises and shock excitation. Swanson et al. [65] showed that the transmitted force could be directly minimized in order to determine a truly optimal design of the mounts. The latter approach is applied in this thesis to minimize transmitted forces from the engine to the foundation in the excitation frequency range of 2-200Hz, which corresponds to the engine speed of 60-6000rpm. In order to save computer-running time, twenty frequencies with unequal intervals were used in the optimization program.

The objective function U for this study is defined as the sum of the RMS values of the transmitted forces and moments from bounce, roll and pitch vibrations. By applying weighting factors for the RMS values, one can adjust the computed values in different frequencies to allow for their significance in a particular context. The objective function is obtained by considering the transmitted force and moments in the entire frequency range. Twenty frequencies are selected and divided into two frequency bands. The ten frequencies selected in the low frequency band are from 2-51Hz, which includes all the frequencies where peak values of transmitted force/moment occur, while another ten frequencies are selected in the high frequency band of 51-200Hz. The peak values at the low frequency band and the maximum values at the high frequency band are employed, respectively. The rest of the transmitted force and moment values in the two frequency bands also play an important role in order to reduce the transmitted force in the entire frequency range. Therefore, the sum of the corresponding forces is also taken into account in the objective function.

The weighted transmitted force and moments in bounce, roll and pitch axes at low and high frequencies are thus represented in four separate equations, such that:

1. Weighted three peak values of transmitted force and moments at low frequency band are expressed as:

$$F_{tp\_1} = \alpha_{11}[\max(F_{ti\_rms}; i = 1,2,...10)] + \alpha_{12}[\max(M_{txi\_rms}; i = 1,2,...10)] + \alpha_{13}[\max(M_{tyi\_rms}; i = 1,2,...10)] \quad (6.1)$$

where i is the number of the selected frequencies, i is from 1 to 10 in low frequency band.

2. Weighted three maximum values of transmitted force and moments at the high frequency band is given as:

$$F_{tp\_2} = \alpha_{21}[\max(F_{ti\_rms}; i = 11,12,...20)] + \alpha_{22}[\max(M_{txi\_rms}; i = 11,12,...20)] + \alpha_{23}[\max(M_{tyi\_rms}; i = 11,12,...20)] \quad (6.2)$$

where the number of the selected frequencies i is from 11-20 in high frequency band.

3. Weighted sum value of three transmitted force and moments at low frequency band, excluding the frequencies selected in Equation (6.1), is described as:

$$F_{ts\_1} = \alpha_{31}(\sqrt{\sum_{i=1}^{10} F_{ti\_rms}^2} + \sqrt{\sum_{i=1}^{10} M_{txi\_rms}^2} + \sqrt{\sum_{i=1}^{10} M_{tyi\_rms}^2}) \quad (6.3)$$

where, i does not include the one selected in Equation (6.1).

4. Weighted sum value of three transmitted force and moments at high frequency band, excluding the frequencies selected in Equation (6.2), such that:

$$F_{ts\_2} = \alpha_{32}(\sqrt{\sum_{i=11}^{20} F_{ti\_rms}^2} + \sqrt{\sum_{i=11}^{20} M_{txi\_rms}^2} + \sqrt{\sum_{i=11}^{20} M_{tyi\_rms}^2}) \quad (6.4)$$

where i does not include the one selected in Equation (6.2).

5. The objective function is finally formed by the four terms described above, such that:

$$U = F_{tp\_1} + F_{tp\_2} + F_{ts\_1} + F_{ts\_2} \tag{6.5}$$

where, $\alpha_{11}, \alpha_{12}, \alpha_{13}, \alpha_{21}, \alpha_{22}, \alpha_{23}, \alpha_{31}, \alpha_{32}$ are weighting factors used to represent the importance of the relevant terms. Weighting factors are user-defined numbers ranging from zero to one. The weighting factors, α_{11}, α_{12} and α_{13}, which represent the peak values of the transmitted force and moments are selected larger due to their significant effect on the characteristics of the vibration isolation of the engine mount system.

F_{tp_1} and F_{tp_2} are the weighted sum of the peak values of the RMS of the transmitted force and moments in the low and high frequency band, respectively. F_{ts_1} and F_{ts_2} are the weighted sum of the RMS of the transmitted force and moments excluding the values corresponding to the peak response as identified by F_{tp_1} and F_{tp_2}. F_{ti_rms} , M_{txi_rms} and M_{tyi_rms} are the overall RMS value of the transmitted force and moments, along the vertical, roll and pitch axes.

The constraints are imposed to limit the displacement of the engine in bounce, roll and pitch motion. The constraints for static deflection of the engine mass center are limited in the vertical and pitch axes, due to the roll angle which is set to zero at the static equilibrium and expressed as:

$$z_{st} \leq c_1 \tag{6.6}$$

$$\varphi_{st} \leq c_2 \tag{6.7}$$

where c_1, c_2 are constants and are the maximum allowable static displacement of the

engine. The constraints for the dynamic displacements of the engine in bounce, roll and pitch axes are given as:

$$\max(z_i) \leq c_3 \tag{6.8}$$

$$\max(\theta_i) \leq c_4 \tag{6.9}$$

$$\max(\varphi_i) \leq c_5 \tag{6.10}$$

where i=1, 2...20, c_3 and c_4 are constants and are the maximum allowable dynamic displacement of the engine. In addition, constraints must be imposed to keep the design variables within the lower (lb) and upper (ub) bounds:

$$lb \leq b \leq ub \tag{6.11}$$

where, b represents variables applied in the optimal process. The stiffness coefficients of front and rear mounts k_{f1}, k_{f2}, k_{f3}, k_{r1},k_{r2}, k_{r3}, k_y and the damping coefficients c_{fa}, c_{fs} and c_{rea} of the front and rear mounts, as well as the engine mounts location parameters $a_1, a_2, b_1, b_2, h, \alpha$ are considered as the sixteen variables in the optimization process.

6.3 Optimization Method

For the purpose of effectively minimizing the total amount of transmitted forces from engine to chassis, the target value which is considered as the value of the objective function is computed by using the optimization program. The flow chart of the optimization process is shown in Figure 6.1.

The optimization program **fmincon**, which is chosen from the MATLAB optimization package, is applied to find a minimum of a constrained nonlinear multivariable function. The algorithm **fmincon** uses a Sequential Quadratic Programming

(SQP) method. The SQP implementation consists of three main stages: updating of the Hessian matrix of the Lagrangian function, solving a Quadratic Programming (QP) subproblem at each iteration, and performing a line search using a merit function. The QP subproblem is solved using an active set strategy. The solution procedure involves two phases. The first phase involves the calculation of a starting point. The second phase involves the generation of an iterative sequence of feasible points that converge to the solution. In this method an active set is maintained that is an estimate of the active constraints at the solution point. As a result, the SQP method is widely used for solving nonlinear constrained optimization problems in terms of minimizing computer time and number of function evaluations.

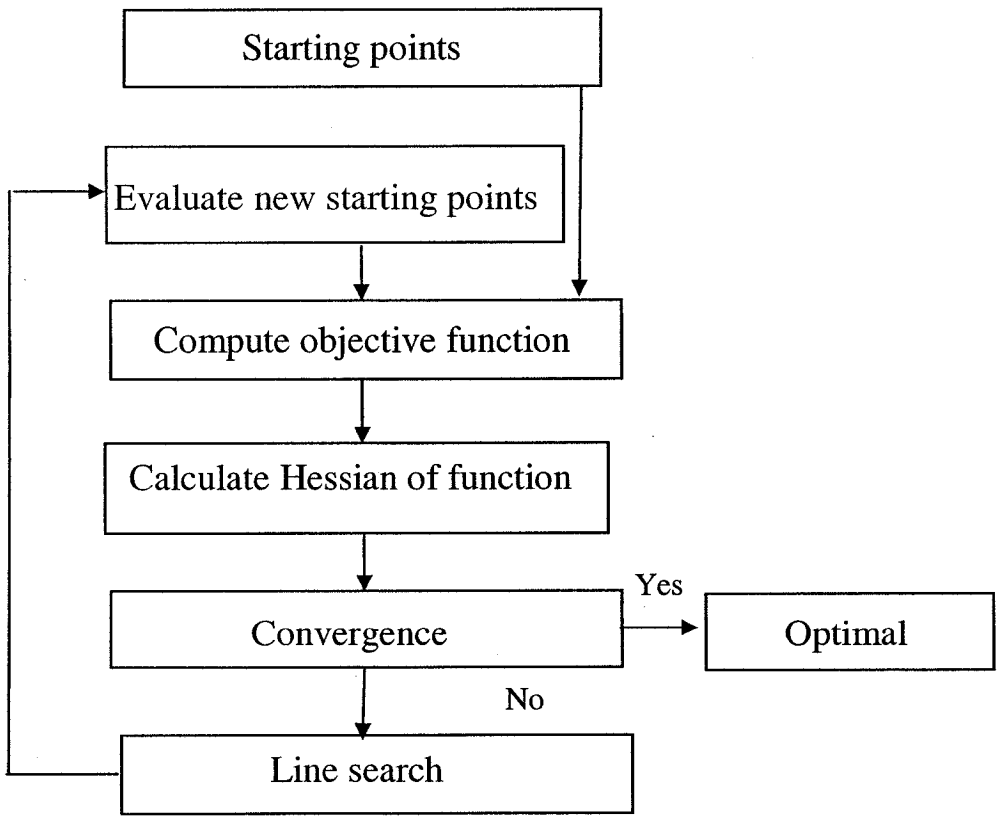

Figure 6.1: Algorithm of optimization

6.4 Optimization Results for Elastomeric Mounts

To optimize the objective function U, the transmitted forces are obtained by solving the differential equations (4.19), (4.20) and (4.21). The design parameters, shown in Table 5.1, are considered as initial conditions to complete the optimization. The design constrains for nominal design parameters are determined in reference to paper [67]. Typically, due to engine bay space limitations, the engine mount locations may be constrained. The design constraints, including mount stiffness and damping coefficients, as well as mount location, are shown in Table 6.1. The engine and mount displacements, including both static and dynamic motion for engine mass center and each individual mounts, are also constrained, owing to the limitation of the engine bay. The corresponding constrains, shown in Table 6.2, are selected as referred to in paper [57].

Table 6.3 presents the weighting factors of the objective function, which are empirical coefficients that determine the influence of the dynamic transmitted forces and moments to enable different dimensions to be converted into a unique one. A few trial iterations were performed to select the correct weighting factors, which can minimize the optimal value of the objective function. The weights for the peak of transmitted force and pitch moment in the low frequency band are selected to be larger values owing to their large magnitudes, while roll transmitted moment has minor effect due to its small values. The factors for the sum of the other transmitted force and moments are much smaller compared to the former. The optimal result proved that the influences of the peak value of transmitted force and moments are significant on the objective function.

It is well known that all methods of nonlinear programming will converge to the nearest minimum but depends on the proper estimation of the starting points of the optimizing parameters [67, 55]. The trail method is used to start the optimization program.

The nominal parameters determined from the analysis in Chapter 5 are used as the initial condition of the optimization operation at the first iteration. The optimal result from the first iteration is used as a feedback to modify the initial values for the next iteration. This method is repeated until the final optimal result is reached. The nominal design parameters, the initial conditions of the final iteration in the optimal process and the optimal results for the sixteen parameters are listed in Table 6.4. The comparison between nominal design and optimal result can thus be implemented. The optimal results appear that the stiffness coefficient of the front mount (k_{f1}) decreased from 160 to $127.79\,N/mm$. The stiffness coefficient of the rear mount (k_{r1}) shows a slight decrease from 272 to 252.53. The damping coefficients of the front and rear mount are also decreased. On the other hand, the locations and the inclination angle of the mounts are adjusted slightly. The front and rear mounts are located closer in the longitudinal direction in the optimal result and the distance between the front left and right mounts is wider to some extent. The optimal inclination angle of the front mounts on roll plane, $54.2°$, is larger than the nominal angle $45°$. However, the static deflection of the mounts shows larger than that of the nominal design due to the mount softening in the optimal results. A comparison of the target value, between that of nominal and optimal results, shows a decrease from 304.30 to 27.25. The ratio of the target value reduction is up to 91%.

Table 6.1: The band of nominal design parameters

Variables	Band
Axial stiffness coefficient of the front mount k_{f1}	$100 \le k_{f1} \le 300$ (N/mm)
Axial stiffness coefficient of the front mount k_{f2}	$-40 \le k_{f2} \le 10(N/mm^2)$
Axial stiffness coefficient of the front mount k_{f3}	$2 \le k_{f3} \le 4(N/mm^3)$
Axial stiffness coefficient of the rear mount k_{r1}	$136 \le k_{r1} \le 340$ (N/mm)
Axial stiffness coefficient of the rear mount k_{r2}	$-68 \le k_{r2} \le 170$ (N/mm)
Axial stiffness coefficient of the rear mount k_{r3}	$1.0 \le k_{r3} \le 2.3$ (N/mm)
Shear stiffness coefficient of the front mount k_y	$200 \le k_y \le 350$ (N/mm)
Axial damping coefficient of the front mount c_{fa}	$150 \le c_{fa} \le 500$ (Ns/m)
Shear damping coefficient of the front mount c_{fs}	$100 \le c_{fs} \le 300$ (Ns/m)
Axial damping coefficient of the rear mount c_{rea}	$150 \le c_{rea} \le 500$ (Ns/m)
Longitudinal location of mounts a_1	$0.28 \le a_1 \le 0.34$ (m)
Longitudinal location of mounts a_2	$0.3 \le a_2 \le 0.38$ (m)
Lateral location of mounts b_1	$0.25 \le b_1 \le 0.32$ (m)
Lateral location of mounts b_2	$0.28 \le b_2 \le 0.32$ (m)
Vertical location of mount h	$0.18 \le h \le 0.22$ (m)
Inclination of the front mounts in the lateral plane α	$\frac{\pi}{6} \le \alpha \le \frac{\pi}{3}$ rad

Table 6.2: Constraints of engine and mount displacement

Constrained variables	Constrain bond
Static displacement of engine mass center z_{st}	$z_{st} \le 0.010$ (m)
Static pitch angle of engine mass φ_{st}	$\varphi_{st} \le 0.035$ rad
Static deflection of front mounts z_{stf}	$z_{stf} \le 0.010$ (m)
Static deflection of rear mount z_{str}	$z_{str} \le 0.010$ (m)
Maximum displacement of engine mass center $\max(z_{1i})$	$\max(z_{1i}) \le 0.006$ m
Maximum roll angle of engine mass $\max(\theta_i)$	$\max(\theta_i) \le 0.006$ rad
Maximum pitch angle of engine mass $\max(\varphi_i)$	$\max(\varphi_i) \le 0.006$ rad
Maximum displacement of front left mount $\max(z_{fli})$	$\max(z_{fli}) \le 0.006$ (m)
Maximum displacement of front right mount $\max(z_{fri})$	$\max(z_{fri}) \le 0.006$ (m)
Maximum displacement of rear mount $\max(z_{ri})$	$\max(z_{ri}) \le 0.006$ m

Table 6.3: Weighting factors of objective function

Factors of weighting	Values
Peak of transmitted bounce force at low frequency band	$\alpha_{11} = 0.25$
Peak of transmitted roll moment at low frequency band	$\alpha_{12} = 0.15$
Peak of transmitted pitch moment at low frequency band	$\alpha_{13} = 0.2$
Highest value of transmitted bounce force at high frequency band	$\alpha_{21} = 0.2$
Highest value of transmitted roll moment at high frequency band	$\alpha_{22} = 0$
Highest value of transmitted pitch moment at high frequency band	$\alpha_{23} = 0.1$
Sum of total transmitted force and moment exclude the peak value at low frequency band in bounce, roll and pitch axes	$\alpha_{31} = 0.06$
Sum of three transmitted force and moments exclude the highest value at high frequency band in bounce, roll and pitch axes	$\alpha_{32} = 0.04$

Table 6.4: Comparisons of nominal, starting and optimal parameter values

Variables	Nominal value	Starting value	Optimal value
Axial stiffness of the front mount k_{f1} (N/mm)	160	160	127.79
Axial stiffness of the front mount k_{f2} (N/mm^2)	-24	-24	-40
Axial stiffness of the front mount k_{f3} (N/mm^3)	1.40	3.00	2.00
Axial stiffness of the rear mount k_{r1} (N/mm)	272	272	252.53
Axial stiffness of the rear mount k_{r2} $((N/mm^2)$	-40.8	-40.8	-45.12
Axial stiffness of the rear mount k_{r3} (N/mm^3)	2.38	1.3	4.00
Shear stiffness of the front mount k_y (N/mm)	304	260	261.69
Axial damping coefficient of the front mount c_{fa} (Ns/m)	300	300	150
Shear damping coefficient of the front mount c_{fs} (Ns/m)	150	150	100
Axial damping coefficient of the rear mount c_{rea} (Ns/m)	300	300	219
Longitudinal location of mount a_1 (m)	0.30	0.30	0.2910
Longitudinal location of mount a_2 (m)	0.35	0.35	0.3350
Lateral location of mount b_1 (m)	0.30	0.30	0.3073
Lateral location of mount b_2 (m)	0.30	0.30	0.3048
Vertical location of mount h (m)	0.20	0.20	0.18
Inclination of the front mounts in the lateral plane α	45°	45°	54.2°
Static displacement of engine mass center z_{st} (m)	0.0032	0.0118	0.0040
Static pitch angle of engine φ_{st} (rad)	0.0049	0.0330	0.0029
Static deflection of front mount z_{stf} (m)	0.0017	0.0019	0.0032
Static deflection of rear mount z_{str} (m)	0.0049	0.0233	0.0050
Target value U	304.30	268.61	27.25

A performance comparison between the nominal and optimized system is illustrated in Figures 6.2 to 6.4. The results show that the optimal transmitted force and moments are all much lower than the original values in the entire frequency range except at a frequency lower than the natural frequency. Typically, the transmitted bounce force of the optimal system shows a huge reduction as compared to that of the nominal design system from low to high frequencies, while the peak decreases from 760 to 50 N. The transmitted roll and pitch moments also decrease in the most of the frequency band, and the peaks decrease, respectively, from 30 to 17 Nm and from 260 to 75 Nm. However, the penalty is in the peaks for optimal transmissibilities which are slightly larger than those of the nominal design.

Table 6.5 shows a comparison of natural frequencies between the nominal design and optimal results. The natural frequencies for bounce, roll and pitch motion are all lower than that of the nominal design. The range of the subsystem natural frequencies for a midsize passenger vehicle is listed in Table 6.6 [66]. In analyzing these data, it can be established that the optimized natural frequencies are acceptable because they coincide neither with the resonant frequencies of the vehicle subsystems nor with the engine running speed which is higher than the idle speed usually set at 800 rpm (26.7Hz).

Table 6.5: Natural frequencies comparison of nominal and optimal

Vibration Modes	Nominal natural frequency (Hz)	Optimized natural frequency (Hz)
Bounce	10	6.24
Roll	12	8.77
Pitch	30	14.03

Table 6.6: Modes and frequencies of powertrain and vehicle [66]

Vibration Modes	Freq. (Hz)	Vehicle Modes (Hz)
Vertical	6 ~ 8	Rigid Body Modes(1~2)
Roll	7 ~ 9	Suspension Hop / Tramp(12--13)
Yaw	7 ~ 12	Front End Pitching(17~19)
Pitch	10 ~ 20	Bending(18~24)
Lateral	8 ~ 25	Torsion(23~30)
Fore/Aft	8 ~ 25	Steering Wheel (25~30) Engine Idle Freq.(25~30)

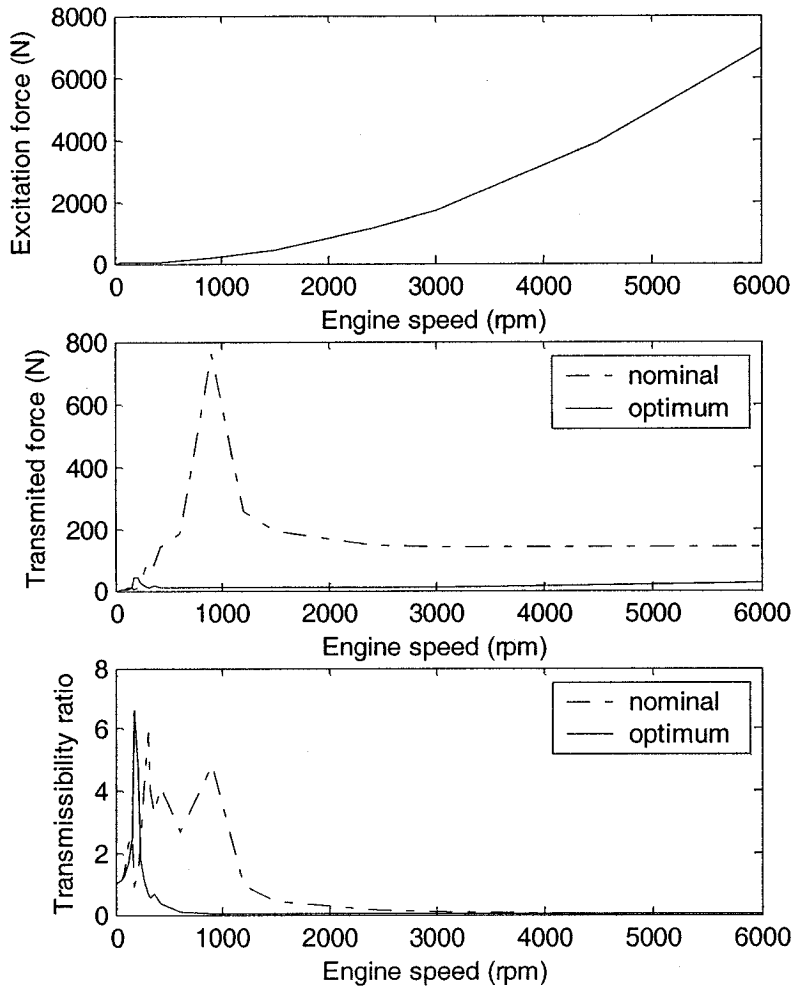

Figure 6.2: Comparison of nominal and optimal vertical transmitted force and transmissibility of the three-DOF engine mount system model with elastomeric mounts.

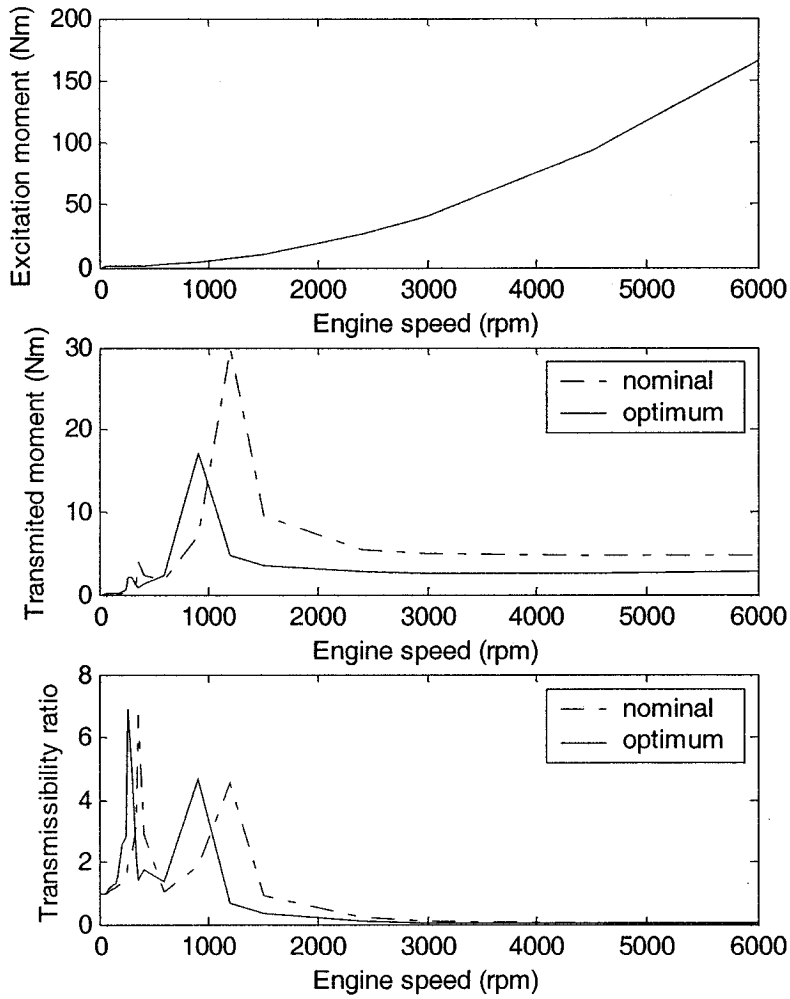

Figure 6.3: Comparison of nominal and optimal transmitted roll moment and transmissibility of the three-DOF engine mount system model with elastomeric mounts.

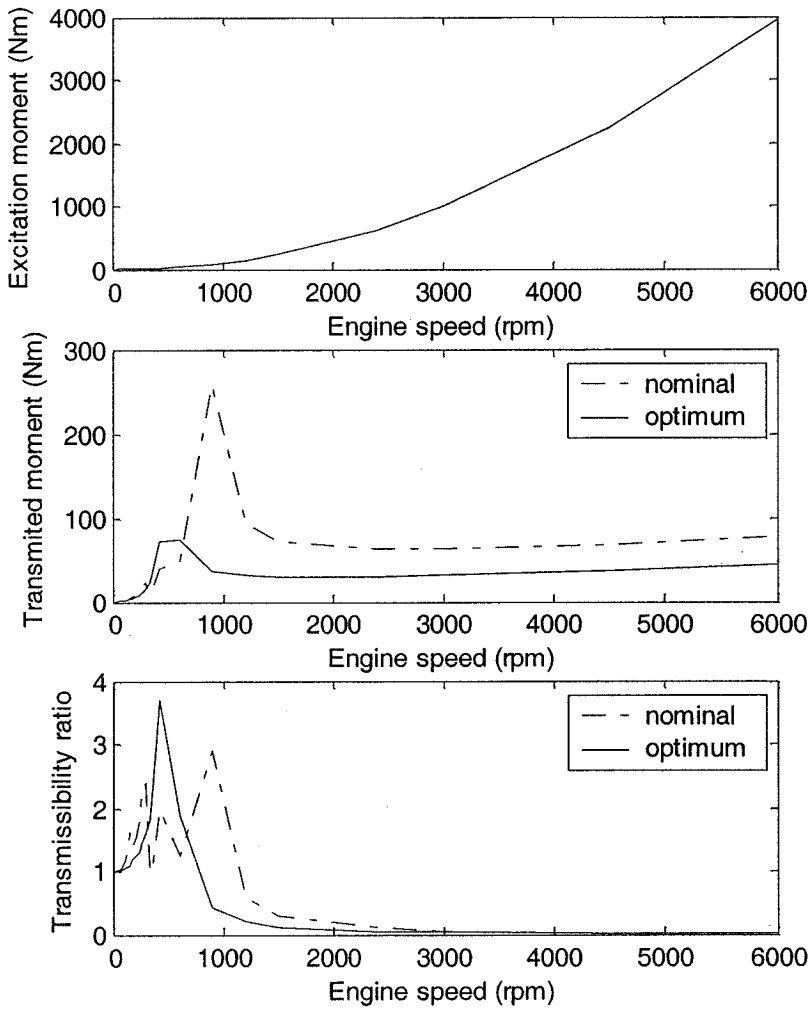

Figure 6.4: Comparison of nominal and optimal transmitted pitch moment and transmissibility of the three-DOF engine mount system model with elastomeric mounts.

6.5 Parameters Sensitivity Analysis:

The optimal results, summarized in Table 6.4, can be used to study parameter sensitivity in order to decide parameters which have primary influence on the transmitted force/moment. Each of the sixteen variables will be selected as a variable while the other 15 parameters stay as constants. The selected variable increase or decrease by 10%, 20% and 30% of its optimal value. The parameters with superscript '*' present the optimal

parameter, the x axial represents the ratio between the varied parameters and the optimal parameters. The influences of the selected variables on the target value along with their variations thus are evaluated and demonstrated in Figures 6.5 to 6.7.

The stiffness coefficients of the front mounts k_{f1}, k_{f2}, k_{f3} and k_y, and the stiffness coefficients of the rear mount k_{r1}, k_{r2} and k_{r3} apparently have the most significant effect on the target value, while either increasing or decreasing the parameter values of the stiffness coefficients. Similarly, the location of the mounts in the longitudinal direction a_1 and a_2, as well as the inclination of the front mounts in the lateral plane α also appear to have large influence in the target value, which are obtained through the integration of the transmitted force or moments in bounce, roll and pitch axes. Meanwhile the damping coefficients c_{fa}, c_{fs} and c_{rea}, as well as the lateral and vertical location of the mounts b_1, b_2 and h reveal nearly no effect. The results can be applied in the optimization design of the engine mount system, so as to identify the most sensitive parameters which can be employed to reduce the transmitted force from the engine to the vehicle chassis. The results further show that the optimal parameters of the sixteen variables all lead to the minimum target value.

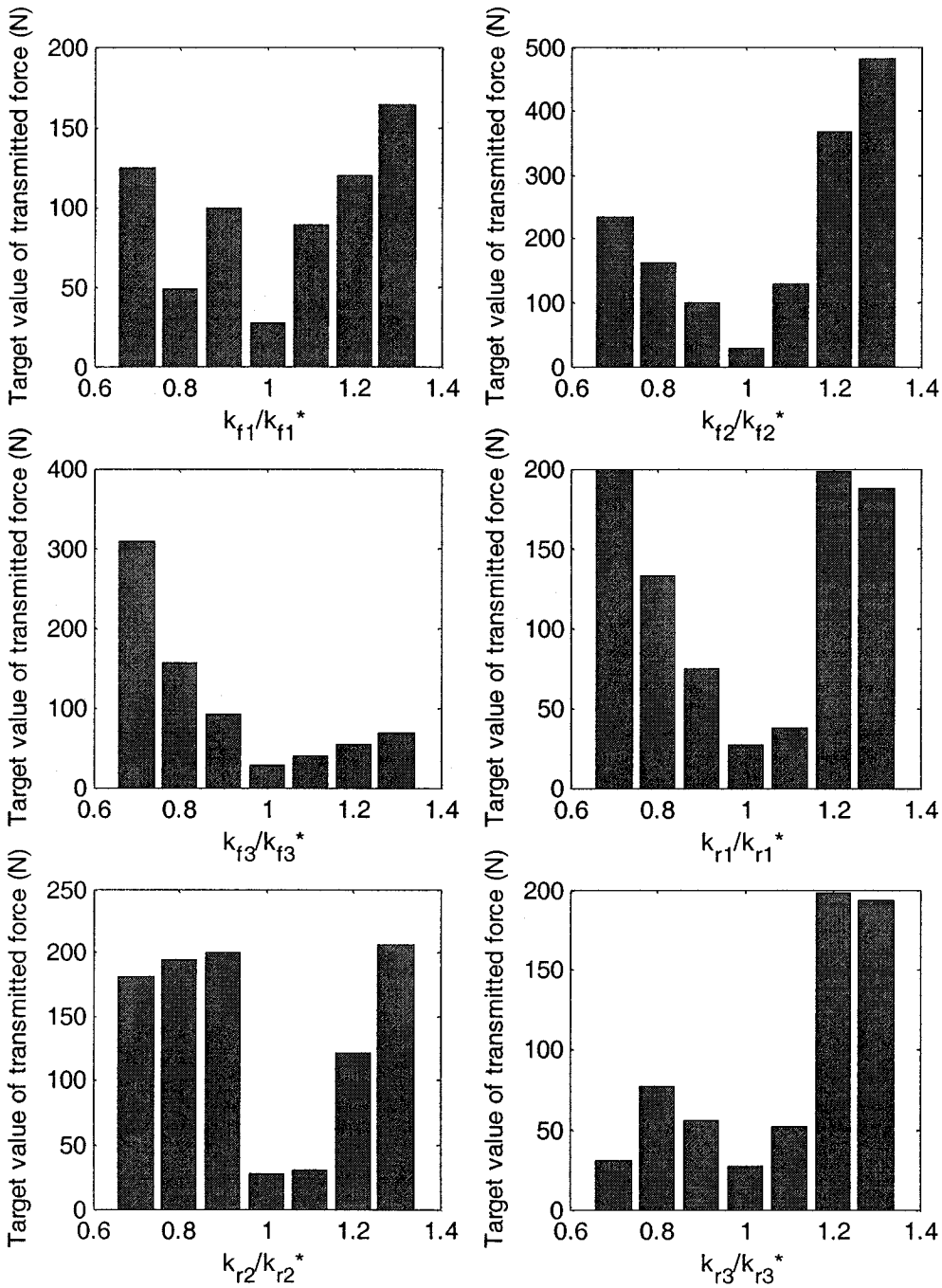

Figure 6.5: The influences of the front and rear mount stiffness coefficients to target value for the three-DOF system with elastomeric mounts.

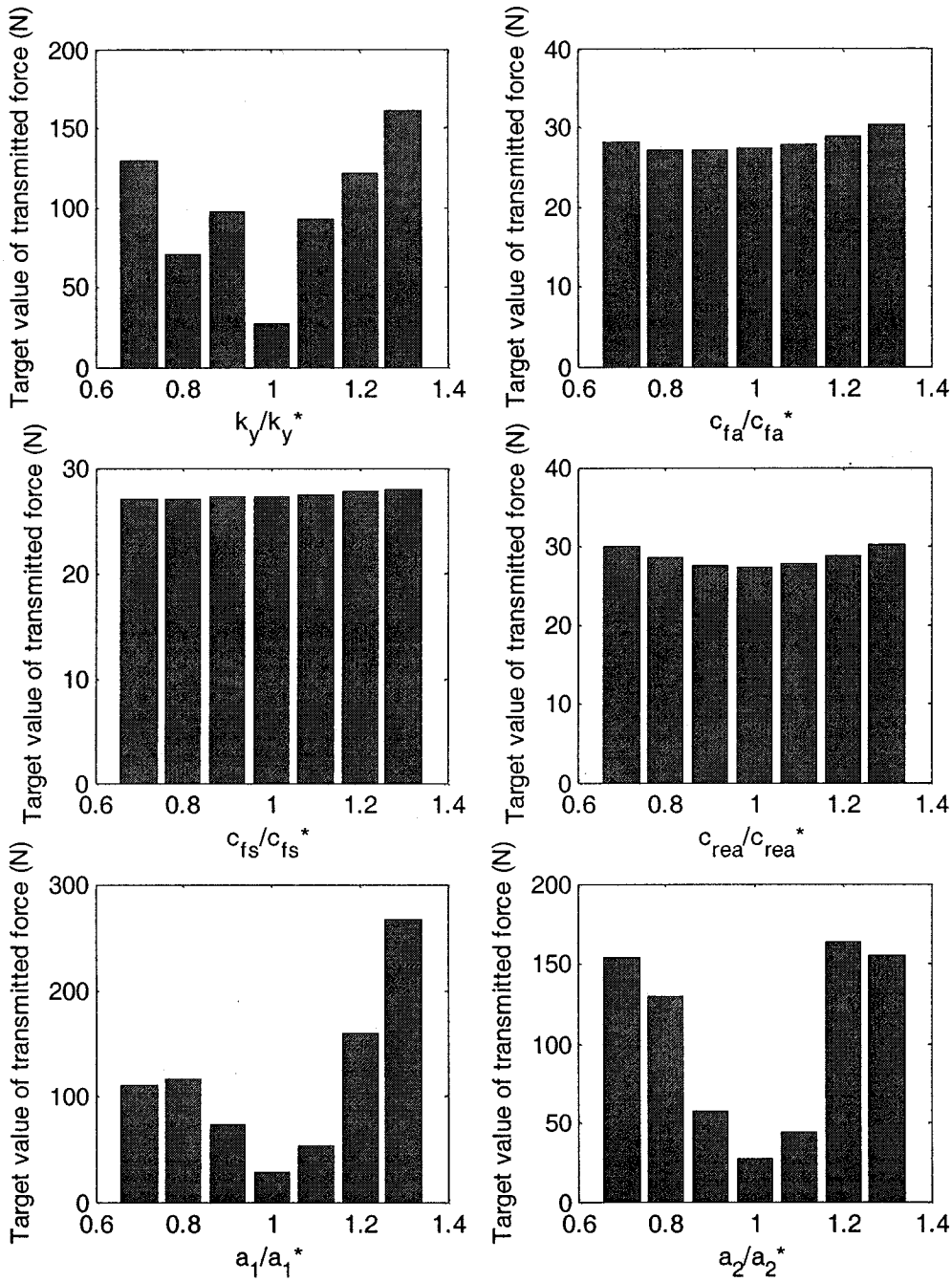

Figure 6.6: The influences of the shear stiffness and damping coefficients, as well as the longitudinal locations to target value for the three-DOF system with elastomeric mounts.

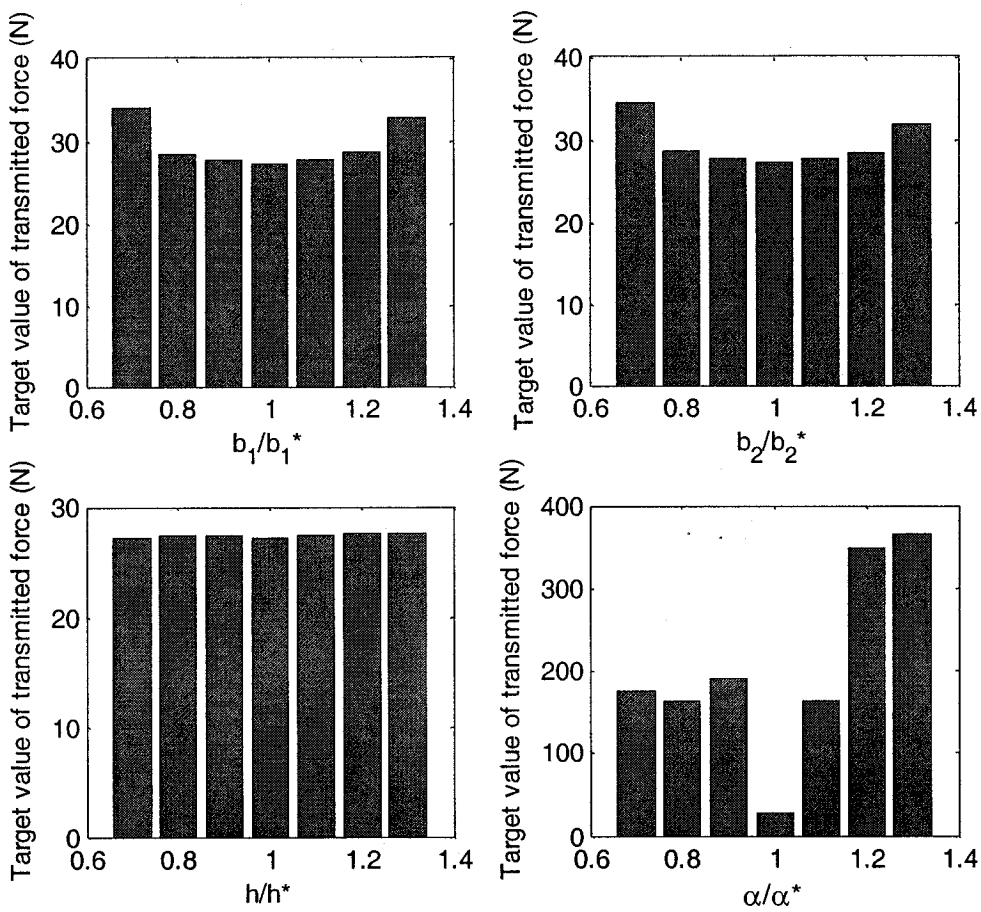

Figure 6.7: The influences of the lateral and vertical locations to target value for the three-DOF system with elastomeric mounts.

6.6 Comparison of Hydraulic System Response Using Optimal Elastomeric Mount Locations

The optimal locations, listed in Table 6.4 for the three-DOF engine mount system with elastomeric mounts are employed to verify the characteristic performance of the three-DOF hydraulic mount system. The simulation results shown in Figures 6.8 to 6.10 indicate that the transmitted force in the vertical direction decrease; however, the transmitted roll and pitch moments increase at the optimal locations due to the higher stiffness of the hydraulic mount. It can be concluded that the optimal location attained

from the optimization result of the elastomeric mount system can not fit for all the other mounts, thus the optimization work for the entire hydraulic mount system is suggested in the future work.

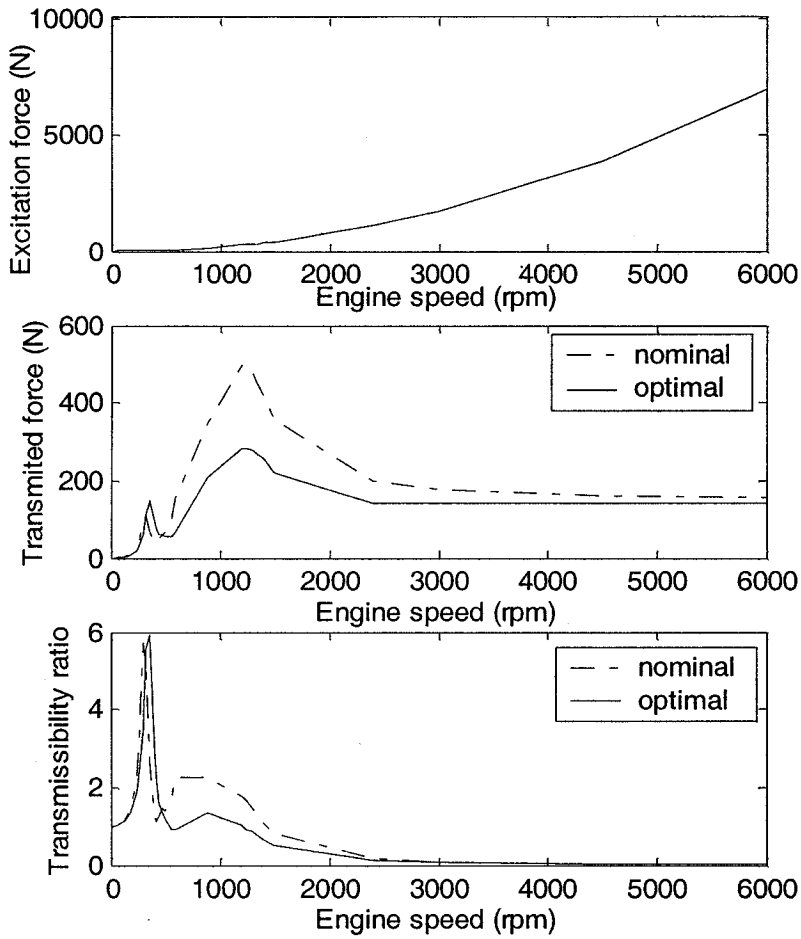

Figure 6.8: Comparison of the transmitted vertical force of three-DOF hydraulic mount system model at the optimal location of the elastomeric mount system.

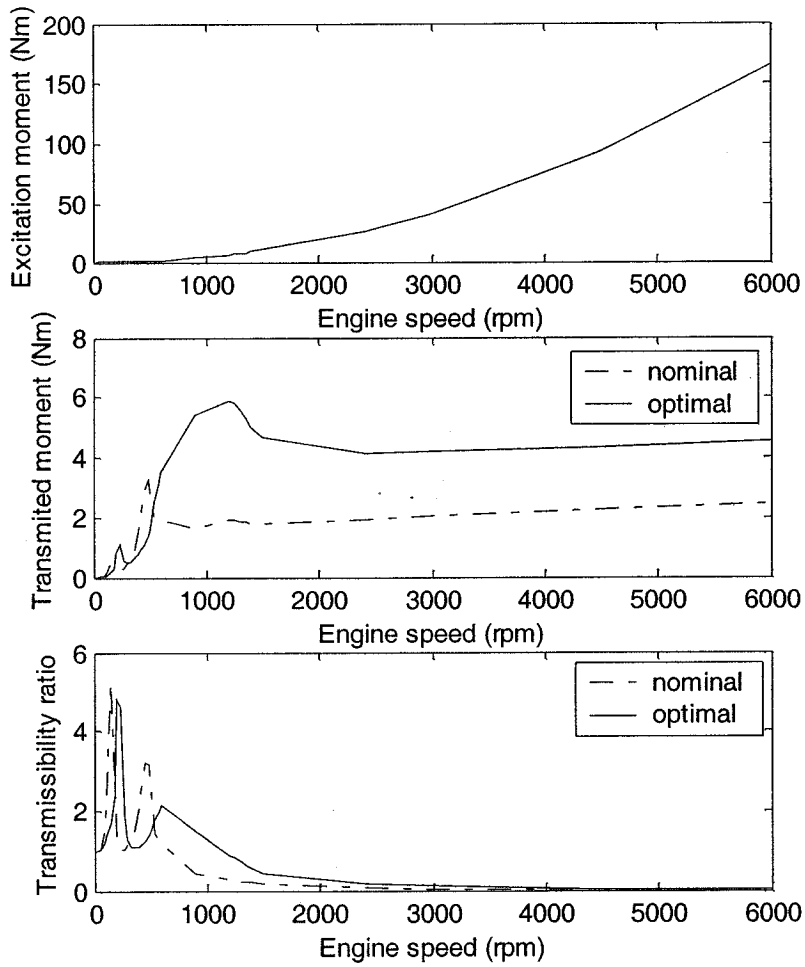

Figure 6.9: Comparison of the transmitted roll moment of three-DOF hydraulic mount system model at the optimal location of the elastomeric mount system.

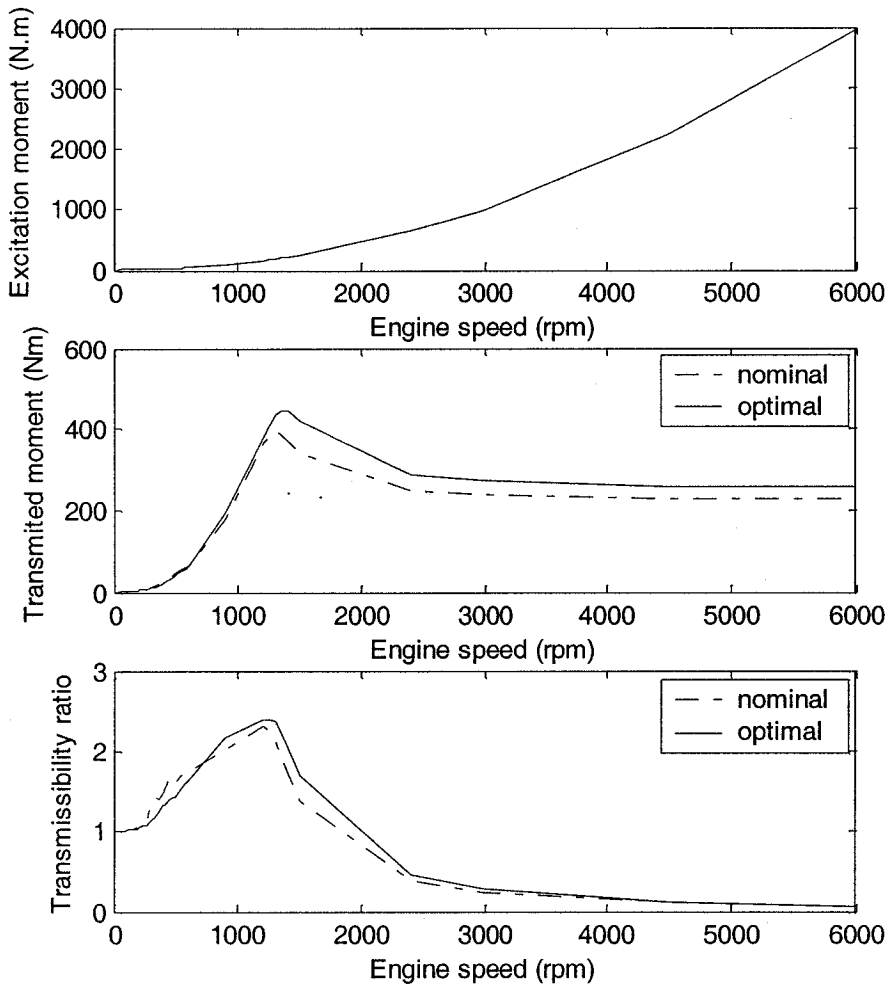

Figure 6.10: Comparison of the transmitted pitch moment of three-DOF hydraulic mount system model at the optimal location of the elastomeric mount system.

6.7 Summary

The simulation and numerical optimization of an engine mounting system is demonstrated with a widely used computer optimization program for nonlinear multi-variable objective functions and nonlinear constraints. Vibratory forces and moments transmitted through the elastomeric mounts under certain engine excitation conditions are minimized by adjusting the stiffness and orientation of the engine mounts. Inequality

constraints on the maximum allowable deflection of the engine to static load and maneuvering conditions must also be satisfied. The constrained variable metric optimization technique is applied to find the optimum design. The technique has been demonstrated successfully after running the program for over 20 hours under the final closest initial conditions. The last optimal result will be used as the reference for the initial conditions for the next optimization procedure until no better an optimal result can be obtained.

The weighting factors of the objective function are applied to specify the relative importance of each individual vibratory excitation or force condition in each direction, and at the entire frequency range of engine operation. The procedure has been rerun many times with different sets of weighting factors until the optimization has been completed successfully with satisfied optimal results under the weighting factors in Table 6.3. The optimal characteristics of the system can be observed considerably reducing the transmitted force and moments. The Sequential Quadratic Programming (SQP) method has proven reliable and effective to solve such a complex nonlinear multi-variable vibration isolation problem under imposing nonlinear constraints. The optimization of the locations and characteristics of the engine mounts has been achieved.

Even though the optimal locations for the elastomeric mount do not suit well for the hydraulic mount, the procedure developed for the optimization of the engine mount system is applicable to both elastomeric and hydraulic mounts system. The parameter sensitivity analysis can also provide a guide to the design engineer of the engine mounting system.

CHAPTER 7

CONCLUSION

7.1 General

The primary focus of this thesis research is to study vibration isolation of an engine mounting system, using both nonlinear elastomeric mounts and flexible chamber hydraulic mounts, under engine gas pressure and unbalanced force excitations. The research is conducted in six phases including: (i) Establishment of a dynamic engine vibration model to identify the engine excitation forces. (ii) Development and validation of the analytical nonlinear elastomeric mount model and complex flexible chamber hydraulic mount model. (iii) Derivation of a three-DOF engine mounting system model using the elastomeric mount and hydraulic mounts, and the simulation of the established systems to determine their respective performance. (iv) Application of an optimization method to the 3DOF elastomeric mounting system to determine optimal design parameters and mount locations. (v) Sensitivity analysis of the design parameters. (vi) Application of the optimal elastomeric mount locations in the three-DOF engine mount system replaced by the hydraulic mounts. The major highlights and contributions of this investigation are summarized as follows:

(i) Develop the engine dynamic performance with a separate model of the reciprocating and rotating parts, as well as cylinder component to derive the excitation force transmitted from the engine to the chassis.

(ii) Identify the engine vertical unbalanced inertia force and related roll and pitch moments, arising from unbalance force and gas pressure attained from reported data.

(iii) Determine nonlinear elastomeric mount parameters by using the experimental characterization of the elastomeric mount in order to perform its static and dynamic properties in the time and frequency domains with both base and force excitations.

(iv) Validate and modify the reported flexible chamber hydraulic mount model, while simulating the static and dynamic performance of the mount with its detailed parameter study, including chamber pressure and its volume change, flow through the orifice etc., under base excitation loaded with a rigid mass.

(v) Analyze the influence of the frequency and amplitude on the vibration of the single-DOF engine mount system with the hydraulic mount.

(vi) Establish a three-DOF engine mount system with elastomeric and hydraulic mounts respectively, with three-point mounts (two front mounts, one rear mount) supporting the engine as a rigid mass.

(vii) Analyze the vibration transmissibility characteristics of the three-DOF engine mount system with both elastomeric and hydraulic mounts in the entire frequency range (1-200Hz) of engine operation.

(viii) Apply the advanced optimization method with a three-DOF elastomeric mount system to realize the optimal design for the purpose of minimizing the transmitted force from the engine to the vehicle chassis by setting the mount parameters and their locations as sixteen variables.

(ix) Evaluate the sensitivity of the parameters, such as mount stiffness, damping coefficients, mount locations and orientation in order to evaluate the influence

of the parameters on the vibration isolation of the three-DOF engine mount system.

(x) Assess the performance of the three-DOF system with the hydraulic mounts at the optimal locations of the elastomeric mount system.

7.2 Conclusions

On the basis of the results attained in this study, the following are the major conclusions drawn:

(i) Engine excitation forces are identified as the unbalance inertia force in the vertical axis, the roll moment is generated by the unbalance force and gas pressure, while the pitch excitation force is caused by the sum of the vertical forces.

(ii) The nonlinear elastomeric mount and hydraulic mount static characteristics are nonlinearly dependent on the preload. The dynamic properties of the mounts, typically for the hydraulic mount, are a strong nonlinear function of the frequency and amplitude of excitation. The detailed parameters of the hydraulic mount change along with the frequency and amplitude.

(iii) The dynamic properties of the engine mounting system with the hydraulic mounts present highly nonlinear characteristics, which rely on their nonlinear chamber compliance. The three mounts show different characteristic response due to their different deflections.

(iv) The optimization method of **Sequential Quadratic Programming (SQP)** was successfully used to optimize the system design to find the optimal placement of all sixteen parameters including the stiffness and damping coefficients, as

well as the mount locations. The reduction ratio of the target value, which is combined with transmitted force and moments in bounce, roll and pitch axes in the entire frequency range, decreases 91.1%. As a result, the greatly obvious improvement has been achieved in vibration isolation of engine mounting system by the implementation of the effective optimization method.

(v) The sensitivity analyses provided suggestions for the design of the system by giving the influence of the design parameters.

(vi) The optimal location only fits well with the specific mounts involved in the optimization process.

7.3 Future Work

The following studies described are recommended for future research:

(i) The optimization of the three-DOF engine mount system with hydraulic mounts is suggested to further improve the system design.

(ii) Experimental work is required to validate the developed model and simulation results for the engine mounting systems.

(iii) The stiffness variation along with the frequency, typically for higher frequencies should be considered in the performance identification of the hydraulic mount since lower stiffness in high frequency is required to perform better vibration isolation characteristics.

(iv) In order to evaluate further performances of the engine mount system in a realistic environment, studies incorporating a full-scale or scaled–down vehicle model are recommended.

REFERENCES

1. Wilson, W.K., "Practical Solution of Torsional Vibration Problems", Vol. 2, 3rd. Edition, New York, 1963.
2. Lumley, J. L., "Engines- an introduction", Cambridge University Press, 1999.
3. Lichty, L. C., "combustion engine processes", McGraw-Hill book Company Press,1967,
4. Taylor, C. F., 'The Internal Combustion Engine in Theory and Practice", 2nd Edition, The M.I.T. press, Cambridge, MA, 1985.
5. Lichty, L. C. "Internal-combustion Engines", 6th Edition, Yale University, 1951.
6. Rizzoni, G. "A Dynamic Model for the Internal Combustion Engine", PhD dissertation, The University of Michigan, USA, 1986.
7. Rabeih, E. M. A. 'Torsional Vibration Analysis of Automotive Drivelines', PhD dissertation, The University of Leeds, UK, 1997.
8. Yu, Y., Peelamedu, S. M., Naganathan, N.G. and Dukkipati, R.V., "Automotive Vehicle Engine Mounting Systems: A Survey", ASME, Vol. 123, pp.186-104, June 2001.
9. Doughty, S., "Fundamentals of IC Engine Torsional Vibration", Presented at the Energy-Sources Technology Conference and Exhibition, New Orleans, Louisiana, January 10-14, 1988.
10. Rizzoni, G., "Estimate of Indicated Torque from Crankshaft Speed Fluctuations: A Model for the Dynamics of the IC Engine", IEEE Transactions on Vehicular Technology, Vol.38, No.3, pp. 168-179, Aug. 1989.

11. Jacob, P.J., Gu, F., "Non-parametric Models in the Monitoring of Engine Performance and Condition, Part1: Modeling of Non-linear Engine Processes", IMechE, Journal of Automobile Engineering, Part D, Vol. 213, pp. 73-81, 1999.

12. Cho, H., Song, H., Lee, J. and Kauh, S., "Simulation of a Transient Torque Response for Engine Performance in a Spark Ignition Engine", IMechE, Journal of Automobile Engineering, Part D, Vol. 215, pp. 127-140, 2001.

13. Jeong, T. and Singh, R., "Analytical Methods of Decoupling the Automotive Engine Torque Roll Axis", Journal of Sound and Vibration, Vol. 234, No.1, pp. 85-114, 2000.

14. Van Nieuwstadt, M.J. and Kolmanovsky, I.V., "Detecting and Correcting Cylinder Imbalance in Direct Injection Engines", Journal of Dynamic Systems, Measurement, and Control, Vol.123, pp. 413-425, Sept.2001.

15. Cho, S.W. and Yun, J.E., "The Friction Force of Piston Assembly in an IDI Diesel Engine", Int. J. Vehicle Design, Vol.19, No.1, pp. 50-64, 1998.

16. Zweiri, Y.H., Whidborne, J.F. and Seneviratne, L.D., "Dynamic Simulation of a Single-cylinder Diesel Engine Including Dynamometer Modeling and Friction", IMechE, Journal of Automobile Engineering, Part D, Vol 213, pp. 391-402, 1999.

17. Zweiri, Y.H., Whidborne, J.F. and Seneviratne, L.D., "Instantaneous Friction Components Model for Transient Engine Operation", IMechE, Journal of Automobile Engineering, Part D, Vol. 214, pp. 809-824, 2000.

18. Zweiri, Y.H., Whidborne, J.F. and Seneviratne, L.D., "Detailed Analytical Model of A Single-cylinder Diesel Engine in the Crank Angle Domain", IMechE, Journal of Automobile Engineering, Part D, Vol 215, pp.1197-1216, 2001.

19. Drew S.J., Hesterman, D.C. and Stone, B.J., "The Torsional Excitation of Variable Inertia Effects in a Reciprocating Engine", Mechanical Systems and Signal Processing, Vol.13, No.1, pp. 25-144, 1999.

20. Tao, J.S., Liu, G.R. and Lam, K. Y., "Excitation Force Identification of an Engine with Velocity Data at Mounting Points", Journal of Sound and Vibration, Vol.242, No.2, pp. 321-331 2001.

21. Masmoudi, R.A. and Hedrick J.K., "Estimation of Vehicle Shaft Torque using Nonlinear Observers", Transactions of the ASME, Vol.114, pp. 394-400, Sept.1992.

22. Moskwa, J.J. and Hedrick J.K., "Modeling and Validation of Automotive Engines for Control Algorithm Development", Transactions of the ASME, Vol.114, pp. 278-284, June 1992.

23. Moskwa, J.J., Wang, W. and Bucheger, D.J., "A New Methodology for Use in Engine Diagnostics and Control, Utilizing "Synthetic" Engine Variables: Theoretical and Experimental Results", Transactions of the ASME, Vol.123, pp. 528-534, Sept.2001.

24. Stotsky, A., Egardt, B. and Eriksson, S., "Variable Structure Control of Engine Idle Speed With Estimation of Unmeasurable Disturbances", Journal of Dynamic Systems, Measurement, and Control, Vol.122, Dec.2000.

25. Weeks, R.W. and Moskwa, J.J., "Automotive Engine Modeling for Real-Time Control Using MATLAB/SIMULINK", SAE Paper 950417, 1994.

26. Du, H., Zhang, L. and Shi, X., "Reconstructing Cylinder Pressure from Vibration Signals Based on Radial Basis Function Networks", IMechE, Journal of Automobile Engineering, Part D, Vol. 215, pp. 761-767, 2001.

27. Kao, M. and Moskwa, J. J., "Nonlinear Diesel Engine Control and Cylinder Pressure Observation", Journal of Dynamic Systems, Measurement, and Control, Vol.117, pp. 183-192, June 1995.

28. Schmitt, R. V. and Charles, J. L., "Design of Elastomeric Vibration Isolation Mounting Systems of Internal Combustion Engines", SAE Paper 760431, 1976.

29. Rivin, E. I., "Passive Engine Mounts—some Directions for Further Development", SAE Paper 850481, 1985.

30. Richards, C. M. and Singh, R., "Characterization of Rubber Isolator Nonlinearities in the Context of Single and Multi-degree-of –freedom Experimental Systems", Journal of Sound and Vibration, Vol.247, No.5, pp. 807-834, 2001.

31. Kim, J. J. and Kim, H. Y., "Shape Design of an Engine Mount by a Method of Parametric Shape Optimization", IMechE, Journal of Automobile Engineering, Part D, Vol.211, pp. 155-159, 1997.

32. Bernuchon, M., "A New Generation of Engine Mounts", SAE Paper 840259, 1984.

33. Corcoran, P. E. and Tick, G.H., "Hydraulic Engine Mounts Characteristics", SAE Paper 840407, 1984.

34. Muzechuk, R. A., "Hydraulic Mounts-improved Engine Isolation", SAE Paper 840410, 1984.

35. Matthew Brach, R. and Haddow, A.G., "On the Dynamic Response of Hydraulic Engine Mounts", SAE Paper 931321, 1993.

36. Kim, G. and Singh, R., "Resonance, Isolation and Shock Control Characteristics of Automotive Nonlinear Hydraulic Engine Mounts", ASME, Transportation Systems, DSC-Vol.44, pp. 165-179, 1992.

37. Kim, G. and Singh, R., "Nonlinear Analysis of Automotive Hydraulic Engine Mount", Transactions of the ASME, Vol. 115, pp. 482-487, 1993.

38. Ahmed, A.K.W., Haque, M.M. and Rakheja, S., "Nonlinear Analysis of Automotive Hydraulic Mounts for Isolation of vibration and Shock", Int. J. of Vehicle Design, Vol. 22, Nos. ½, pp. 116-128, 1999.

39. Geisberger, A., Khajepour, A. and Golnaraghi, F., "Non-linear Modeling of Hydraulic Mounts: Theory and Experiment", Journal of Sound and Vibration, Vol.249, No.2, pp. 371-397, 2002.

40. Marjoram, R.H., "Pressurized Hydraulic Mounts for Improved Isolation of Vehicle Cabs", SAE Paper 852349, 1985

41. Haque, M. M., "Evaluation of a class of Hydraulic Dampers for Isolation of Vibration and shock", PhD Dissertation, Concordia University, Montreal, Canada, 1996.

42. Kim, G., "Study of Passive and Adaptive Hydraulic Engine Mounts", PhD Dissertation, The Ohio State University, USA, 1992.

43. Flower, W.C., "Understanding Hydraulic Mounts for Improved Vehicle Noise, Vibration and Ride Qualities", SAE Paper 850975, 1985.

44. Singh, R., Kim, G., and Ravindra, P.V., "Linear Analysis of Automotive Hydro-Mechanical Mount with Emphasis on Decoupler Characteristics", Journal of Sound and Vibration, Vol.158, No.2, pp. 219-243, 1992.

45. Royston, T.J., and Singh, R., "Periodic Response of Nonlinear Engine Mounting Systems", SAE Paper 951297, 1995.

46. Ushijima, T., Takano, K. and Kojima, H., 1988, "High Performance Hydraulic Mount for Improving Vehicle Noise and Vibration", SAE Paper 880073, 1988.

47. Petec, N.K., Goudie, R.J., and Boyle, F.P., "Actively Controlled Damping in Electrorheological Fluid-Filled Engine Mounts", SAE Paper 881785, 1988.

48. Duclos, T.G., "Design Devices using Electrorheological Fluids", SAE Paper 881134, 1988.

49. Kim, G. and Singh, R., "A Study of Passive and Adaptive Hydraulic Engine Mount Systems with Emphasis on Non-linear Characteristics", Journal of Sound and Vibration, Vol.179, No.3, pp. 427-453, 1995.

50. Swanson, D. A., "Active Engine Mounts for Vehicles", SAE Paper 932432, 1993.

51. Nakaji, Y., Satoh, S., Kimura, T., Hamae, T., Akatsu, Y. and Kawazoe, H., "Development of an Active Control Engine Mount system", Vehicle System Dynamics, 32, P185-198, 1999.

52. Muller, M., Weltin, U., "The Effect of Engine Mounts on the Noise and Vibration Behavior of Vehicles", SAE Paper 940607, 1994.

53. Ushijima, T., and Kumakawa, S., " Active Engine Mount with Piezo-Actuator for Vibration Control", SAE Paper 930201, 1993

54. Ford, D.M., "An Analysis and Application of a Decoupled Engine Mount System for Idle Isolation", SAE Paper 850976, 1985.

55. Okuma, M., Ohara, T., Nagao, K. and Nagamatsu, A., "Application of a New Experimental Identification Method to Engine Rigid Body Mount System", SAE Paper 891139, 1989.

56. Lee, J.M., Yin, H.J. and Kim, J.H., "Flexible Chassis Effects on Dynamic Response of Engine Mount Systems", SAE Paper 951094, 1995.

57. Bretl, J., "Optimization of Engine Mounting Systems to Minimize Vehicle Vibration", SAE Paper 931322, 1993.

58. Kim, J.H. and Lee, J.M., "Elastic Foundation Effects on the Dynamic Response of Engine Mount Systems", IMechE, Journal of Automobile Engineering, Part D, Vol. 214, pp. 45-53, 2000.

59. Ashrafiuon, H. and Nataraj, C., "Dynamic Analysis of Engine-Mount Systems", Journal of Vibration and Acoustics, Vol.114, pp. 79-83, Jan. 1992.

60. Winkler, K., "Guidelines for Optimizing Vibration Mass Dampers", SAE Paper 880076, 1988.

61. Geck, P.E. and Patton, R.D., "Front Wheel Drive Engine Mount Optimization", SAE Paper 840736, 1984.

62. Wise, K.A. and Reid, R.E., "Modeling and Identification of a Light Truck Engine Mounting System for Ride Quality Optimization", SAE Paper 841142, 1984.

63. Arai, T., Kubozuka, T. and Gray, S.D., "Development of an Engine Mount Optimization Method Using Model Parameters", SAE Paper 932898, 1993.

64. Swanson, D.A., Wu, H.T. and Ashrafiuon, H., "Optimization of Aircraft Engine Suspension Systems", Journal of Aircraft, Vol. 30, No. 6, Nov.-Dec. 1993.

65. Ashrafiuon, H., "Design Optimization of Aircraft Engine-Mount Systems", Journal of Vibration and Acoustics, Vol. 115, pp. 463-467, Oct. 1993.

66. Oh, T., Lim, J. and Lee, S.C., "An Engineering Practice in Optimal Design of Power train Mounting System for 2.0L FF Engine". SAE Paper 912523, 1991.

67. Demic, M., "A Contribution to the Optimization of the Position and the Characteristics of Passenger Car Powertrain Mounts", Int. J. of Vehicle Design, Vol.11, No. 1, 1990.

68. Tao, J. C., Liu, G.R. and Lam, K.Y., "Design Optimization of Marine Engine-mount system", Journal of Sound and Vibration, Vol.235, No.3, pp. 477-494, 2000.

69. Ahn, Y.K., Song, J.D. and Yang, B., "Optimal Design of Engine Mount Using an Artificial Life Algorithm", Journal of Sound and Vibration, 261, P309-328, 2003.

70. Baldanzini, N., Caprioli, D. and Pierini, M., "Designing the Dynamic Behavior of an Engine Suspension System through Genetic Algorithms", Transactions of the ASME , Vol. 123, Oct. 2001.

71. Kang, J., Kolmanovsky, I. and Grizzle, J. W., "Dynamic Optimization of Lean Burn Engine Aftertreatment", Journal of Dynamic Systems, Measurement, and Control, Vol. 123, pp. 153-160, 2001.

72. Rao, S.S. "Optimization—Theory and Applications", 2nd Edition, San Diego State University, USA, 1984.

73. Arora, J. S., "Guide to Structural Optimization", Published by ASCE, USA, 1997.

74. Kelly, S.G., "Fundamentals of Mechanical Vibrations", 2nd Edition, The University of Akron. 2000.

75. Shiao, Y., Pan, C. and Moskwa, J.J., "Advanced Dynamic Spark Ignition Engine Modeling for Diagnostics and Control", Int. J. of Vehicle Design, Vol. 15, No.6, pp. 578-596, 1994

76. Heisler, H., " Advanced Vehicle Technology", 2nd Edition, College of North West London, Willesden Centre, London, UK, 2002.

77. Streeter, V. L. and Wylie, E. B. " Fluid Mechanics", 7th Edition, McGraw-Hill, New York, 1981.

在加拿大不同的省份考驾照的要求是不一样的。安大略省的驾照考试程序和要求最近几年发生了很大变化。目前的考试方法较复杂，难度也较大。

在安省考驾照，首先要通过笔试（理论考试），然后参加路考。笔试主要包括交通规则和交通信号及标志，不考机械常识。熟读驾驶指南可帮助顺利通过笔试。笔试试卷为多项选择题。有时也通过计算机答题。如果不能通过，回去准备后可以再考。通过理论考试以后，还要进行视力测试。然后便可取得“学习驾驶执照”，也称临时驾照（G1）。用这个驾照，就可以在持有正式驾照的成年人陪同下上路练习驾驶了。陪同的教练必须有 4 年以上的驾龄。在大多数城市里，一般没有象中国这样的练车场，也没有“钻竿儿”之类的训练。而是第一次开车就上真正的马路，融入街上的车流里。在安大略省，持学习驾照的司机要等很长时间才能排上路考。如果你参加了正规的驾校课程，8 个月以后可以参加路考，对于不参加驾校的初学者则要练习等待至少 12 个月。路考通过后得到可以无教练陪同单独驾车的驾照（G2）了。持有 G2 的司机夜间开车和上高速路有限制。再过 12 个月，将通过一个全面的路考，合格后，得到正式的（G）驾照。如果你已有中国国内驾照并有两年以上驾龄，则可在通过理论考试后立即申请正式 G 驾照的路考，如果通不过，则可用 G1 直接参加 G2 的路考，而不必等很长的时间。如果驾龄超过一年，可直接由 G1 参加 G2 驾照的路考。

各省对考驾照有不同的规定。有些省份的驾照考试相对简单些。在魁北克省，首先必须注册一个驾驶学校，不管你是否真正去上课，只要掌握了教材中的内容，就可参加由政府举办的理论考试。政府不允许没在驾校注册过的人参加笔试。笔试通过后，可以得到一个临时驾照（Temporary Driver′ s License），也称学习驾照（Learner′ s Permit）。凭这个临时驾照，你可以在驾校老师或有正式驾照的其他人陪同下上路练习了。当你练到有把握通过时再进行路考。在安大略省，上驾校不是必须的。加拿大的驾校一般为私人所开，规模不大，收费也不高。一般在三四百加元左右。无论是驾校教练还是私人司机，教车一般都是在普通路上与正常行驶的车辆并驾齐驱。很少有专门的练车场。为了提醒别人注意，可以在车上注明“ Student Driver”字样。

各省的交通规则也有所不同。例如，魁北克省规定红灯时不可以向右拐弯；卑诗省规定绿灯闪动时左拐弯不优先，而这些都与安大略省不相同。

请熟悉当地驾驶规则的朋友或驾校的教练帮助上路练习很有必要。新司机更要做充分的训练才能保证路考通过。如果是新司机，练习 30 个小时以上路考通过的把握性才比较大。路考要事先约定具体时间。路考时，要带身份证明及路考费用（依具体省份和时间而定）。路考过程大概在 15 分钟至 30 分钟。路考时最好用自动档车而不要用手动档车，这样易精神集中，有利通过。在路考前，本人亲自驾车熟悉考试路段是有好处的。只有“轻车熟路”才能稳操胜券。

要做到精神集中但不紧张，放松而不怠慢。路考时，出现任何的“危险动作”都会导致失败。如果没有所谓的危险动作出现，则根据小的误差计点数。点数积累到一定程度即宣布考试失败。

由于加拿大的交通规则和国内的不尽相同，所以，既使是老司机，也不能掉以轻心。对一般人容易忽略的小动作也应该做到位，例如，遇到“STOP”标志牌一定要停稳后一两秒